

**GOLD NANOPARTICLE BASED COLORIMETRIC
SENSORS FOR HEAVY METAL IONS DETECTION**

**AĐIR METAL İYONLARI TAYİNİNE YÖNELİK ALTIN
NANOPARTİKÜL TEMELLİ KOLORİMETRİK SENSÖRLER**

GÜLSU ŞENER YİLDİRİM

PROF. DR. ADİL DENİZLİ

Supervisor

Submitted to Graduate School of Science and Engineering of Hacettepe University
as a Partial Fulfillment to the Requirements
for the Award of the Degree of Doctor of Philosophy
In Nanotechnology and Nanomedicine

2014

This work named “**Gold Nanoparticle Based Colorimetric Sensors for Heavy Metal Ions Detection**” by **GÜLSU ŞENER YİLDİRİM** has been approved as a thesis for the Degree of **DOCTOR OF PHILOSOPHY IN NANOTECHNOLOGY AND NANOMEDICINE** by the below mentioned Examining Committee Members.

Prof. Dr. Adil DENİZLİ

Head and Supervisor

.....

Prof. Dr. Emir Baki DENKBAŞ

Member

.....

Prof. Dr. Handan YAVUZ ALAGÖZ

Member

.....

Prof. Dr. Serap ŞENEL

Member

.....

Assist. Prof. Dr. Fatma YILMAZ

Member

.....

This thesis has been approved as a thesis for the Degree of **DOCTOR OF PHILOSOPHY IN NANOTECHNOLOGY AND NANOMEDICINE** by Board of Directors of the Graduate School of Science and Engineering.

Prof. Dr. Fatma SEVİN DÜZ
Director of the Graduate School of
Science and Engineering

To my dear family and Adem...

ETHICS

In this thesis study, prepared in accordance with the spelling rules of Graduate School of Science and Engineering of Hacettepe University,

I declare that

- all the information and documents have been obtained in the base of the academic rules
- all audio-visual and written information and results have been presented according to the rules of scientific ethics
- in case of using other Works, related studies have been cited in accordance with the scientific standards
- all cited studies have been fully referenced
- I did not do any distortion in the data set
- and any part of this thesis has not been presented as another thesis study at this or any other university

10/12/2014

GÜLSU ŞENER YİLDİRİM

ÖZET

AĞIR METAL İYONLARI TAYİNİNE YÖNELİK ALTIN NANOPARTİKÜL TEMELLİ KOLORİMETRİK SENSÖRLER

Gülsu ŞENER YİLDİRİM

Doktora, Nanoteknoloji ve Nanotıp Anabilim Dalı

Tez Danışmanı: Prof. Dr. Adil DENİZLİ

İkinci Tez Danışmanı: Doç. Dr. Lokman UZUN

Aralık 2014, 85 sayfa

Suyun toksik metal iyonlarıyla kirlenmesi ciddi çevre ve sağlık sorunlarına yol açmaktadır. Bu nedenle sudaki toksik metal iyonlarının izlenmesi halk sağlığı ve su kalitesi açısından oldukça önemlidir. Toksik metal iyonlarını tayini için sıklıkla kullanılan yöntemler, indüktif olarak eşleştirilmiş plazma kütle spektrometresi (ICP-MS), atomik absorpsiyon spektrometresi (AAS) ve yüksek performans sıvı kromatografisi (HPLC) gibi kromatografik ve spektroskopik tekniklerdir. Bu yöntemler oldukça hassastır ancak karmaşık prosedürleri nedeniyle kullanımları için yoğun teknik eğitim gereklidir. Ayrıca bu yöntemler pahalı ve zaman alıcıdır. Bu nedenle metal iyonları tayini için ucuz, basit ve taşınabilir yöntemlere ihtiyaç vardır.

Bu kapsamda, toksik metal iyonu ile kirlenmiş suların tayini için altın nanopartiküller ve amino asitler kullanılarak kolorimetrik temelli basit yöntemler geliştirilmiştir. Bu tezde, altın nanopartikül temelli iki farklı kolorimetrik yöntem hazırlanmıştır. İlk yaklaşımda sudan Hg^{2+} iyonu tayini için sitrat kaplı altın nanopartiküller ve lizin aminoasidi kullanılarak basit ama oldukça hassas (tayin limiti 2.9 nM) bir yöntem gösterilmiştir. Ayrıca bu yöntem Hg^{2+} iyonuna karşı

oldukça seçicidir ve sadece birkaç dakika içinde tamamlanabilmektedir. İkinci yaklaşımda sudan çoklu toksik metal iyonları (Hg^{2+} , Cd^{2+} , Fe^{3+} , Pb^{2+} , Al^{3+} , Cu^{2+} ve Cr^{3+}) tayini için 11-merkaptoundekanoik asit kaplanmış altın nanopartiküller ve beş amino asit (lizin, sistein, histidin, tirozin ve arjinin) kullanılarak basit kolorimetrik sensör dizisi rapor edilmiştir. Amino asitlerin varlığı (metal iyonları ve altın nanopartiküllerle kompleks yapabilen fonksiyonel grupları olan) partiküllerin agregasyonunu düzenlemekte ve, partikül agregasyonunu arttırabilir ya da azaltabilir. Her amino asit-altın nanopartikül çiftindeki renk değişimi incelenerek test edilen bütün metallerin hassas bir şekilde ayırt edilebilmesi mümkün olmuştur.

Anahtar Kelimeler: Ağır metal iyonu tayini, altın nanopartiküller, kolorimetrik sensörler, amino asitler, sensör dizileri.

ABSTRACT

GOLD NANOPARTICLE BASED COLORIMETRIC SENSORS FOR HEAVY METAL IONS DETECTION

Gülsu ŞENER YİLDİRİM

**Doctor of Philosophy, Nanotechnology and Nanomedicine
Division**

Supervisor: Prof. Dr. Adil DENİZLİ

Co-supervisor: Assoc. Prof. Dr. Lokman UZUN

December 2014, 85 pages

Contamination of water by toxic metal ions can lead to serious environmental and health problems. Therefore, monitoring of toxic metal ions in water is very important in terms of improving public health and water quality. Common methods for toxic metal ion detection are often based on chromatographic and spectroscopic techniques such as inductively coupled plasma mass spectrometry (ICP-MS), atomic absorption spectrometry (AAS), and high performance liquid chromatography (HPLC). These methods are highly sensitive but they require intense technical training because of their complicated procedures, and they are expensive and time-consuming. Therefore, low cost, simple, rapid, and portable methods for metal ion detection are still highly desired.

In this context, this thesis seeks development of facile colorimetric based methods for detection of toxic metal ion contaminated water using gold nanoparticles and amino acids. In this thesis, we report the preparation of two different gold nanoparticle based colorimetric method for this purpose. In the first approach, we demonstrate the preparation of a simple yet very sensitive (detection limit is 2.9 nM) colorimetric assay for rapid detection of Hg²⁺ in water using as-prepared citrate-capped gold nanoparticles and amino acid lysine. In addition, the assay

showed good selectivity against Hg^{2+} and the analysis can be completed within only a few minutes. In the second approach, we report a facile colorimetric sensor array for detection of multiple toxic heavy metal ions (Hg^{2+} , Cd^{2+} , Fe^{3+} , Pb^{2+} , Al^{3+} , Cu^{2+} , and Cr^{3+}) in water using 11-mercaptoundecanoic acid-capped gold nanoparticles and five amino acids (lysine, cysteine, histidine, tyrosine, and arginine). The presence of amino acids (which have functional groups that can form complexes with metal ions and gold nanoparticles) regulates the aggregation of the particles; it can either enhance or diminish the particle aggregation. Therefore, the color change enables naked-eye discrimination of all of the tested metal ions.

Keywords: Heavy metal ion detection, gold nanoparticles, colorimetric sensors, amino acids, sensor array.

ACKNOWLEDGEMENTS

First and foremost, I would like to express my special appreciation and thanks to my advisor Prof. Dr. Adil Denizli, who always believed in and supported me with every aspect of research and life. I thank him for all the resources that he provided, all the ideas that he shared, and all the time that he spent during my Ph.D. experience. He will always be an excellent example for me as both a chemist and a professor.

I owe my special thanks to my patient co-advisor Assoc. Prof. Dr. Lokman Uzun. He always supported me with the research projects. I gained an indispensable experience during the time that I have worked with him.

My sincere thanks go to the most cheerful professor, Handan Yavuz Alagöz, for her continuous support and encouragement since then my undergraduate.

Also, I would like to thank my thesis committee members: Prof. Dr. Serap Şenel, Prof. Dr. Emir Baki Denkbaş and Assist. Prof. Dr. Fatma Yılmaz, for their time, interest, and insightful comments.

My time at Bioreg was very enjoyable, thanks to the many great friends. I would like to thank my sincere and helpful office mates Emoş, Işık and Ahmet for the enjoyable time spent together. To my teammate Erdoğan, for his continuous support and dear friendship. To the best couple Canan and Emin and to the fearless Bahoş for all the moments shared together.

Also, I would like to thank all of the current and past Bioreg members; Erkut, Ali, Deniz, Nilay, Müge, Gözde, Engin, İlker, Veyis, Esmâ, Recep, Çiğdem, Mine, Aykut, Sabina, Gizem, Sevgi, Yeşeren, Ilgım, Duygu, Semra, Monireh, Kemal, Fatma, Dilara, and Seda.

I wish to give special thanks to Adem, who stood by me for all those times. None of this could have happened without his continuous support, patience and encouragement. With him, we will continue to peruse our dreams.

Last but not least, I would like to thank my family: my parents Zehra and Metin and my sister Başak, for all their love and support. The last words go to for, our newest member of the family, my adorable niece, Duru. She cheered me up in these hard working days.

The ten years in Bioreg family was a great experience and will always be remembered.

CONTENTS

	<u>Page</u>
ÖZET	i
ABSTRACT	iii
ACKNOWLEDGEMENTS.....	v
CONTENTS.....	vi
TABLES.....	viii
FIGURES	ix
SYMBOLS AND ABBREVIATIONS.....	xiv
1. INTRODUCTION.....	1
2. GENERAL INFORMATION	4
2.1. Toxicity of Metal Ions.....	4
2.2. Gold Nanoparticles	6
2.3. Synthesis of Gold Nanoparticles	6
2.3.1. Citrate Based and Related Methods.....	6
2.3.2. The Brust-Schiffrin Method.....	7
2.3.3. The Seed-Mediated Methods	8
2.3.4. Photochemical Method	10
2.3.5. Electrochemical Method	11
2.3.6. Sonochemical Method	12
2.3.7. Templates Based Methods.....	13
2.3.8. Galvanic Replacement Method	15
2.4. Surface Modification of Gold Nanoparticles.....	16
2.5. Optical Properties of Gold Nanoparticles.....	18
2.6. Colorimetric Detection of Metal Ions Using Metal Nanoparticles	19
2.6.1. Detection of Heavy Metal Ions.....	20
2.6.2. Detection of Other Metal Ions.....	24
2.6.3. Selective Detection of Multiple Metal Ions	25
2.6.4. New Approaches	27
3. MATERIALS AND METHODS.....	29
3.1. Ultrasensitive Colorimetric Sensing of Hg ²⁺ using Citrate-Capped AuNPs and Lysine	29
3.1.1. Materials.....	29

3.1.2. Methods.....	29
3.1.2.1. Synthesis of Citrate Capped Gold Nanoparticles	29
3.1.2.2. Colorimetric Sensing of Hg ²⁺ in Deionized and Tap Water	30
3.1.2.3. Recovery Experiments	31
3.1.2.4. Effect of Other Amino Acids on the Response Colorimetric Sensor	31
3.1.2.5. Selectivity of the Colorimetric Sensor	31
3.1.3. Characterization	32
3.2. Development of a Colorimetric Sensor Array for Detection of Multiple Metal Ions based on AuNPs and Amino Acids	32
3.2.1. Materials.....	32
3.2.2. Methods.....	32
3.2.2.1. Synthesis of MUA capped AuNPs	32
3.2.2.2. Determination of Optimum Amino Acid Concentrations in the Colorimetric Assay.....	33
3.2.2.3. Colorimetric Detection of Multiple Metal Ions	33
3.2.3. Characterization	33
3.2.4. Data Analysis for Multiple Ion Detection	34
4. RESULTS AND DISCUSSION	35
4.1. Ultrasensitive Colorimetric Sensing of Hg ²⁺ using Citrate-Capped AuNPs and Lysine	35
4.1.1. Sensing Mechanism	36
4.1.2. Effect of Amino Acids on Aggregation of Hg ²⁺ -Capped AuNPs	39
4.1.3. Colorimetric Detection of Hg ²⁺	41
4.1.4. Selectivity of the Colorimetric Assay.....	47
4.1.5. Practical Application	49
4.2. Development of a Colorimetric Sensor Array for Detection of Multiple Metal Ions based on AuNPs and Amino Acids	52
4.2.1. Amino Acid Binding onto the MUA-capped AuNP Surface	53
4.2.2. Sensing Mechanism	57
4.2.3. Colorimetric Sensing of Metal Ions Using the Colorimetric Array	59
4.2.4. Simultaneous Sensing of Multiple Metal Ions	68
5. CONCLUSIONS	70
REFERENCES.....	72
CURRICULUM VITAE	83

TABLES

Table 4.1: Comparison of our assay with other colorimetric approaches.	46
Table 4.2: Ion concentrations of tap water of Ankara ^a	49
Table 4.3: Results of the recovery experiments performed in tap water samples.	51
Table 4.4: Zeta potentials of MUA capped AuNPs before and after interacting with different amino acids.	56

FIGURES

Figure 2.1. TEM images of citrate capped AuNPs prepared using different amounts of sodium citrate. Decreasing the sodium citrate amount increases the particle size (A-F). Reprinted with permission from ref. [44].	7
Figure 2.2. (a) Low magnification and (b) high magnification TEM images of the small AuNPs prepared according to the Brust-Schiffrin method. Reprinted with permission from ref. [45].	8
Figure 2.3. TEM images of AuNRs with different aspect ratios. Reprinted with permission from ref. [55].	10
Figure 2.4. (a) SEM and (b) and (c) TEM images of star-shaped platelet-like asymmetric AuNPs. Inset in (a) shows the cross section of the plates. Adopted with permission from ref. [62].	11
Figure 2.5. TEM images of short (a) and long (b) AuNRs prepared using the electrochemical method. Adopted with permission from ref. [69].	12
Figure 2.6. TEM images of Au nanobelts at different magnifications. Adopted with permission from ref.[72].	13
Figure 2.7. (a) Cross-sectional SEM image of the AAO template. (b) SEM image of the Au deposited AAO template. (c, d) SEM images of Au nanotubes after template removal. (e) TEM image of the Au nanotubes. Reprinted with permission from ref. [82].	14
Figure 2.8. (a) Schematic representation of synthesis steps of iron oxide templated rice-shaped gold nanoshell fabrication. (b-e) SEM (left panel) and TEM (right panel) images of the particles at every step of synthesis. Reprinted with permission from ref. [84].	15
Figure 2.9. (a) TEM image of Ag nanoparticle templates. (b and c) TEM and SEM images of hollow AuNPs, respectively. (d) Electron reflection pattern of the hollow AuNPs. (e and f) TEM images of hollow Au nanotubes. Reprinted with permission from ref. [86].	16
Figure 2.10. Schematic representation of PEG and peptide modification of AuNRs. Reprinted with permission from ref. [95].	17
Figure 2.11. Major SPR bands of AuNPs with different shapes. Reprinted with permission from ref. [97].	18

Figure 2.12. (a) Absorption spectra of AuNPs (spherical) with different sizes. (b) pH-induced reversible aggregation of surface functionalized AuNPs. Aggregation of AuNPs results in a red shift in the absorption spectrum. Reprinted with permission from refs. [99,100].	19
Figure 2.13. Schematic representation of heavy metal ions sensing using the MUA capped AuNPs. Reprinted with permission from ref. [7].	20
Figure 2.14. Schematic representation of Hg ²⁺ sensing using DNA functionalized AuNPs. Reprinted with permission from ref. [18].	21
Figure 2.15. Schematic representation of Hg ²⁺ induced self-assembly of N-alkylaminopyrazole functionalized AuNRs. Reprinted with permission from ref. [105].	22
Figure 2.16. Schematic representation of the Ni ²⁺ coordinated octahedral complex between histidine and NTA functionalized AuNPs. Adopted with permission from ref. [107].	23
Figure 2.17. Schematic representation of catalytic etching based sensing of Cu ²⁺ ions using AuNRs. [108]	23
Figure 2.18. Schematic representation of K ⁺ sensing in the presence of Na ⁺ ions using 15-crown-5 functionalized AuNPs. Reprinted with permission from ref. [109].	24
Figure 2.19. Bright-field microscopic images of HeLa cells incubated with pentapeptide functionalized AuNPs and different amounts of Al ³⁺ ions; (a) 0 mM, (b) 5 mM, (c) 10 mM, (d) 50 mM and (e) 100 mM. (f) After F ⁻ etching the AuNPs in (e). Reprinted with permission from ref. [114].	25
Figure 2.20. Results of selective Hg ²⁺ and Ag ⁺ sensing using Tween 20 stabilized AuNPs. (a) Hg ²⁺ in the presence of NaCl and (b) Ag ⁺ sensing in the presence of EDTA. Reprinted with permission from ref. [15].	26
Figure 2.21. Schematic representation of the smart-phone based sensing of Hg ²⁺ . Reprinted with permission from ref. [120].	28
Figure 2.22. Schematic representation of Hg ²⁺ sensing using the paper-based colorimetric sensor. Reprinted with permission from ref. [121]	28
Figure 3.1. Photograph of as-prepared citrate capped AuNP solution.	30
Figure 4.1. Schematic representation of the proposed Hg ²⁺ sensing mechanism of the colorimetric assay	37

Figure 4.2. Colorimetric response of the assay. (a) Photographs of AuNP solutions showing the color change occurs only in the presence of lysine (0.4 mM) and Hg ²⁺ (10 μM). (b) Extinction spectra of the AuNP solutions.	38
Figure 4.3. TEM images of AuNP solutions. (a) Bare AuNPs, (b) in the presence of lysine, (c) in the presence of Hg ²⁺ ions, and (d) in the presence of both lysine and Hg ²⁺ ions. AuNPs aggregated when both lysine and Hg ²⁺ were added.	39
Figure 4.4. Effect of amino acids on colorimetric response of the assay. Extinction spectra of the colorimetric assay tested with 14 different amino acids: (a) in the presence and (b) in the absence of 10 μM Hg ²⁺ . (c) Extinction intensity ratios (EX ₇₂₅ /EX ₅₂₅) of the colorimetric assay for 14 different amino acids in the presence or absence of 10 μM Hg ²⁺ ions. (Lys: lysine, Cys: cysteine, His: histidine, Tyr: tyrosine, Asp: aspartic acid, Arg: arginine, Ala: alanine, Gly: glycine, Phe: phenylalanine, Trp: tryptophan, Met: methionine, Leu: leucine, Ile: isoleucine).....	41
Figure 4.5. Effect of lysine concentration on the response (EX ₇₂₅ /EX ₅₂₅) of the colorimetric assay (Hg ²⁺ concentration is 10 μM in all measurements).	42
Figure 4.6. Change of the colorimetric array response with time.	43
Figure 4.7. Colorimetric sensing of Hg ²⁺ . (a) Photographs of AuNP solutions with different Hg ²⁺ concentrations. (b) Extinction spectra of the solutions. (c) Response (EX ₇₂₅ /EX ₅₂₅) of the colorimetric assay against increasing Hg ²⁺ concentrations. Inset shows the response linearity of the assay at low Hg ²⁺ concentrations (Lysine concentration is 0.4 mM in all measurements)	44
Figure 4.8. Linearity of the array response against Hg ²⁺ in distilled water.	45
Figure 4.9. Selectivity of the sensor. (a) Photographs showing the AuNP solutions in the presence of lysine (0.4 mM) and several competing metal ions (50 μM) or Hg ²⁺ (1 μM). (b) Response (EX ₇₂₅ /EX ₅₂₅) of the colorimetric assay against several competing metal ions (50 μM) or mixture of competing metal ions (Cu ²⁺ , Ni ²⁺ , Pb ²⁺ , Co ²⁺ , Zn ²⁺ , Ca ²⁺ , Al ³⁺ , K ⁺ , Fe ³⁺ , Cd ²⁺ , Ag ⁺ , Na ⁺) (10 μM) and Hg ²⁺ (1 μM) in the presence (0.4 mM) or absence of lysine.	48
Figure 4.10. Colorimetric sensing of Hg ²⁺ in tap water. (a) Photographs of AuNP solutions in tap water with different Hg ²⁺ concentrations. (b) Colorimetric response of the assay against Hg ²⁺ containing tap water samples at different concentrations (Lysine concentration is 0.4 mM in all measurements).....	50
Figure 4.11. Linearity of the assay response against Hg ²⁺ in tap water.	51

Figure 4.12. Raman Spectra of glass substrate and MUA capped AuNPs and amino acid treated AuNPs which were dried on glass substrates.53

Figure 4.13. Schematic Representation of Proposed Metal Ions, Amino Acids, and AuNP Interactions: (a) No interaction, (b) Metal Ions Induce the Aggregation of AuNPs, (c) Amino Acids Interact with Metal Ions and Prevent Aggregation of AuNPs; and (d) Metal Ions and Amino Acids Co-Contribute the Aggregation of AuNPs57

Figure 4.14. Structure of MUA capped AuNPs and some possible interaction between metal ions and amino acid or MUA molecules.58

Figure 4.15. Effect of metal ion concentration (0-50 μM) on the response ($\text{Ex}_{625}/\text{Ex}_{525}$) of the colorimetric sensor array. (a) Hg^{2+} , (b) Cd^{2+} , (c) Fe^{3+} , (d) Pb^{2+} , (e) Al^{3+} , (f) Cu^{2+} , and (g) Cr^{3+} 60

Figure 4.16. Representative UV-Vis spectra for AuNPs in the presence or absence of metal ions and amino acids.61

Figure 4.17. TEM images of well-dispersed as prepared MUA capped AuNPs (a) and aggregated AuNPs in the presence of 20 μM of Cd^{2+} and 200 μM of lysine. .61

Figure 4.18. Colorimetric response ($\text{Ex}_{625}/\text{Ex}_{525}$) of AuNPs depending on amino acid concentrations in the absence of metal ions.62

Figure 4.19. Time dependent colorimetric response ($\text{Ex}_{625}/\text{Ex}_{525}$) of AuNPs in the presence of amino acids at their concentrations used in the assay.63

Figure 4.20. Effect of salinity on the stability of MUA capped AuNPs.64

Figure 4.21. (a) Representative photograph of the colorimetric sensor array response against 20 μM of metal ions. (b) Blue-scale representation of the colorimetric sensor array response. White corresponds to no aggregation and blue corresponds to aggregation of AuNPs.65

Figure 4.22. Representative photograph of the colorimetric sensor array response against (a) 20 μM of 9 nonresponsive metal ions with the assay (b) mixture of all metal ions.66

Figure 4.23. Hierarchical cluster analysis of colorimetric sensor array of seven different metal ions at different metal ion concentrations: (a) at 2 μM , (b) at 10 μM , (c) at 20 μM , and (d) at 50 μM67

Figure 4.24. (a) Dendrogram showing the discrimination between all the tested metal ions at different concentrations. (b) Table listing the names and concentrations of analytes in (a).68

Figure 4.25. Colorimetric response of the colorimetric array against Hg^{2+} , Cd^{2+} and Fe^{3+} ions (20 M) and their binary and ternary mixtures. (a) Representative photograph and (b) Hierarchical cluster analysis.....69

SYMBOLS AND ABBREVIATIONS

Symbols

Ex Extinction value

Abbreviations

EPA	U. S. Environmental Protection Agency
ICP-MS	Inductively Coupled Plasma Mass Spectrometry
AAS	Atomic Absorption Spectrometry
HPLC	High Performance Liquid Chromatography
XRF	X-Ray Fluorescence Spectroscopy
UV-Vis	Ultraviolet–Visible Spectroscopy
SEM	Scanning Electron Microscope
TEM	Transmission Electron Microscope
SPR	Surface Plasmon Resonance
AuNPs	Gold Nanoparticles
MUA	11-Mercaptoundecanoic Acid
PBS	Phosphate Buffered Saline
LOD	Limit of Detection
HCA	Hierarchical Cluster Analysis

1. INTRODUCTION

Contamination of water by toxic metal ions (e.g., mercury, silver, and lead) can cause serious environmental and health problems because of their acute and/or chronic toxicity to biological organisms [1,2]. For instance, mercury -most common and stable form of mercury in water is the solvated divalent mercuric ion (Hg^{2+})- which is widely released to the environment by industrial activities (e.g., gold mining and combustion of fossil fuels and wastes), shows great toxicity mainly on renal and nervous systems through the disruption of enzyme activity [3,4]. Lead ions (Pb^{2+}), on the other hand, released to the environment by many end-user products such as dyes, gasoline and batteries and it can cause neurological, cardiovascular and developmental disorders in especially children [5]. Similarly, another highly toxic metal ion; cadmium (Cd^{2+}) may be found in many end user products such as plastics, batteries, cigarettes and dyes [5]. In addition, many other metal ions such as aluminum, copper, zinc and silver have proved acute and chronic toxicity against biological organisms.

Therefore, monitoring of toxic metal ion levels in water (drinking, sea, lake, etc.) is very important in terms of waste management, environmental analysis, toxicology, water safety, and water quality [6]. Common methods for the detection of metal ions are based on chromatographic and spectroscopic techniques such as inductively coupled plasma mass spectrometry (ICP-MS), atomic absorption spectrometry (AAS), high performance liquid chromatography (HPLC) and X-ray fluorescence spectroscopy (XRF) [7-9]. Although, these methods are highly sensitive they require intense technical training because of their complicated procedures, and they are expensive and time-consuming. Also, many electrochemical and membrane based methods are available for detection of aqueous metal ions. However, these methods are generally insufficient in terms of sensitivity for real-world applications. Therefore, low cost, simple, rapid, and portable methods for metal ion detection are still highly desired.

In this context, colorimetric methods (based on dyes or surface modified metal nanoparticles) are very promising due to their simplicity, cost effectiveness, and rapid detection times. The colorimetric response of these sensors can be easily monitored with the naked eye or by using a UV-Vis spectrophotometer, without needing any complicated instruments [10,11]. In particular, colorimetric sensors of

metal (mostly gold and silver) nanoparticles attracted a great deal of interest due to their size- and shape-dependent optical properties and large absorption coefficients [12,13].

Recently, metal nanoparticle-based colorimetric assays for toxic metal ion detection have been emerged as a simple and low-cost alternative of above mentioned based methods [13-20]. These assays are based on controlled aggregation of surface modified (with aptamers, peptides, proteins, small organic molecules etc.) metal nanoparticles in the presence of metal ions [18,21-32]. Aggregation of metal nanoparticles in the presence of analyte ions changes the color of nanoparticles solution. Therefore, rapid and sensitive detection of metal ions without the need of any equipment (i.e., naked eye observation of color changes) or using a simple UV-Vis absorption spectrophotometer can be achieved.

In this thesis, we focused on preparation of novel gold nanoparticle (AuNP) based colorimetric sensors for toxic metal ion detection. This thesis cover two main research projects; 1) ultrasensitive colorimetric sensing of Hg^{2+} using citrate-capped AuNPs and lysine and 2) development of a colorimetric sensor array for detection of multiple metal ions based on AuNPs and amino acids.

In the first part, we reported a simple yet very sensitive colorimetric assay for rapid detection of Hg^{2+} in water. The colorimetric assay is based on the aggregation of as-prepared citrate-capped AuNPs in the presence of Hg^{2+} ions and the positively charged amino acid, lysine. The detection limit of this inexpensive colorimetric assay is 2.9 nM, which is below the limit value (10 nM) defined by the U.S. Environmental Protection Agency (EPA) in drinkable water. Also, the colorimetric response of citrate-capped AuNPs in the presence of lysine is very selective to the Hg^{2+} . In addition, the colorimetric assay is very fast, and all analyses can be completed within a few minutes.

In the second part, we reported a facile colorimetric sensor array for detection of multiple toxic heavy metal ions (Hg^{2+} , Cd^{2+} , Fe^{3+} , Pb^{2+} , Al^{3+} , Cu^{2+} , and Cr^{3+}) in water is demonstrated using 11-mercaptoundecanoic acid (MUA)-capped AuNPs and five amino acids (lysine, cysteine, histidine, tyrosine, and arginine). The presence of amino acids (which have functional groups that can form complexes with metal ions and MUA) regulates the aggregation of MUA-capped particles; it

can either enhance or diminish the particle aggregation. The combinatorial colorimetric response of all channels of the sensor array (i.e., color change in each of AuNP and amino acid couples) enables naked-eye discrimination of all of the metal ions tested in this study with excellent selectivity.

2. GENERAL INFORMATION

2.1. Toxicity of Metal Ions

Safe and adequate water for drinking and as well as for other vital activities (e. g. agricultural activities) available to all is needed to sustain life. Also, quality of water is very important in terms of improving the public health. There are three major aspects to determine the quality of drinking water, which are microbial, chemical and radiological aspects. Microbial contaminants in water such as pathogenic bacteria, viruses and helminths have acute effects and they can cause serious infections and diseases. Chemical contaminants such as organic compounds and heavy metal ions, on the other hand, have generally chronic effects and may cause diseases such as cancer and Alzheimer's disease. Also, radiological contaminants such as radioactive compounds may cause both serious acute and chronic diseases including cancer. Therefore, to provide safe drinking water to humans, fast and reliable analysis of drinking water is very important to determine the risk factors and decide appropriate treatment methods [33]. In this thesis, we will discuss the colorimetric sensing of toxic metal ions (Hg^{2+} , Pb^{2+} , Cd^{2+} etc.) in drinking water. Therefore, below we briefly discuss their health effects and current methods for their detection in aqueous media.

Metal ions are widely released to the environment by industrial activities such as mining, combustion of fossil fuels and industrial wastes. Lead, mercury and cadmium are the most toxic three among the toxic metal ions and their use in electronic equipment prohibited by the European Union [5]. Other than these three, many metal ions including copper, zinc, aluminum and silver have proved toxicity to humans. Even very low levels exposure to these metal ions may cause serious health problems. For example, lead may cause neurological, cardiovascular and developmental disorders in especially children [5]. Similarly, cadmium has many serious effects on human health; chronic exposure to cadmium may cause cancer, cardiovascular diseases and renal failure [5]. Mercury accumulation in the body, on the other hand, can mainly cause diseases related with the nervous system such as motor disorders and Minamata disease [1,34]. Another toxic metal ion copper can cause anemia, gastrointestinal distress, and liver and kidney damage [35]. Also, recent studies demonstrated the effects of long-term exposure of

several metal ions including aluminum, iron, copper and zinc, on neurological diseases such as Alzheimer's and Parkinson's diseases [36,37].

The most common methods developed for detection of metal ions in water are based on chromatographic and spectroscopic techniques such as ICP-MS, AAS, HPLC and XRF. These methods offer very sensitive and reliable measurement of several metal ions. For example, Karunasagar et al. reported the aqueous Hg^{2+} detection with a detection limit of 1 ng/L by cold vapor introduction into an ICP-MS system in plasma [38]. Maciel et al. demonstrated the detection of Cd^{2+} ions with a detection limit of 80 ng/L by using AAS [39]. Although, these methods have good sensitivity they often have complicated and expensive procedures.

Electrochemical methods such as anodic stripping voltammetry, stripping chronopotentiometry and competitive ligand equilibration-adsorptive cathodic stripping voltammetry have been also extensively applied for metal ion detection in aqueous media [40]. These methods are very selective due to the specificity of the potential chosen for an electrochemical reaction, $\text{M}^{n+}_{\text{aq}} + n\text{e}^- = \text{M}^0$ [41]. However, electrochemical methods need relatively long time (around 20 min) to provide adequate sensitivity. In addition, many other methods have been also applied for detection of metal ions such as ion exchange and complexing resins techniques, diffusive gradients in thin-film gels, permeation liquid membrane technique and Donnan membrane technique. More information about these methods can be found in previous excellent reviews [40,41].

Recently, metal nanoparticle (mostly gold or silver) based colorimetric assays for toxic metal ion detection have been emerged as a simple and low-cost alternative of above mentioned methods [13-20]. These assays are based on controlled aggregation of surface modified (with aptamers, peptides etc.) metal nanoparticles in the presence of metal ions. Aggregation of metal nanoparticles in the presence of analyte ions changes the color of nanoparticles solution. Therefore, rapid and sensitive detection of metal ions without the need of any equipment (i.e., naked eye observation of color changes) or using a simple UV-Vis absorption spectrophotometer can be achieved. In the Section 2.7, gold nanoparticle based colorimetric metal ion sensors will be discussed in detail.

2.2. Gold Nanoparticles

Gold nanoparticles (AuNPs) can be synthesized in different size and shape (spheres, rods, shells, plates etc.) and their surface chemical modification is easy and well established. More importantly, they have size and shape dependent optoelectronic properties which make them a strong candidate for optical detection applications [13]. Below, we will discuss the common AuNP synthesis methods, their surface modifications and their optical properties.

2.3. Synthesis of Gold Nanoparticles

2.3.1. Citrate Based and Related Methods

In 1857, Micheal Faraday synthesized colloidal gold hydrosols by reduction of chloroaurate solution with phosphorus dissolved in carbon disulfide [42]. This work can be accepted as first demonstration of colloidal gold synthesis. Almost a century later, in 1951, Turkevich developed an easy method to synthesize AuNPs in water in which the HAuCl_4 (chloroauric acid) salt is reduced to Au using sodium citrate [43]. This approach became most widely used method for obtaining AuNPs. In this method, preheated sodium citrate solution was added to boiling water containing HAuCl_4 salt to reduce the Au^{3+} ions to metallic Au^0 . In this reaction, citrate also stabilizes the formed AuNPs by covering their surfaces. Later, Frens extend the method to control size of AuNPs (in the range of 16 to 150 nm) by changing of sodium citrate amount in the solution (Figure 2.1) [44].

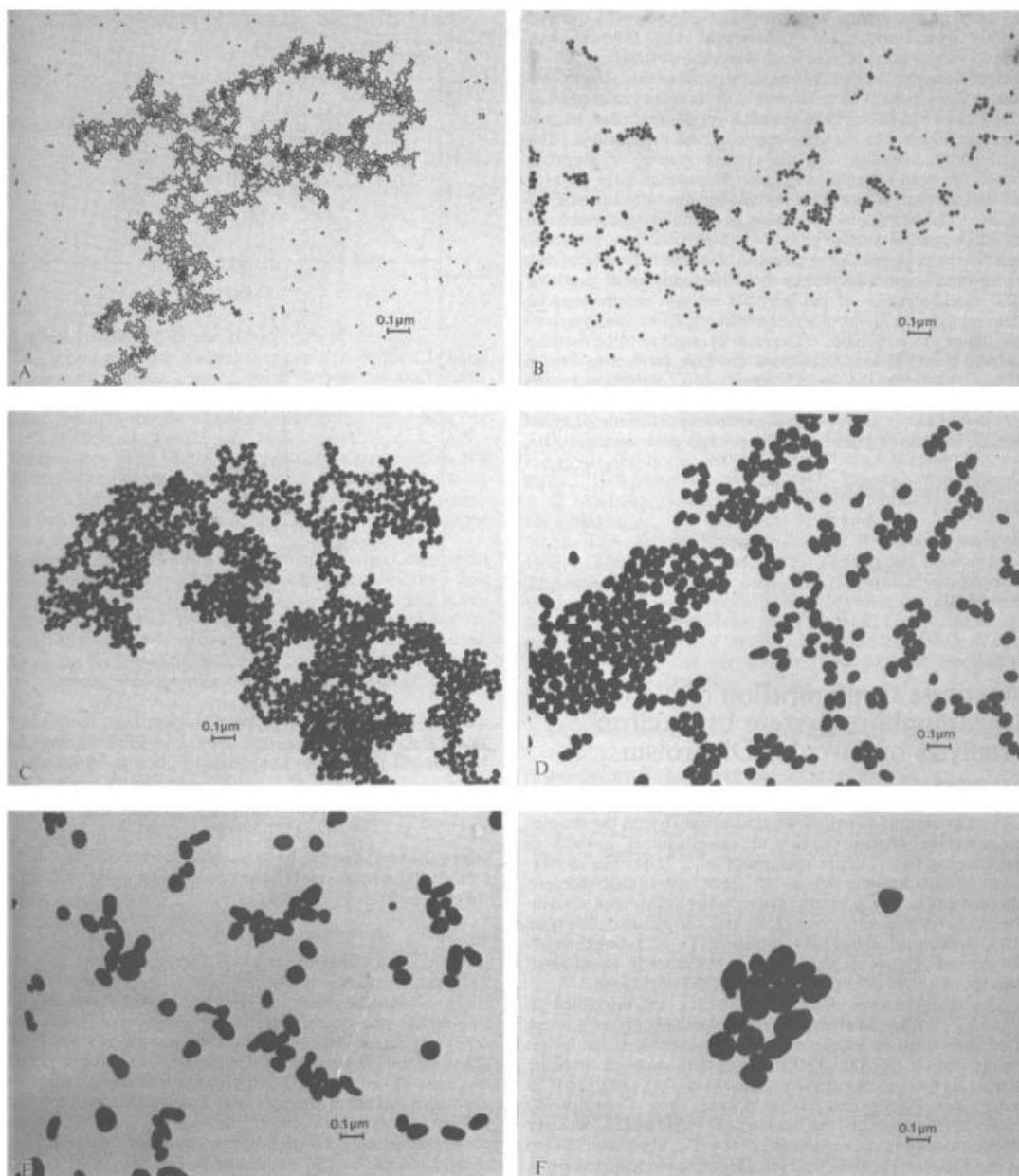


Figure 2.1. TEM images of citrate capped AuNPs prepared using different amounts of sodium citrate. Decreasing the sodium citrate amount increases the particle size (A-F). Reprinted with permission from ref. [44].

2.3.2. The Brust-Schiffrin Method

In 1994, Brust and Schiffrin used strong thiol-gold interaction to stabilize ultra-small AuNPs (Figure 2.2). In this method, AuNPs were synthesized in organic phase [45]. Thanks to the surfactant of tetraoctylammonium bromide (TOAB) AuCl_4^- got into toluene from aqueous phase. Gold ions reduced by sodium borohydride (NaBH_4) in presence of dodecanethiol. After that a color change can be seen from orange to brown. The method enables the control of AuNPs diameter

in the range of 1.5 to 5 nm with changing of reaction conditions (gold/thiol ratio, reduction rate and temperature). Obtained AuNPs were very stable because of the strong thiol-gold interaction. Later, other reducing agents such as superhydride [46] and glutathione [47] was also used instead of NaBH₄.

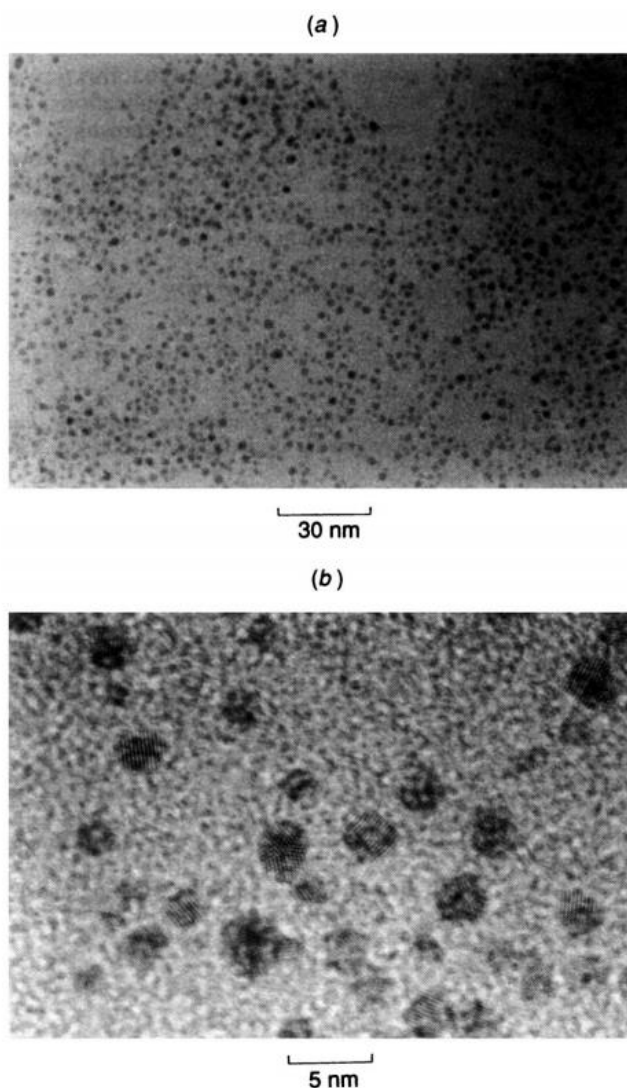


Figure 2.2. (a) Low magnification and (b) high magnification TEM images of the small AuNPs prepared according to the Brust-Schiffrin method. Reprinted with permission from ref. [45].

2.3.3. The Seed-Mediated Methods

As the particle size becomes bigger particles become polydisperse in the single-step citrate based methods. More importantly, shape control is very limited in the single-step methods. To address these limitations seed-mediated methods, in

which AuNPs were prepared step by step using generally citrate stabilized small AuNPs, have been developed. This method enables preparation of variety of AuNPs with various size and shapes. The seed growth includes in general two steps. In the first step, small AuNP seeds are prepared and added in a 'growth' solution. The growth solution also contains HAuCl_4 , stabilizing and reducing agents. Thus, large AuNPs can be formed growing reduced Au^0 on the seed surface. Amount and nature of the reducing agent, stabilizer and their ratio to Au precursor provide to control size, shape and surface properties in the seed-growth synthesis [48].

Murphy's group reported a procedure to synthesize gold nanorods (AuNRs) using the seed mediated growth method where ascorbic acid reduces HAuCl_4 to HAuCl_2 in the presence of cetyl triammonium bromide (CTAB) and AgNO_3 after that citrate-capped spherical AuNPs are mixed with HAuCl_2 solution [49]. In this approach, ascorbic acid reduces Au^+ to Au^0 over AuNP seeds and CTAB surfactant directs the structure. High aspect ratio (length/width) AuNRs with the ratios of up to 25 can be prepared using a three-step procedure [50-53]. Interestingly, addition of nitric acid to the third seeding growth solution improves the yield and monodispersity [54]. Later, El-Sayed's group improved the yield and polydispersity of the AuNRs by replacing the citrate stabilizer of seeds with a stronger stabilizer of CTAB [55]. Similarly, they used AgNO_3 to control the aspect ratio of the AuNRs. By controlling the reaction parameters they obtained AuNRs with high yields of up to 99% and aspect ratios between 1.5 and 4.5 (Figure 2.3).

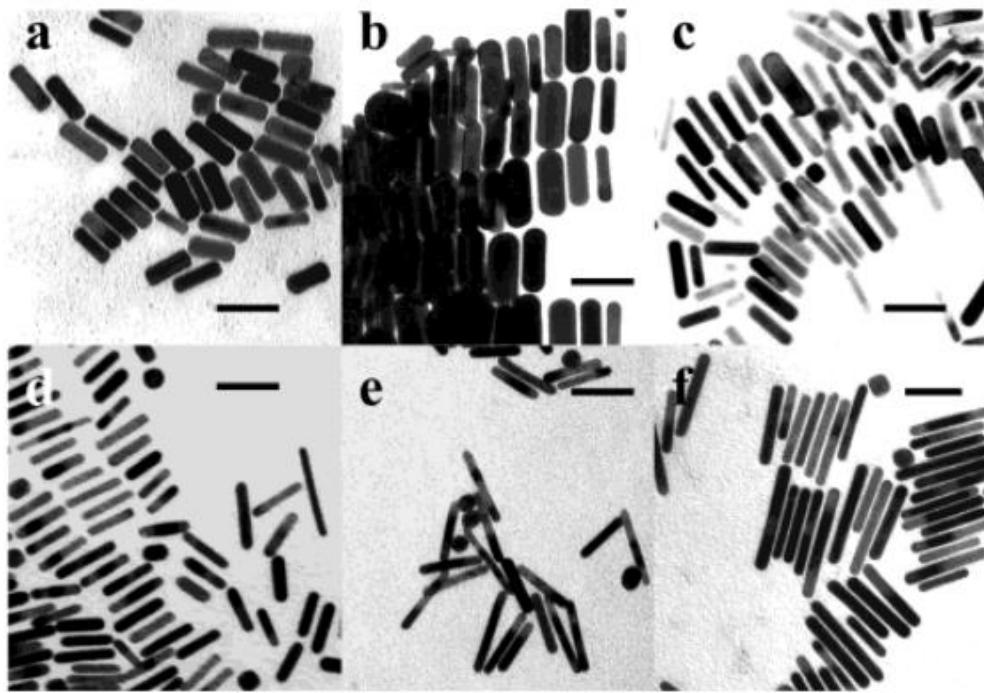


Figure 2.3. TEM images of AuNRs with different aspect ratios. Reprinted with permission from ref. [55].

2.3.4. Photochemical Method

Another method to synthesize anisotropic AuNPs is the photochemistry. UV light can reduce the HAuCl_4 and in the presence of rod shaped cationic micelles to form AuNRs [56,57]. A specific crystal face is stabilized by the micelle surfactant as in the seed-growth procedure. Increase in the aspect ratio of the AuNRs was observed for this method in the presence of NaCl [57] and also Ag^+ ions [58] similar to the seed-growth process.

Additives such poly(vinylpyrrolidone) (PVP) and ethylene glycol [59] or TiO_2 colloids [60-62] can be also used in the photochemical approach to either stabilize or control the shape of the particles. For instance, Zhang's group used TiO_2 nanoparticles to prepare star-shaped platelet-like asymmetric AuNPs (Figure 2.4) [62]. Also, Au nanodots were assembled on graphene oxide using the photochemical approach in the presence of graphene oxide [63]. Although photochemical methods eliminate the need of reductants they normally have long reaction times, approximately 30 h, compared to the chemical methods [58,64]. Nevertheless, the photo-reduction time can be reduced to approximately 30 min if ascorbic acid is used as a pre-reductant [65-67].

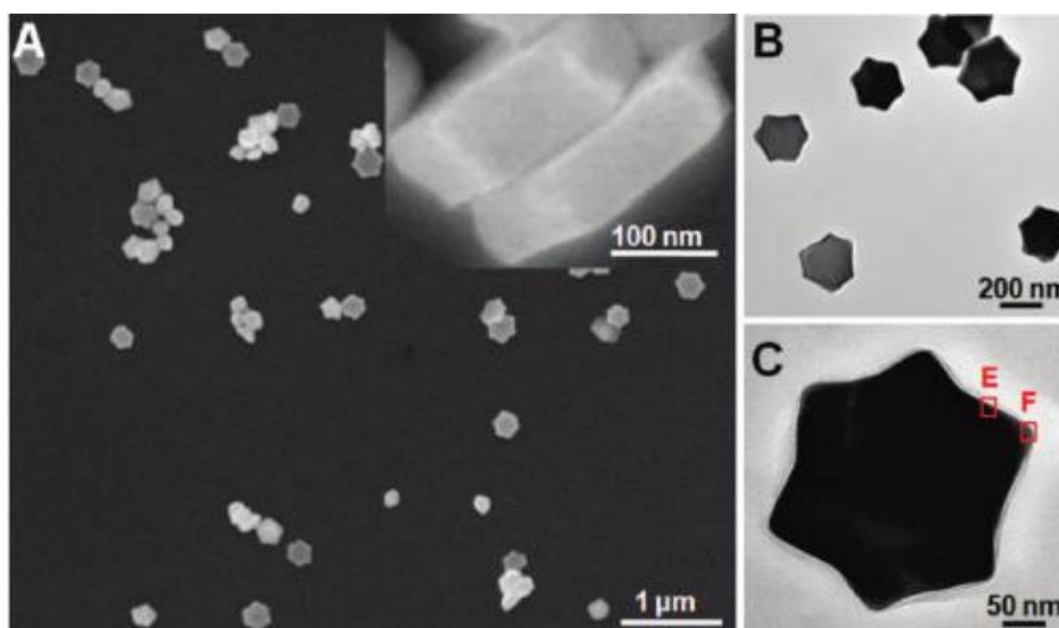


Figure 2.4. (a) SEM, (b) and (c) TEM images of star-shaped platelet-like asymmetric AuNPs. Inset in (a) shows the cross section of the plates. Adopted with permission from ref. [62].

2.3.5. Electrochemical Method

Wang's group immersed an Au plate anode and a Pt plate cathode in an electrolyte containing CTAB and tetradodecylammonium bromide (TOAB) as a co-surfactant. Electrolytic oxidation of the Au anode then formed AuBr_4^- bound to the CTAB micelle, which then underwent migration to the cathode and cathodic reduction to Au^0 . Ag^+ cations produced by the redox reaction between Au^{3+} and an Ag plate controlled the ratio of formed AuNRs. Then ultrasonication process separates the AuNRs from the cathode [68,69]. AuNRs are produced in this method have aspect ratios of between 2 and 7 (Figure 2.5). Also these AuNRs are single crystals without stacking faults, twins, or dislocations.

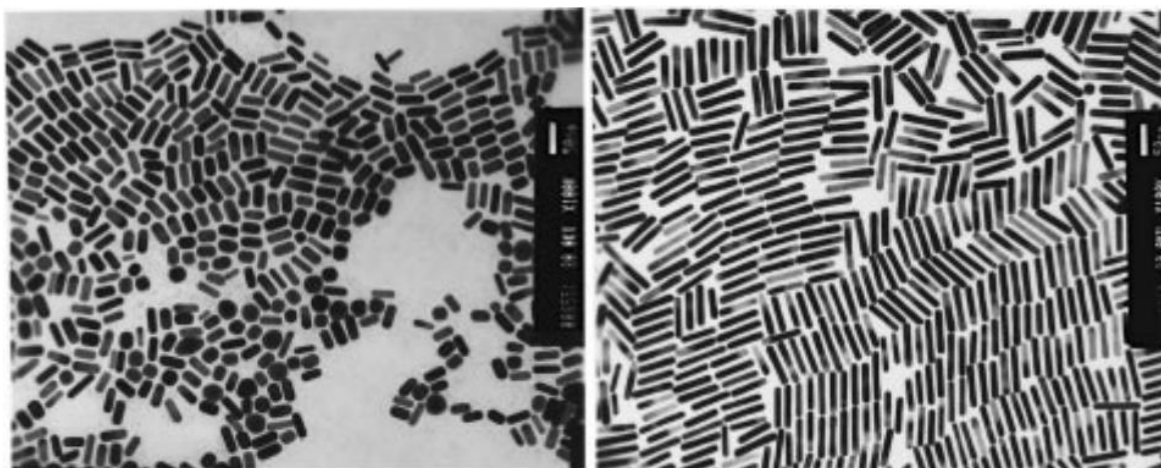


Figure 2.5. TEM images of (a) short and (b) long AuNRs prepared using the electrochemical method. Adopted with permission from ref. [69].

2.3.6. Sonochemical Method

Using the ultrasound approach very small AuNPs can be synthesized thanks to the extreme local temperature and pressure conditions formed due the acoustic cavitation. AuNPs prepared using this method; however, have broad size and shape distribution [48]. To overcome this problem surfactants and alcohols can be added to the synthesis solution [70,71]. One interesting example of this approach is the single-crystalline flexible Au nanobelts with a width of 30-50 nm and a length of several micrometers synthesized by Han's group [72] (Figure 2.6).

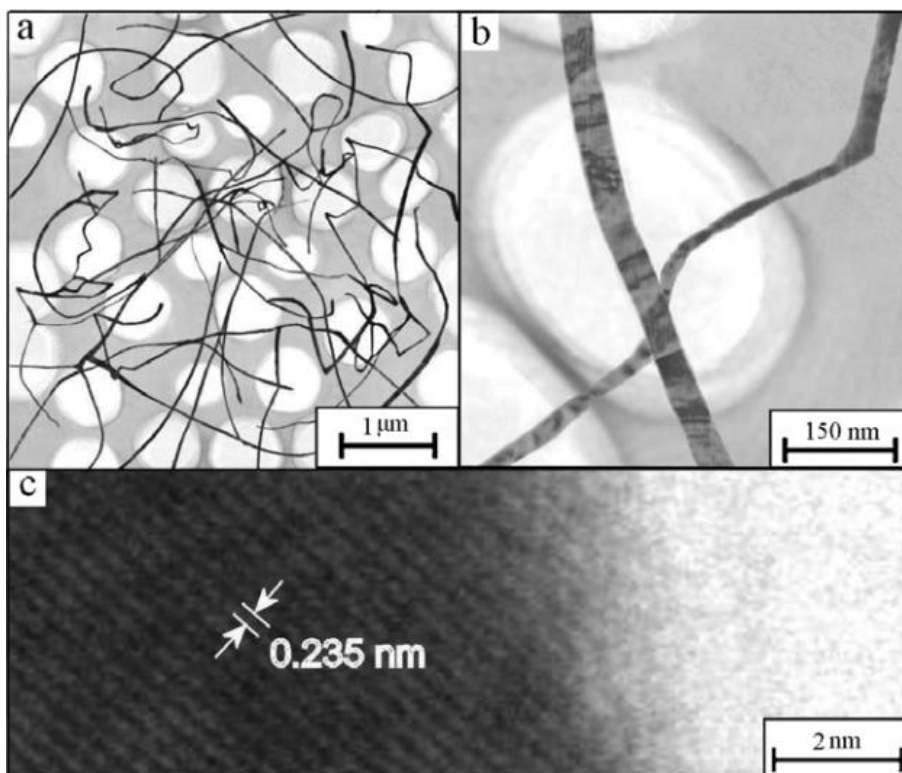


Figure 2.6. TEM images of Au nanobelts at different magnifications. Adopted with permission from ref.[72].

2.3.7. Templates Based Methods

Another approach to prepare nonspherical AuNPs is the template based methods where gold salts first reduced into the proper templates and after removal of the template AuNPs are obtained. In this method shape and size of the resulting AuNPs are determined by the template properties such as pore shape and length [73]. Variety of templates have been employed up to date such as porous silica [74] or silicon membranes [75], block copolymers [76], nanoparticles [77], carbon nanotubes [78], surfactants micelles [51,52,68,79], viruses, [80], and DNA [81].

Also, some groups report the use of template based methods in combination with other methods such as photochemical, electrochemical, and sonochemical methods. For example, Lee et al. prepared gold nanotubes by electrochemically reducing of gold salts into the pores of anodized aluminum oxide (AAO) templates [82]. The nanotubes have very narrow size distribution and high aspect ratio thanks to the well-organized pores of AAO templates (Figure 2.7).

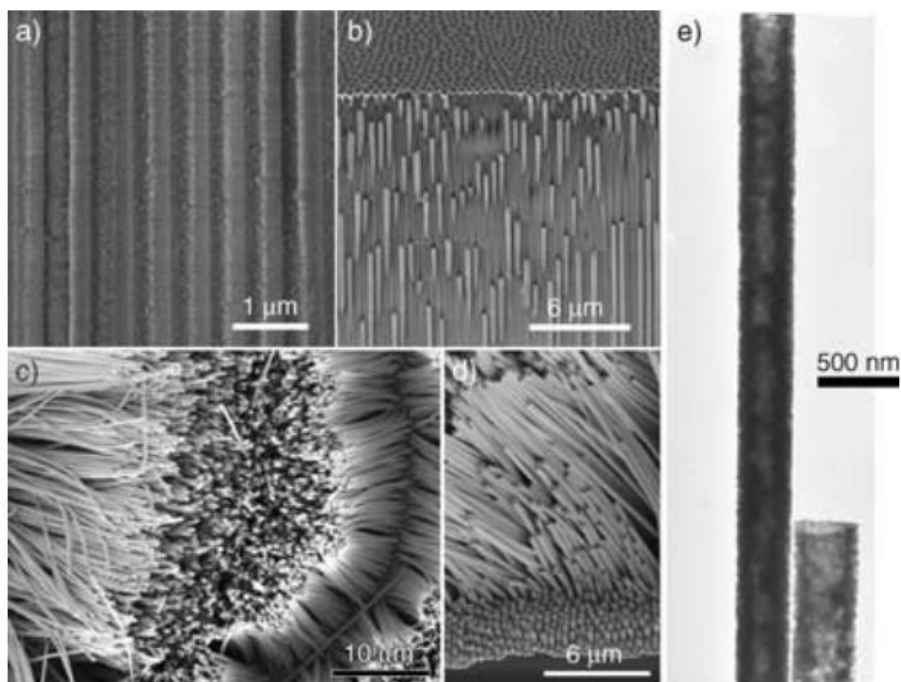


Figure 2.7. (a) Cross-sectional SEM image of the AAO template. (b) SEM image of the Au deposited AAO template. (c, d) SEM images of Au nanotubes after template removal. (e) TEM image of the Au nanotubes. Reprinted with permission from ref. [82].

One of the most popular applications of template based methods is the preparation gold shells using silica micro/nano particles as templates. In this approach Au ions reduced around the positively charged silica cores. Halas and co-workers demonstrated the can control of size and shell thickness of the gold layers by tuning the reaction time and the concentration of the plating solution [83]. Later, same group demonstrated preparation rice-shaped gold nanoshells using iron-oxide particles as templates (Figure 2.8) [84].

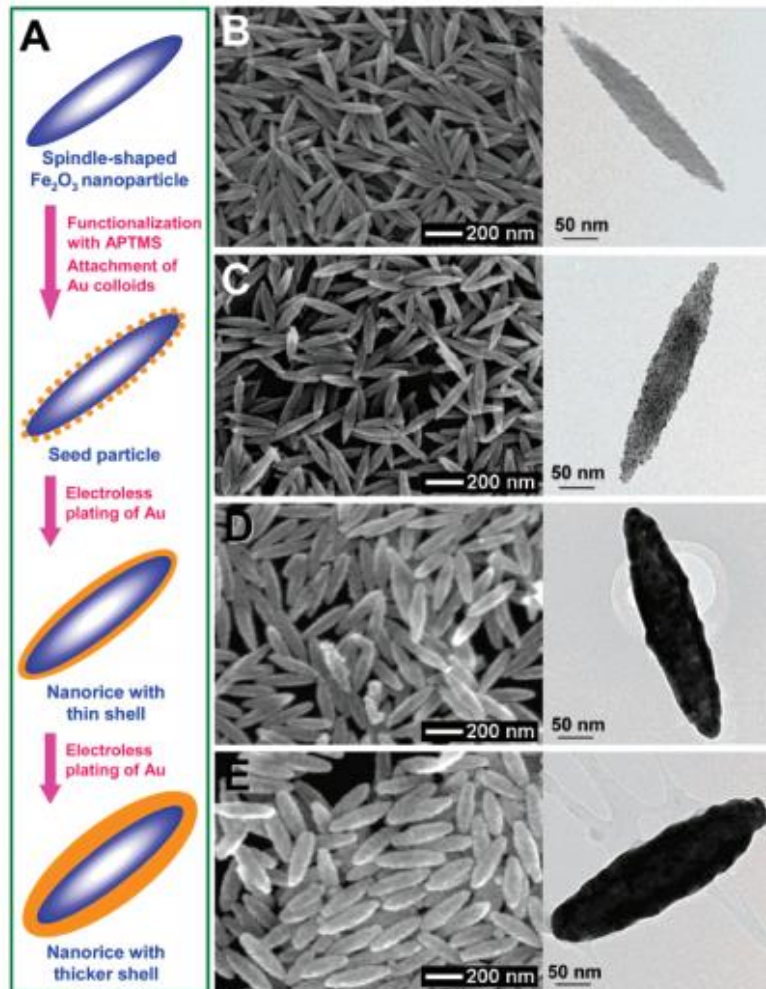


Figure 2.8. (a) Schematic representation of synthesis steps of iron oxide templated rice-shaped gold nanoshell fabrication. (b-e) SEM (left panel) and TEM (right panel) images of the particles at every step of synthesis. Reprinted with permission from ref. [84].

2.3.8. Galvanic Replacement Method

The galvanic replacement approach is based on the spontaneous reduction of gold ions by another metal. Redox potential differences between the reducing metal and the Au^{3+}/Au system make the reaction favorable. Using the galvanic replacement, Xia and coworkers reported the preparation of gold nanostructures with hollow interiors. They used silver nanostructures as sacrificial templates (Figure 2.9) [85-88]. The method is based on the oxidation of Ag to templates to AgCl using AuCl_4^- salt. Since AgCl is soluble at elevated temperatures at the end of the reaction all Ag dissolved and hollow particles are obtained [85].

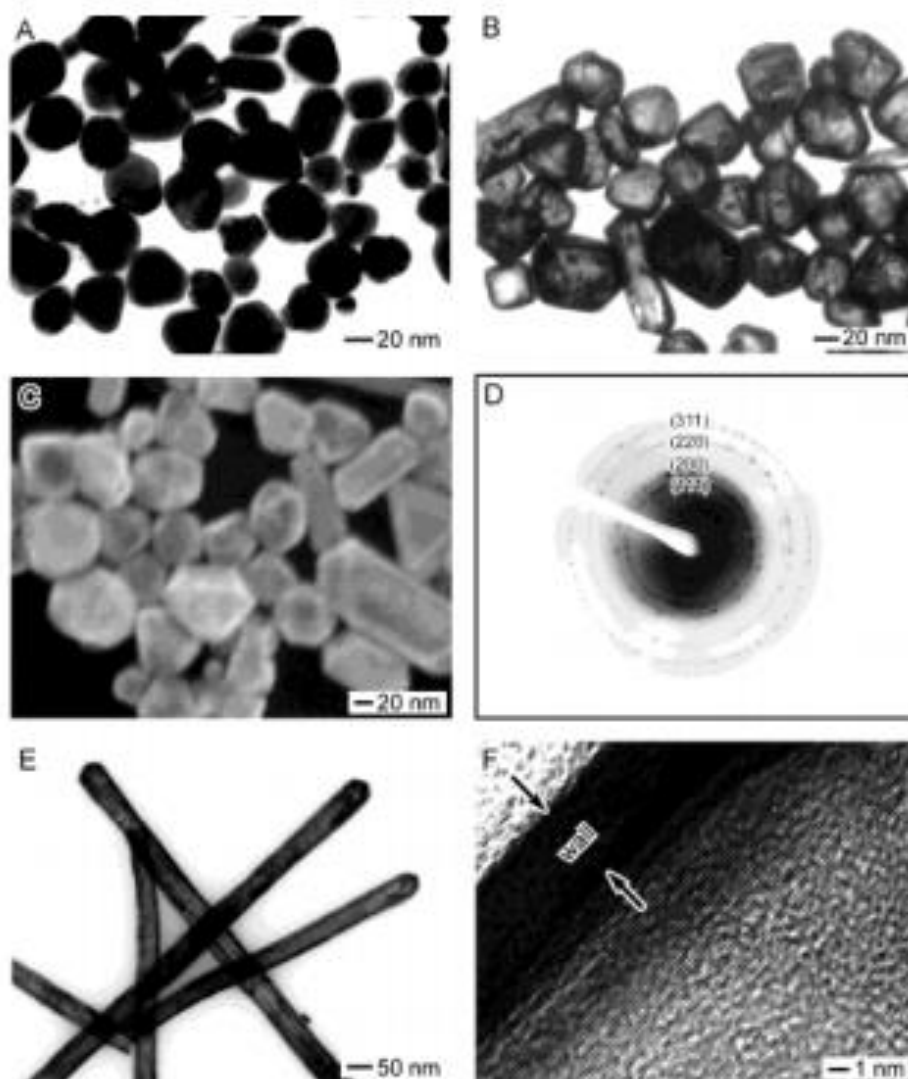


Figure 2.9. (a) TEM image of Ag nanoparticle templates. (b and c) TEM and SEM images of hollow AuNPs, respectively. (d) Electron reflection pattern of the hollow AuNPs. (e and f) TEM images of hollow Au nanotubes. Reprinted with permission from ref. [86].

2.4. Surface Modification of Gold Nanoparticles

Surface of as prepared AuNPs is covered with surface stabilizing agents which protect them from aggregation. The AuNPs prepared using the Turkevich method is covered with citrate ions which is both stabilizer and reductant in the reaction [43]. The AuNPs prepared using Brust-Schiffrin method, on the other hand, contains alkylthiols such as dodecanethiol, on their surfaces [45]. Surface of anisotropic AuNPs (nanorods, plates etc.) generally covered with surfactant molecules such as CTAB. In the recent years, alternative synthesis methods have been also reported. One interesting approach is the use of amino acids as both

reducing and stabilization agent in the AuNP synthesis, which yields amino acid functionalized AuNPs [89,90].

For biological and chemical applications, these ligands were generally replaced with proper ligands in order to improve colloidal stability of the particles and make the particles water soluble, biocompatible and/or specific to a chemical or biological molecule. For example, the AuNPs prepared using Brust-Schiffrin method are water insoluble and for many applications ligand exchange with water-soluble thiolated ligands is needed. Due to strong interaction between gold surface and thiol groups the particles can be easily transferred in water phase. Also, surfactant molecules were exchanged with thiolated polyethylene glycol (PEG) polymers prior to the use in biological applications due to the high toxicity of surfactant molecules. Further surface modification over PEG layers to give AuNPs other functionalities, such as targeting or fluorescence property, can be also done (Figure 2.10). Other than PEG, many other polymers such as poly(vinyl alcohol), chitosan, poly(N-vinylpyrrolidone) and poly(methyl methacrylate) were also used to improve the stability of AuNPs [91-94]. For chemical sensing applications, AuNP surfaces was modified with various small organic molecules or biological molecules (e. g. aptamers and peptides) which will be discussed below in more detail.

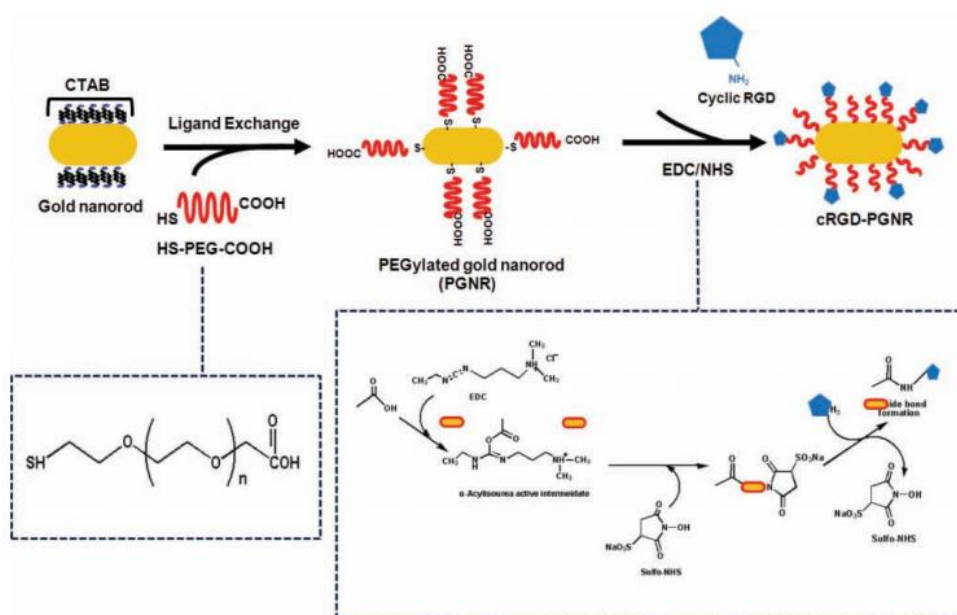


Figure 2.10. Schematic representation of PEG and peptide modification of AuNRs. Reprinted with permission from ref. [95]

2.5. Optical Properties of Gold Nanoparticles

AuNPs have shape and size dependent unique light absorption properties which make them promising for various applications including colorimetric sensors, disease diagnosis and therapy and solar cells. Figure 2.11 shows the absorption bands of the AuNPs with different shapes. The light absorption of nanosized Au is due to the coherent oscillation of the conduction band electrons induced by the interacting with the electromagnetic field. This is only observed in nanosized Au and it is absent either then the particle size roughly below a few nanometers (individual atoms or small clusters) or above a few hundreds of nanometers (bulk form). This special light absorption property of nanosized metal particles is generally known as surface plasmon resonance (SPR) effect [96].

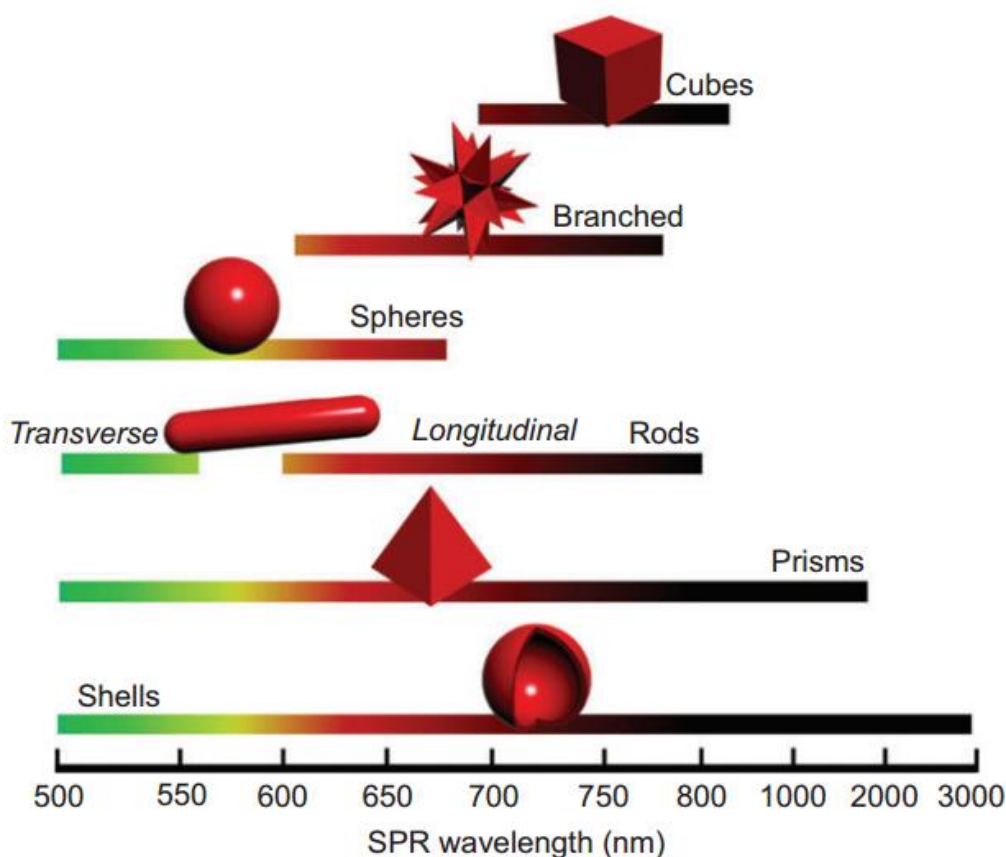


Figure 2.11. Major SPR bands of AuNPs with different shapes. Reprinted with permission from ref. [97].

As the particle size increases, the SPR absorption peak red shifted to longer wavelength (Figure 2.12a). In addition to the size and shape, other parameters like dielectric property of the medium, aggregation state, surface modification, and refractive index of surrounding medium may also affect the SPR frequency of AuNPs [98]. For example, aggregation of AuNPs results in a red shift in the SPR absorption peak of the particles (Figure 2.12b).

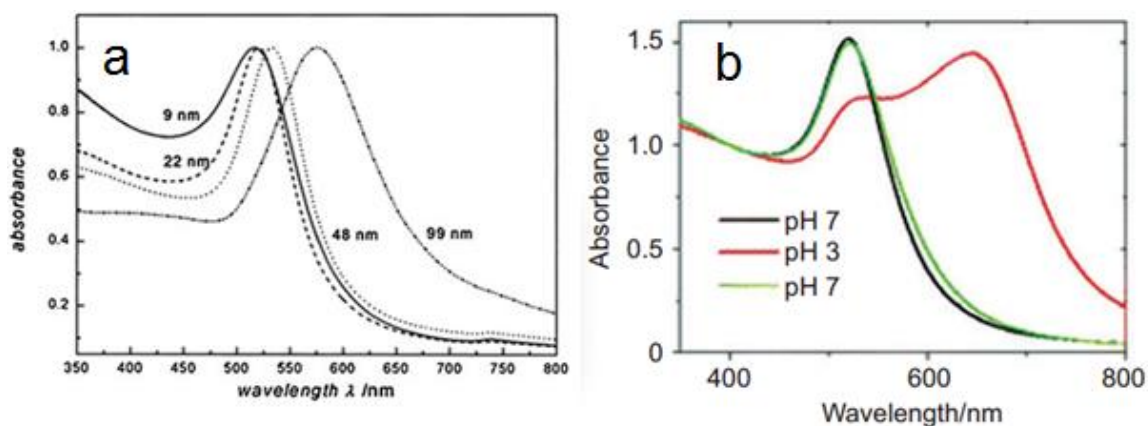


Figure 2.12. (a) Absorption spectra of AuNPs (spherical) with different sizes. (b) pH-induced reversible aggregation of surface functionalized AuNPs. Aggregation of AuNPs results in a red shift in the absorption spectrum. Reprinted with permission from refs. [99,100].

2.6. Colorimetric Detection of Metal Ions Using Metal Nanoparticles

Attachment of chelating agents onto the nanoparticle surface is the basic step of metal nanoparticle (gold or silver nanoparticles, AgNPs) based colorimetric detection of metal ions. Chelating agent forms complexes with metal ions and promotes nanoparticle aggregation, which result in a color change in the nanoparticle solution. The color change can be detected easily by naked-eye and/or using a UV-Vis spectrophotometer. Many different chelating agents including DNA, aptamers, and small organic molecules have been employed to prepare colorimetric sensors for metal ion detection. Below, we will give some important examples in the field.

2.6.1. Detection of Heavy Metal Ions

Metal ion detection using AuNPs, demonstrated by Hupp et al. [7], for the first time, using MUA capped 13 nm spherical AuNPs. The assay can detect three common heavy metals (Pb^{2+} , Cd^{2+} , and Hg^{2+}) through red to blue color change after chelating of heavy metal ions with surface carboxylates of MUA functionalized AuNPs (Figure 2.13). However, the selectivity of the sensor is poor and its detection limit is in μM level for all of the three metal ions which limit their practical applications.

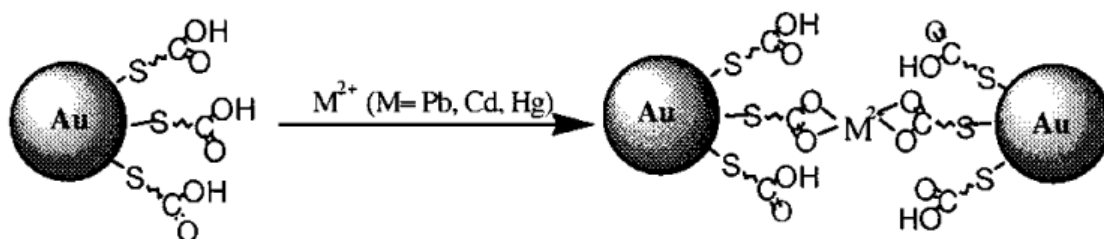


Figure 2.13. Schematic representation of heavy metal ions sensing using the MUA capped AuNPs. Reprinted with permission from ref. [7].

The selectivity and sensitivity (100 nM) of this system was improved by Chang et al. [31] by changing the buffer composition and monolayer structure. Also, Chen et al. [101] reported the colorimetric detection of Pb^{2+} ions using AuNPs functionalized with both carboxylate and 15-crown-5. At the beginning, functionalized AuNPs were aggregated in methanol containing water because of hydrogen bonding between carboxylic acid residues. Then a color change from blue to red was observed with the addition of Pb^{2+} ions due to breakage of the hydrogen bonding [101].

Recently Lee et al. reported very sensitive and selective detection of Pb^{2+} using triazole-acetate functionalized AuNPs (TTA-AuNPs). In the presence of Pb^{2+} , a bridge between Pb^{2+} and TTA was formed through the carboxyl group and triazole. Hence, an aggregation of AuNPs occurred and resulted with a color change from red to purple. This sensor can detect Pb^{2+} ion as low as 16.7 nM. This sensitive colorimetric sensor also worked in lake water including interfering metal ions [102].

Many efforts have been also devoted to detect Hg^{2+} in water using colorimetric sensors. For instance, Mirkin's group synthesized DNA functionalized AuNPs for the detection of Hg^{2+} ions through the thymidine- Hg^{2+} -thymidine bond formation above the melting point of DNA functionalized AuNPs (Figure 2.14) [18]. The assay can detect Hg^{2+} selectively and sensitively (100 nM).

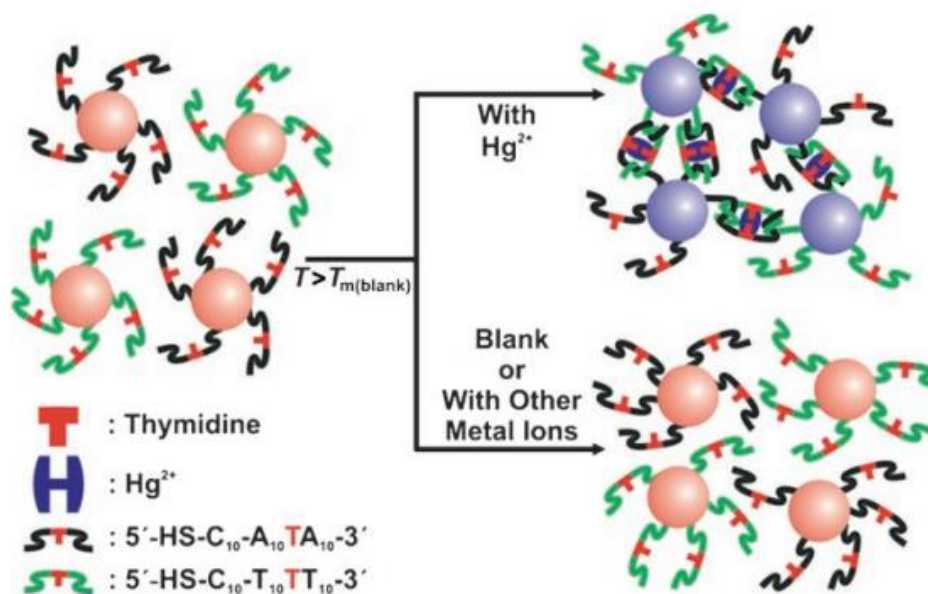


Figure 2.14. Schematic representation of Hg^{2+} sensing using DNA functionalized AuNPs. Reprinted with permission from ref. [18].

Yu et al. reported 3-mercaptopropionic acid (MPA) and adenosine monophosphate (AMP) functionalized AuNPs for the colorimetric detection of Hg^{2+} ions [103] AMP provided high negatively charge density to AuNP surface which makes the MPA/AMP capped AuNPs dispersible in salt solutions. In contrast, MPA/AMP capped AuNPs aggregated in salt solutions in the presence of Hg^{2+} ions due to the interactions between surface carboxyl groups and Hg^{2+} ions, which increase the zeta potential and destabilize the AuNPs in salt solutions. In this scheme, Hg^{2+} detection limit is lowered to 50 nM. Thiocetic acid functionalized AuNPs (TA-AuNPs) were also used for detection of Hg^{2+} ion in water. In the presence of Hg^{2+} , Hg^{2+} ions were replaced with thiol groups and aggregation of AuNPs occurred rapidly. This sensor system showed selectivity over 13 other metal ions and detection limit was 10 nM [104].

AuNRs were also applied for ultrasensitive detection of Hg^{2+} ions (<1 nM). The N-alkylaminopyrazole functionalized AuNRs interact with Hg^{2+} ions to form aggregates which cause both red shift and broadening of the plasmon band of the AuNR solution (Figure 2.15) [105].

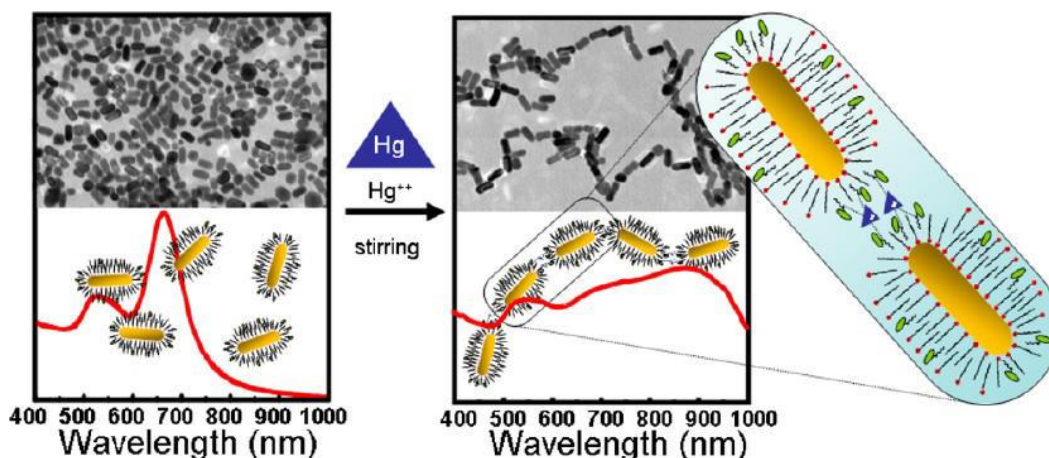


Figure 2.15. Schematic representation of Hg^{2+} induced self-assembly of N-alkylaminopyrazole functionalized AuNRs. Reprinted with permission from ref. [105].

Recently, in the concept of this thesis, our group also demonstrated a very simple method for ultrasensitive detection of Hg^{2+} ions in water (3 nM) [14] which will be discussed in Section 4.1 in detail.

Metal nanoparticle based colorimetric sensors were prepared for many other heavy metal ions. For example, Yao et al. [106] synthesized triazole-carboxyl functionalized AgNPs to determine Co^{2+} selectively in aqueous solution. In the presence of Co^{2+} ions, AgNPs aggregated through metal-ligand interactions and so a color change from yellow to red was observed. The detection limit of the sensor was 10 μM and it was highly selective to Co^{2+} ions compared to 12 other metal ions. Graham's group designed a colorimetric sensor for detection of Ni^{2+} ions in aqueous solution using histidine and nitrilotriacetic acid (NTA) functional AuNPs [107]. An octahedral coordination complex formed between histidine and NTA moieties in the presence of Ni^{2+} ions (Figure 2.16), which enables sensitive detection of Ni^{2+} ions.

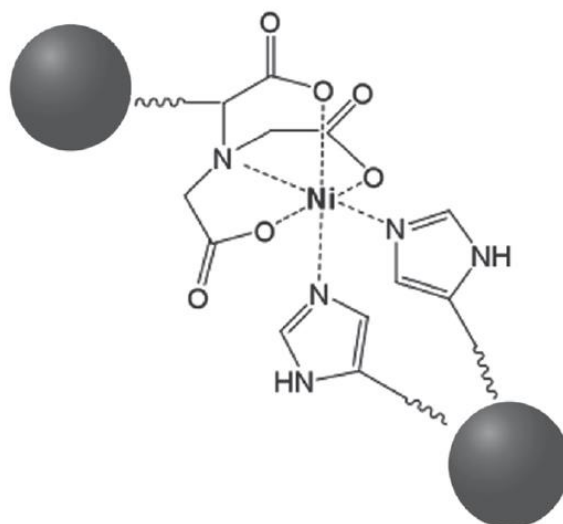


Figure 2.16. Schematic representation of the Ni²⁺ coordinated octahedral complex between histidine and NTA functionalized AuNPs. Adopted with permission from ref. [107].

CTAB stabilized AuNRs were synthesized by Chen et al. which were used for the detection of Cu²⁺ ions in aqueous solution [108]. Unlike the above mentioned chelating based colorimetric sensors, this assay is based on the catalytic etching of AuNRs with the aid of S₂O₃²⁻ in the presence of Cu²⁺ (Figure 2.17). Even a very low concentration (30 nM) of Cu²⁺ produces a color change which can be seen by naked eye. Similar to this approach, Chen et al. reported the detection Hg²⁺ ions based on the shape transformation of Ag nanoprisms to spheres due to the dissolution of destabilized Ag nanoprisms in the presence of Hg²⁺ ions [6].

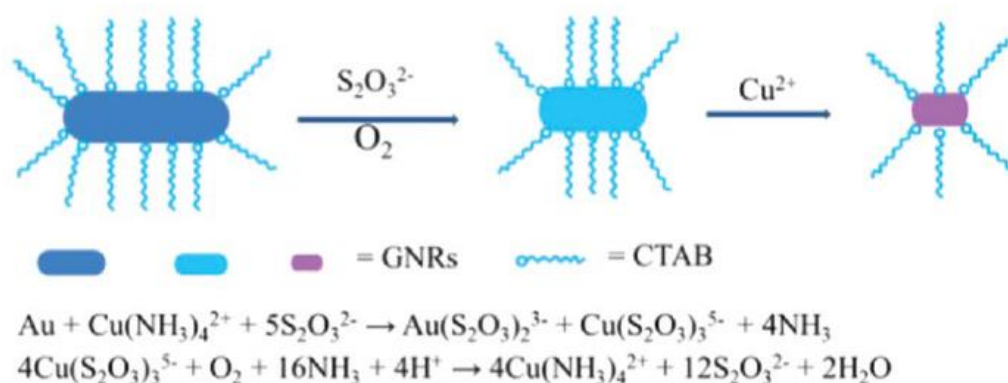


Figure 2.17. Schematic representation of catalytic etching based sensing of Cu²⁺ ions using AuNRs. [108]

2.6.2. Detection of Other Metal Ions

Non-heavy metal ions have been also detected using metal nanoparticles based sensors. For example, Lin et al. [109] reported the colorimetric detection of K^+ ions by using 15-crown-5 functionalized AuNPs (Figure 2.18). 15-crown-5 functionalized AuNPs and K^+ ions formed a complex and aggregates AuNPs; accordingly a color change of AuNP from red to blue was observed. This assay can detect K^+ ions selectively and in micromolar level. Later, same group improved the sensitivity of the sensor by modifying the AuNP surface with thiocetic acid in addition to crown thiols [110]. The improved sensitivity of the sensor might be attributed to the negatively charged carboxylate moiety of the thiocetic acid, which can electrostatically interact with K^+ ions and increase its concentration around the AuNP surface. Using the same principle, colorimetric sensors for Li^+ and Ca^{2+} have been also prepared [111,112].

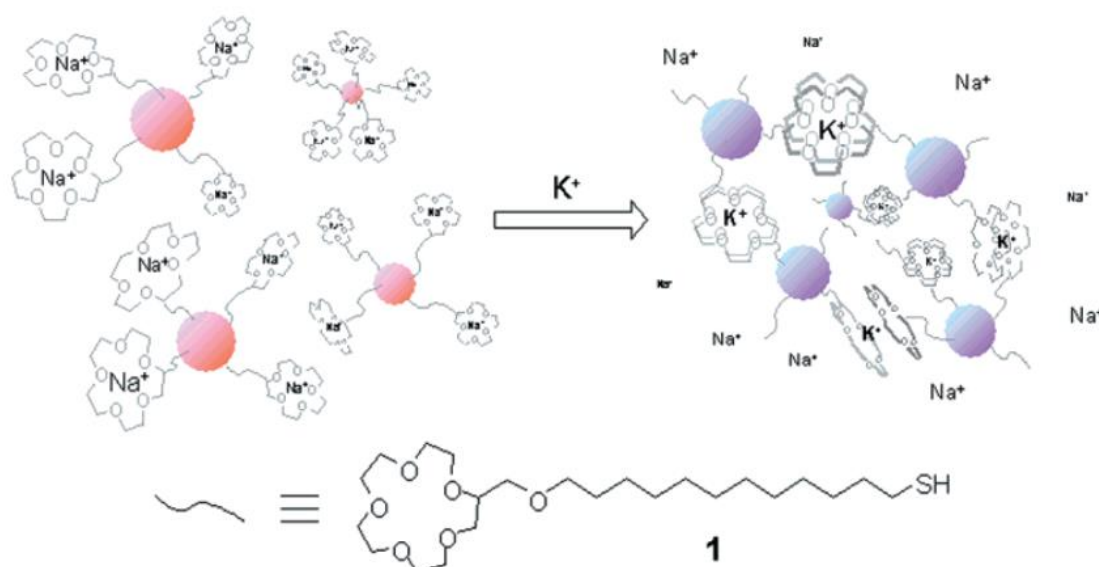


Figure 2.18. Schematic representation of K^+ sensing in the presence of Na^+ ions using 15-crown-5 functionalized AuNPs. Reprinted with permission from ref. [109].

Hutchison et al. [113] reported a colorimetric sensor for the detection of lanthanide ions (Ln^{3+}) based on AuNPs functionalized with tetramethylmalonamide (TMMA). Addition of Ln^{3+} to the AuNPs solution caused formation of TMMA- Ln^{3+} complex so the color of the solution changed from red to blue. Wang et al., [114] synthesized

pentapeptide (CALNN) functionalized AuNPs for the determination of Al^{3+} ions. Carboxylic groups of CALNN caught Al^{3+} and caused a color change due to AuNPs aggregation. They also demonstrated the measurement of intracellular Al^{3+} levels (Figure 2.19). Uranyl (UO_2^{2+}) ions have been also detected using AuNP based colorimetric sensors. In the first step, AuNPs aggregated using DNAzymes which is specific to the uranyl ion. Uranyl ions cleave the bond between aggregates and releases AuNPs, which changes the color of solution from purple to red. The detection limit is 50 nM, which is below the maximum contamination limit have defined by the EPA [115].

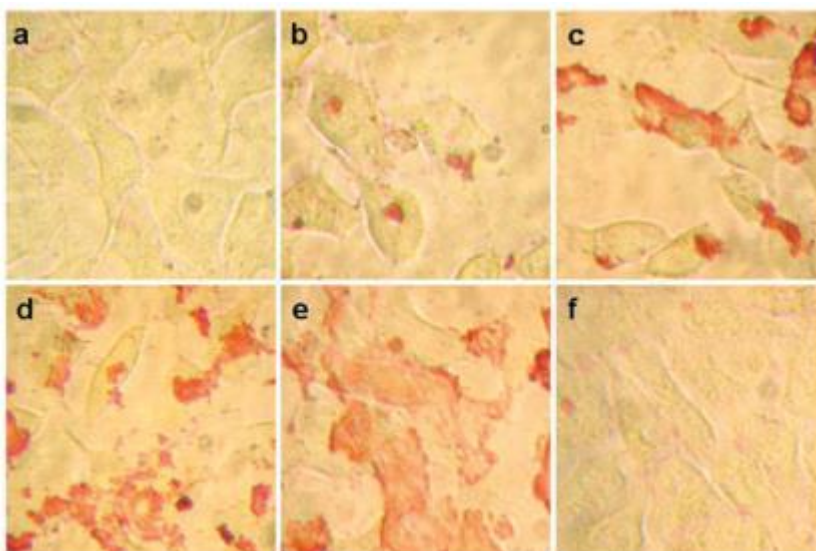


Figure 2.19. Bright-field microscopic images of HeLa cells incubated with pentapeptide functionalized AuNPs and different amounts of Al^{3+} ions; (a) 0 mM, (b) 5 mM, (c) 10 mM, (d) 50 mM and (e) 100 mM. (f) After F^- etching the AuNPs in (e). Reprinted with permission from ref. [114].

2.6.3. Selective Detection of Multiple Metal Ions

It is very attractive to detect more than one metal ion using the same assay for practical applications since it will decrease the cost and time needed for analysis. For this purpose, Lou et al. [15] reported a simple and rapid colorimetric assay to simultaneously detect Hg^{2+} and Ag^+ ions. They reduced Hg^{2+} or Ag^+ on to the Tween 20 stabilized AuNPs with the help of ascorbic acid (AA). The metal layer protects the AuNPs against aggregation, which enable blue to red detection of both metal ions. To give the selectivity to the assay one of the metal ions can be

eliminated from the solution or chelated using proper chemicals; EDTA for Hg^{2+} and NaCl for precipitate Ag^+ (Figure 2.20). The sensor was able to detect Hg^{2+} levels as low as 5 nM, and Ag^+ levels as low as 10 nM. They validated this sensitive and selective method both in drinking and tap water.

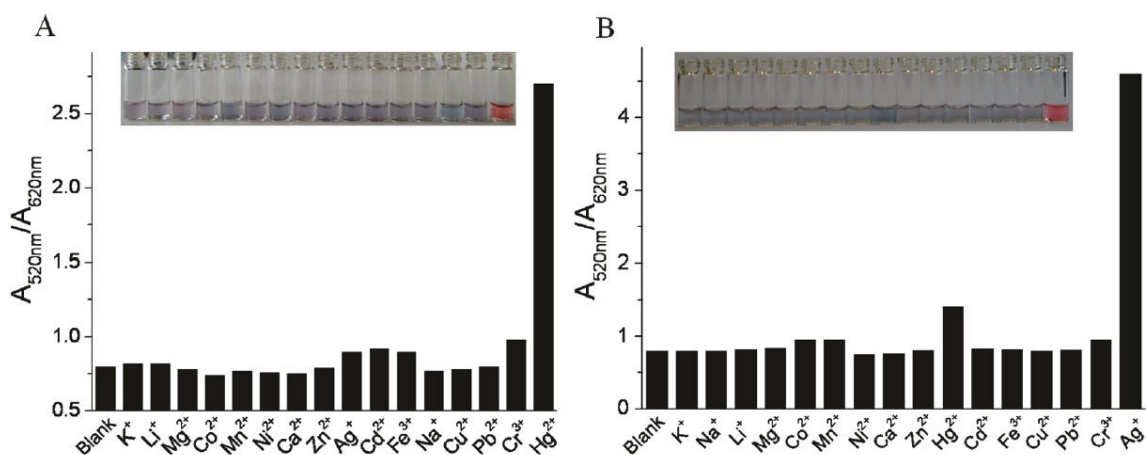


Figure 2.20. Results of selective Hg^{2+} and Ag^+ sensing using Tween 20 stabilized AuNPs. (a) Hg^{2+} in the presence of NaCl and (b) Ag^+ sensing in the presence of EDTA. Reprinted with permission from ref. [15].

In the study by Modi et al. [116] 6-mercaptopyridonic acid (MNA) and melamine (MA) functionalized AgNPs were prepared to detect Cr^{3+} and Ba^{2+} ions at the same time, in aqueous solutions. MNA and MA molecules attached to the AgNPs surface through Ag-S and Ag-N linkage. Cr^{3+} and Ba^{2+} ions interacted through strong cooperative metal-ligand interactions with functionalized AgNPs and it caused quick aggregation and a color change from yellow to reddish brown for Cr^{3+} and to orange for Ba^{2+} . They also applied this method successfully for determination of Cr^{3+} and Ba^{2+} ions in drinking, tap and river water samples simultaneously. Simultaneous detection of Cu^{2+} and Ag^+ ions reported by Alizadeh et al. [117] using the chelidamic acid and 2-aminopyridine modified AuNPs. The moieties of chelidamic acid on the AuNPs surface had ability to make complexes with Cu^{2+} and similarly 2-aminopyridine had ability to make complexes with Ag^+ ions. In the presence of Cu^{2+} ions modified AuNPs aggregated and formation of black precipitates observed. In the presence of Ag^+ ions a quick color change from brown to purple occurred because of aggregation of AuNPs.

In a recent study, green AgNPs which were synthesized by reducing extracts of different plants (neem, mango, pepper and tea plants) were utilized to detect several heavy metal ions (Hg^{2+} , Pb^{2+} , Zn^{2+}) in aqueous solutions [118]. The complicated interactions between surface bound plant extracts and metal ions enables detection of Hg^{2+} , Pb^{2+} , Zn^{2+} ions in a wide pH range. In a similar manner, Kumar et al. [119] reported the detection of Cd^{2+} , Hg^{2+} and Pb^{2+} ions using the AgNPs that are functionalized with different organic ligands such as N-(2-hydroxybenzyl)-valine (VP) and N-(2-hydroxybenzyl)-isoleucine (ILP).

Recently, our group reported the simultaneous detection of 7 metal ions with excellent selectivity using an array of MUA stabilized AuNPs and amino acids which will be discussed in Section 4.2 in detail.

2.6.4. New Approaches

In order to develop on-field colorimetric devices for metal ion detection based on metal nanoparticles, some recent studies reported smart phone coupled systems which make these devices very compact by eliminating the need of bulky UV-Vis spectrophotometers. For instance, Ozcan group developed a compact device for detection of mercury contamination in water using a smart phone for both collecting and analyzing the colorimetric response data [120] (Figure 2.21). The device uses green and red LEDs to analyze the color of solution. Also, it calculates the mercury concentration automatically using a custom-developed application. Using this lightweight (smart phone + 40 g of apparatus) device, they produced a mercury contamination map for California (USA) by investigating the samples taken from more than 50 locations.

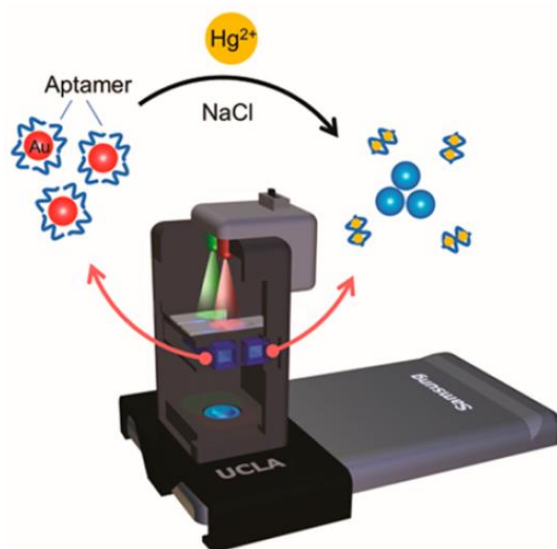


Figure 2.21. Schematic representation of the smart-phone based sensing of Hg^{2+} . Reprinted with permission from ref. [120].

In another recent study, Chen et al. [121] developed a compact paper-based sensor for detection of mercury contamination in water. They produced the paper-based sensor array using a conventional printer and read and analyze the data using a smart phone (Figure 2.22). They reached a mercury detection limit of 50 nM in real samples using this portable device.

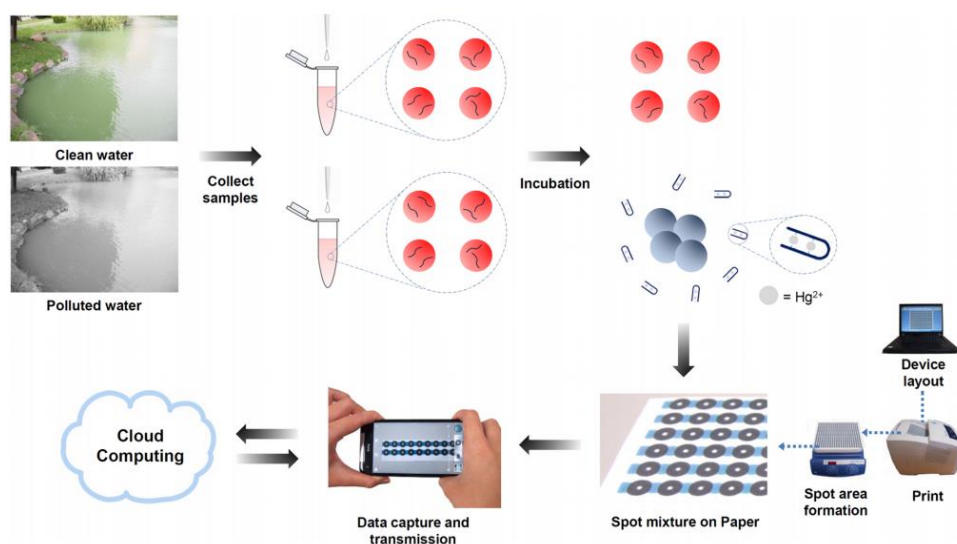


Figure 2.22. Schematic representation of Hg^{2+} sensing using the paper-based colorimetric sensor. Reprinted with permission from ref. [121]

3. MATERIALS AND METHODS

3.1. Ultrasensitive Colorimetric Sensing of Hg²⁺ using Citrate-Capped AuNPs and Lysine

3.1.1. Materials

Sodium citrate tribasic dehydrate, gold(III) chloride trihydrate, lysine, cysteine, histidine, tyrosine, aspartic acid, arginine, alanine, glycine, phenylalanine, tryptophan, methionine, leucine, isoleucine, Cu(NO₃)₂·6H₂O, Ni(NO₃)₂·6H₂O, Pb(NO₃)₂, Fe(NO₃)₃·9H₂O, Hg(NO₃)₂·H₂O, AgNO₃, NaCl, Zn(NO₃)₂·6H₂O, Co(NO₃)₂·6H₂O, KNO₃, Ca(NO₃)₂·4H₂O, Al(NO₃)₃·H₂O, Cd(NO₃)₂·4H₂O were obtained from Sigma-Aldrich (St Louis, MO). All water used in the experiments was purified using a Barnstead (Dubuque, IA) ROpure LP® reverse osmosis unit with a high flow cellulose acetate membrane (Barnstead D2731) followed by a Barnstead D3804 NANOpure® organic/colloid removal and ion exchange packed bed system.

3.1.2. Methods

3.1.2.1. Synthesis of Citrate Capped Gold Nanoparticles

The AuNPs were prepared according to Turkevich method in which HAuCl₄ salt is reduced to Au using sodium citrate [122]. Briefly, 12 mL preheated sodium citrate solution (1%, w/w) was added to the 100 mL of boiling water containing 8.5 mg of HAuCl₄ salt. The solution was vigorously stirred while heating for 20 min until color of the solution turned to deep red (Figure 3.1). Finally, the solution was cooled to room temperature and volume of the AuNP solution was adjusted to 100 mL. The average particle size of the AuNPs was determined to be 24.5 ± 3.7 nm from TEM images.

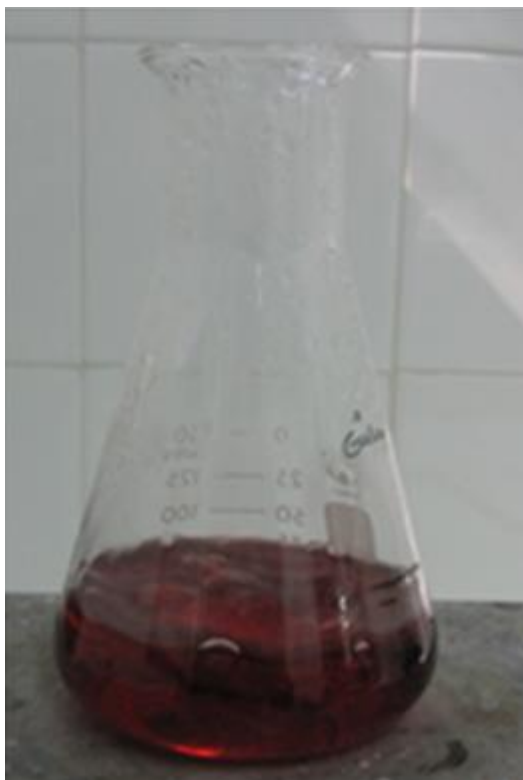


Figure 3.1. Photograph of as-prepared citrate capped AuNP solution.

3.1.2.2. Colorimetric Sensing of Hg^{2+} in Deionized and Tap Water

In a typical experiment 0.5 mL of AuNPs (0.4 nM, which was calculated according a previous report [123]) was mixed with 0.2 mL of Hg^{2+} solutions (in deionized or tap water) at different concentrations to give final Hg^{2+} concentrations in the range of 1 nM to 20 μM . Then, 0.5 mL of lysine solution (final concentration is 0.4 mM) in water (pH 7.0) was added to this solution. Finally, the color changes were detected by naked eye and/or recording the UV-Vis absorption spectra. The photographs were taken with a digital camera (12.1 megapixels) and the absorption measurements were performed using a UV-Vis spectrophotometer between 350 nm and 850 nm. The sensor responses were calculated by dividing the extinction of AuNP suspension at 725 nm to the extinction at 525 nm (E_{725}/E_{525}). All experiments were performed in triplicate.

Limit of detection (LOD) values were calculated using the following formula;

Limit of detectable response = Average response of the blank + (3 × standard deviation of the blank)

3.1.2.3. Recovery Experiments

The recovery experiments were performed at the above-mentioned conditions using Hg²⁺-spiked tap water. The absorption measurements between 350 and 850 nm were performed using a UV–Vis spectrophotometer. The sensor responses were calculated by dividing the extinction of the AuNP suspension at 725 nm by the extinction at 525 nm (EX_{725}/EX_{525}). Then, using the response (EX_{725}/EX_{525}) of the colorimetric assay against spiked tap water samples and linear regression equations, we calculated the Hg²⁺ concentration in the samples. Finally, recovery values were calculated using the following formula:

$$\text{Recovery (\%)} = (\text{calculated Hg}^{2+}/\text{added Hg}^{2+}) \times 100\%$$

3.1.2.4. Effect of Other Amino Acids on the Response Colorimetric Sensor

The experiments were performed at the above-mentioned conditions with the exception of using other amino acids (cysteine, histidine, tyrosine, aspartic acid, arginine, alanine, glycine, phenylalanine, tryptophan, methionine, leucine, and isoleucine) instead of lysine at the same concentration. The final Hg²⁺ concentration was kept constant at 10 μM in all experiments. Also, control experiments were performed in the absence of Hg²⁺. All experiments were performed in triplicate.

3.1.2.5. Selectivity of the Colorimetric Sensor

The selectivity of the colorimetric sensor was investigated using several metal ions (Cu²⁺, Ni²⁺, Pb²⁺, Co²⁺, Zn²⁺, Ca²⁺, Al³⁺, K⁺, Fe³⁺, Cd²⁺, Ag⁺, Na⁺, Au³⁺) under the above-mentioned conditions. The final concentration of the competing metal ions was adjusted to 50 μM, whereas the concentration of Hg²⁺ was 1 μM. In addition, selectivity experiments were performed in the presence of a mixture of all metal ions (each ion concentration was adjusted to 10 μM). Also, control experiments were performed in the absence of lysine. All experiments were performed in triplicate.

3.1.3. Characterization

The morphology and size of the AuNPs were characterized using TEM. The AuNPs were dropped onto a copper-coated grid and then dried at room temperature. TEM micrographs were taken at 200 kV by TEM microscope (FEI, Tecnai G2 F30). Extinction spectra were recorded by a double beam UV-Vis spectrophotometer (UV-1601, Shimadzu) at room temperature.

3.2. Development of a Colorimetric Sensor Array for Detection of Multiple Metal Ions based on AuNPs and Amino Acids

3.2.1. Materials

Sodium citrate tribasic dehydrate, gold(III)chloride trihydrate (HAuCl_4), MUA, lysine, cysteine, histidine, tyrosine, arginine, $\text{Hg}(\text{NO}_3)_2 \cdot \text{H}_2\text{O}$, $\text{Cd}(\text{NO}_3)_2 \cdot 4\text{H}_2\text{O}$, $\text{Fe}(\text{NO}_3)_3 \cdot 9\text{H}_2\text{O}$, $\text{Pb}(\text{NO}_3)_2$, $\text{Al}(\text{NO}_3)_3 \cdot \text{H}_2\text{O}$, $\text{Cu}(\text{NO}_3)_2 \cdot 6\text{H}_2\text{O}$, $\text{Cr}(\text{NO}_3)_3 \cdot 9\text{H}_2\text{O}$, AgNO_3 , $\text{Ca}(\text{NO}_3)_2 \cdot 4\text{H}_2\text{O}$, $\text{Zn}(\text{NO}_3)_2 \cdot 6\text{H}_2\text{O}$, $\text{Co}(\text{NO}_3)_2 \cdot 6\text{H}_2\text{O}$, $\text{Ni}(\text{NO}_3)_2 \cdot 6\text{H}_2\text{O}$, $\text{Sr}(\text{NO}_3)_2$, KNO_3 , NaCl , and $\text{FeCl}_2 \cdot 4\text{H}_2\text{O}$ were obtained from Sigma-Aldrich (St Louis, MO). All water used in the experiments was purified using a Barnstead (Dubuque, IA) ROPure LP® reverse osmosis unit with a high flow cellulose acetate membrane (Barnstead D2731) followed by a Barnstead D3804 NANOpure® organic/colloid removal and ion exchange packed bed system.

3.2.2. Methods

3.2.2.1. Synthesis of MUA capped AuNPs

First, citrate capped AuNPs were prepared according to Turkevich method [122]. Briefly, 12 mL preheated sodium citrate solution (1%, w/w) was added to the 100 mL of boiling water containing 8.5 mg of HAuCl_4 salt. The solution was vigorously stirred while heating for 20 min until color of the solution turned to deep red. After reaction completed, the volume of AuNP solution was adjusted to 100 mL.

To modify the AuNP surface with MUA, 10 mL of aqueous solution of MUA (3.25 mg) containing NaOH (0.5 M, 30 μL) was added to citrate capped AuNPs solution (50 mL) while heating. Then, the solution was stirred for 1 hour [7]. Solution was cooled to room temperature and volume of the MUA capped AuNP solution was

adjusted to 50 mL. Finally, MUA capped AuNPs were washed with water twice to remove the unbound MUA molecules.

3.2.2.2. Determination of Optimum Amino Acid Concentrations in the Colorimetric Assay

To determine the suitable amino acid concentrations that will be used in the colorimetric sensor array UV-Vis spectra of AuNPs (0.1 nM) in the presence of different amino acid concentrations between 0 μ M and 500 μ M were recorded using a UV-Vis spectrophotometer at different time intervals up to 1 h. The colorimetric responses were calculated by dividing the extinction of AuNPs at 625 nm by the extinction of 525 nm (Ex_{625}/Ex_{525}).

3.2.2.3. Colorimetric Detection of Multiple Metal Ions

The experiments were performed in a 96 well plate. 50 μ L MUA capped AuNPs (0.1 nM) was mixed with 5 μ L of cysteine (1 mM) or 20 μ L of other amino acids (1 mM) (lysine, cysteine, histidine, tyrosine, and arginine) at determined concentrations. Then, metal ions (Hg^{2+} , Cd^{2+} , Fe^{3+} , Pb^{2+} , Al^{3+} , Cu^{2+} , and Cr^{3+}) in water at different concentrations were added to this solution to give final metal ions concentrations in the range of 2 μ M to 50 μ M. Final volume of assay was completed to 100 μ L with water. Finally, color changes were detected by the naked eye and/or by using a plate reader. The colorimetric responses were recorded at 625 nm and 525 nm. The colorimetric responses were calculated by dividing the extinction of AuNPs at 625 nm by the extinction of 525 nm (Ex_{625}/Ex_{525}). The photographs were taken with a digital camera (12.1 megapixels).

3.2.3. Characterization

The morphology and size of the AuNPs were characterized using TEM. The AuNPs were dropped onto a copper-coated grid and then dried at room temperature. TEM micrographs were taken at 200 kV by TEM microscope (FEI, Tecnai G2 F30). Extinction spectra were recorded by double beam UV-Visible spectrophotometers (UV-1601 and UVmini-1240, Shimadzu) at room temperature. A plate reader (Spectra max M5, Molecular Devices) used to read the absorption

values at 525 nm and 625 nm of the colorimetric assay. Raman spectra were collected using a DXR Raman Microscope (Thermo Scientific). Zeta potentials of the AuNPs were measured using a Zetasizer (Nanoseries, Malvern).

3.2.4. Data Analysis for Multiple Ion Detection

The colorimetric responses of the array against metal ions at different concentrations were analyzed using hierarchical cluster analysis (HCA) as the pattern recognition technique. The analyses were performed by built-in HCA algorithms of MATLAB software. Euclidean distance method was used for the obtaining the dendrograms.

MATLAB code for HCA:

```
X = [enter data]
```

```
D = pdist (X)
```

```
Squareform (D)
```

```
Z = linkage (X,'complete','euclidean');
```

```
H = dendrogram (Z,'Orientation','right')
```

```
Set (H,'LineWidth',1)
```

The distance between two data points were calculated using Euclidean distance, which is expressed as follow;

$$d(a, b) = \sqrt{\sum_{i=1}^n (a_i - b_i)^2}$$

4. RESULTS AND DISCUSSION

In this thesis, we focused on two research projects about preparation of novel AuNP based colorimetric sensors for toxic metal ion detection. First part is entitled as “Ultrasensitive Colorimetric Sensing of Hg²⁺ using Citrate-Capped AuNPs and Lysine” and second part is entitled as “Development of a Colorimetric Sensor Array for Detection of Multiple Metal Ions based on AuNPs and Amino Acids”. Below, we will summarize the results of both projects in sections 4.1 and 4.2, respectively.

4.1. Ultrasensitive Colorimetric Sensing of Hg²⁺ using Citrate-Capped AuNPs and Lysine

Facile metal NP-based colorimetric techniques have been developed for Hg²⁺ detection using commercially available simple ligands such as Tween 20 or urine [15,124-126]. However, these methods generally revealed low sensitivity and a poor limit of detection, with values higher than the limit of acceptable Hg²⁺ concentration in drinkable water, which is 10 nM according to the EPA [21].

With these insights, in this part we report a facile yet highly sensitive and selective method for rapid Hg²⁺ detection in both distilled and tap water samples. The colorimetric assay utilizes as-prepared citrate-capped gold nanoparticles without performing any tedious surface modification with Hg²⁺ specific ligands. Instead, we simply use the amino acid, lysine to promote aggregation of gold nanoparticles in the presence of Hg²⁺. Strong affinity of some amino acids (e.g., cysteine) toward Hg²⁺ has been proved, and accordingly they have been used in colorimetric assays [127-129]. However, they are generally used for detection of amino acids, not Hg²⁺. Also, they are used with surface-modified AuNPs, not the citrate-capped as-prepared AuNPs. The colorimetric Hg²⁺ sensing principle of our assay can be explained by a two-step mechanism. In the first step, Hg²⁺ was spontaneously reduced on the AuNP surface and formed a shell around the particles. Then, lysine addition to this solution induced aggregation of Hg²⁺-covered AuNPs and resulted in a rapid color change from red to purple or gray because the distance between the AuNPs became less than the average particle diameter [124]. The color change of the AuNPs was investigated using several Hg²⁺ solutions in distilled or tap water at different concentrations. The detection limit of this inexpensive

colorimetric assay is 2.9 nM, which makes our assay one of the most sensitive colorimetric Hg²⁺ sensors compared with many metal nanoparticle-based methods. To demonstrate the selectivity, several metal ions were tested with the assay, and it was observed that the response of the colorimetric assay is highly selective to Hg²⁺.

4.1.1. Sensing Mechanism

Figure 4.1 shows the proposed Hg²⁺ sensing mechanism of the colorimetric assay. Initially, the surface of the as-prepared AuNPs is covered with citrate ions, which are replaced with Hg²⁺ ions upon the addition of Hg²⁺ solution (final concentration is 10 μM) to the AuNP solution. It is well-known that Hg²⁺ ions can spontaneously react with the AuNP surface to form a mercury layer [124,130]. After addition of lysine (final concentration is 0.4 mM) to the Hg²⁺-capped AuNPs, the color of the AuNP suspension immediately changes from red to purple or gray due to the aggregation of AuNPs (Figure 4.2a). The color change of the solution is very fast and occurs in a few seconds after the addition of lysine. The aggregation of the AuNPs upon addition of lysine can be explained as follows: lysine contains two amino groups which can strongly interact with the Hg²⁺ ions [131], and therefore it forms bridges between Hg²⁺-coated AuNPs and aggregates them. In the presence of only Hg²⁺ ions or lysine, the color of the AuNP solution did not change (Figure 4.2a), which also supports the proposed sensing mechanism.

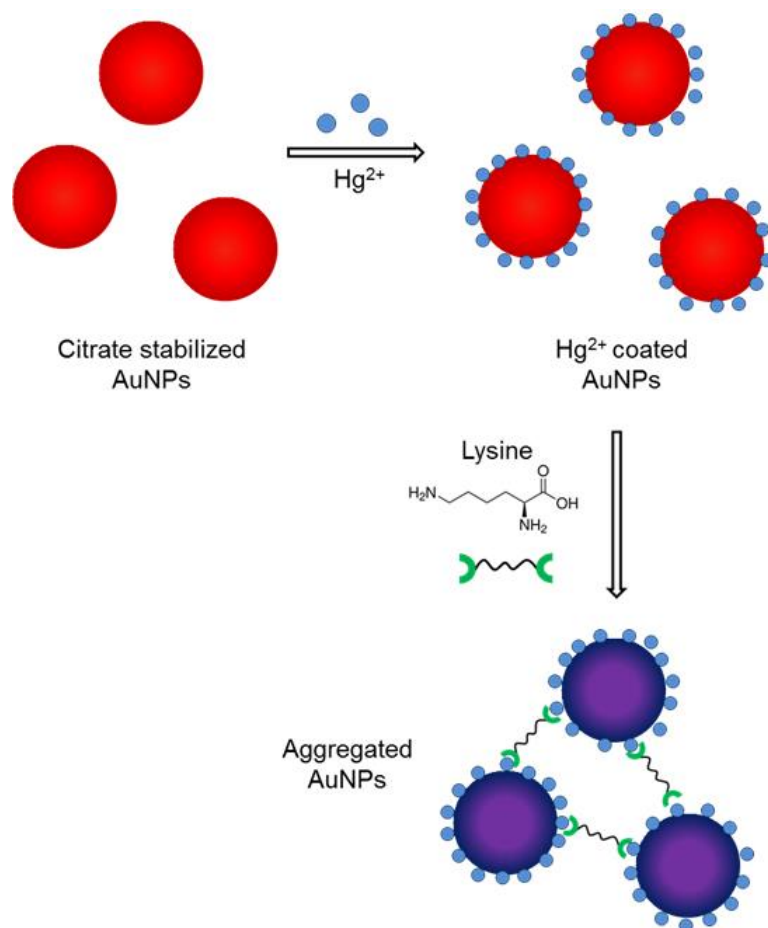


Figure 4.1. Schematic representation of the proposed Hg²⁺ sensing mechanism of the colorimetric assay.

Figure 4.2b shows the UV-Vis spectra of AuNP solutions. As-prepared citrate-capped AuNPs demonstrated typical extinction spectra for such particles with a maximum centered at 525 nm. Upon addition of Hg²⁺ ions, the extinction maxima slightly blue-shifted to around 522 nm, indicating the Hg²⁺ layer formation around the AuNPs (Figure 4.2b) [124,132]. After addition of lysine to the Hg²⁺-capped AuNP solution, a second broad and intense peak appeared at around 725 nm in the extinction spectrum, which indicated the aggregation of AuNPs. Also, the extinction peak at 525 nm of the well-dispersed AuNPs was largely reduced upon lysine addition.

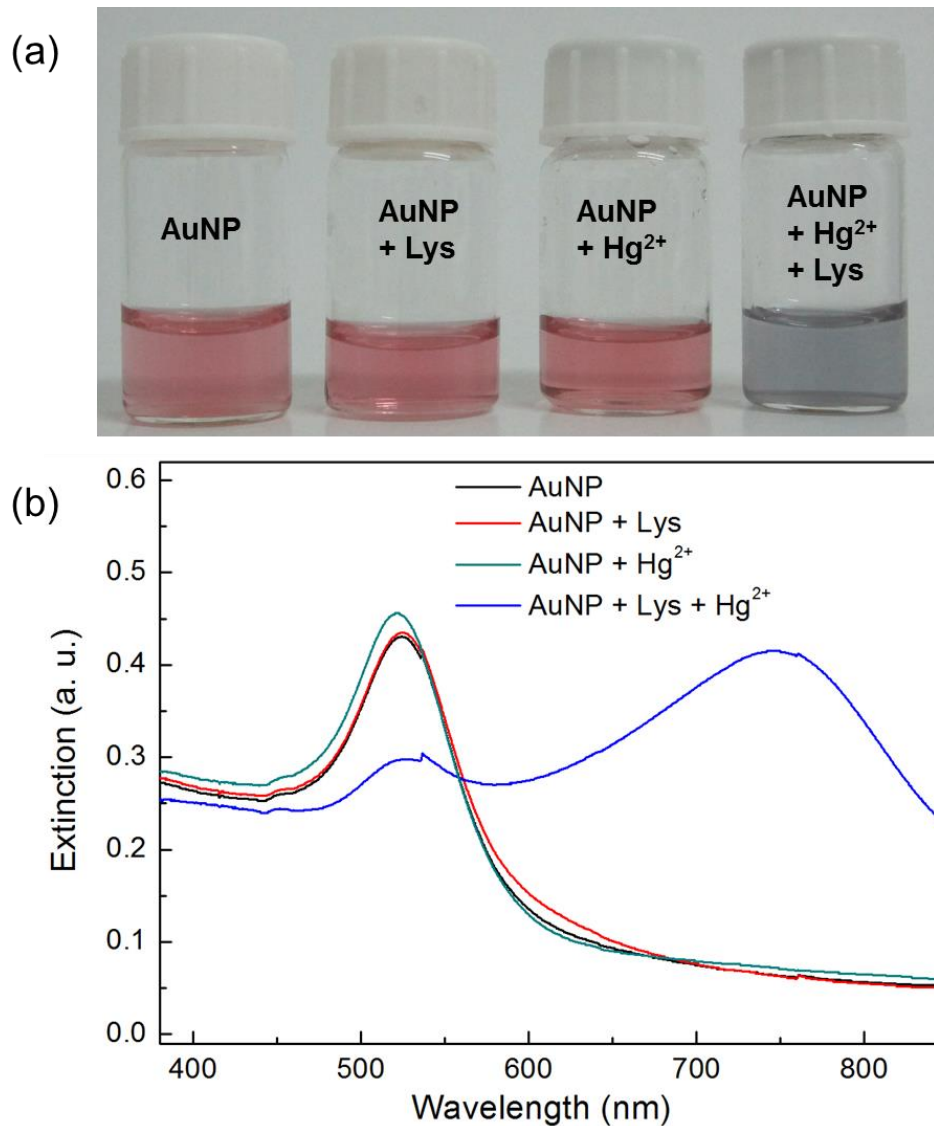


Figure 4.2. Colorimetric response of the assay. (a) Photographs of AuNP solutions showing the color change occurs only in the presence of lysine (0.4 mM) and Hg²⁺ (10 μ M). (b) Extinction spectra of the AuNP solutions.

On the other hand, when only lysine was added to the AuNP solution, the extinction spectrum remained almost unaffected. Hg²⁺-and/or lysine-added AuNP solutions were further investigated using TEM (Figure 4.3). As can be seen from the TEM images for citrate-capped AuNPs with no addition and citrate-capped AuNPs with Hg²⁺-only or lysine-only added solutions, AuNPs were well dispersed on the TEM grid. On the other hand, large aggregates were observed for both Hg²⁺- and lysine-added solution (Figure 4.3d).

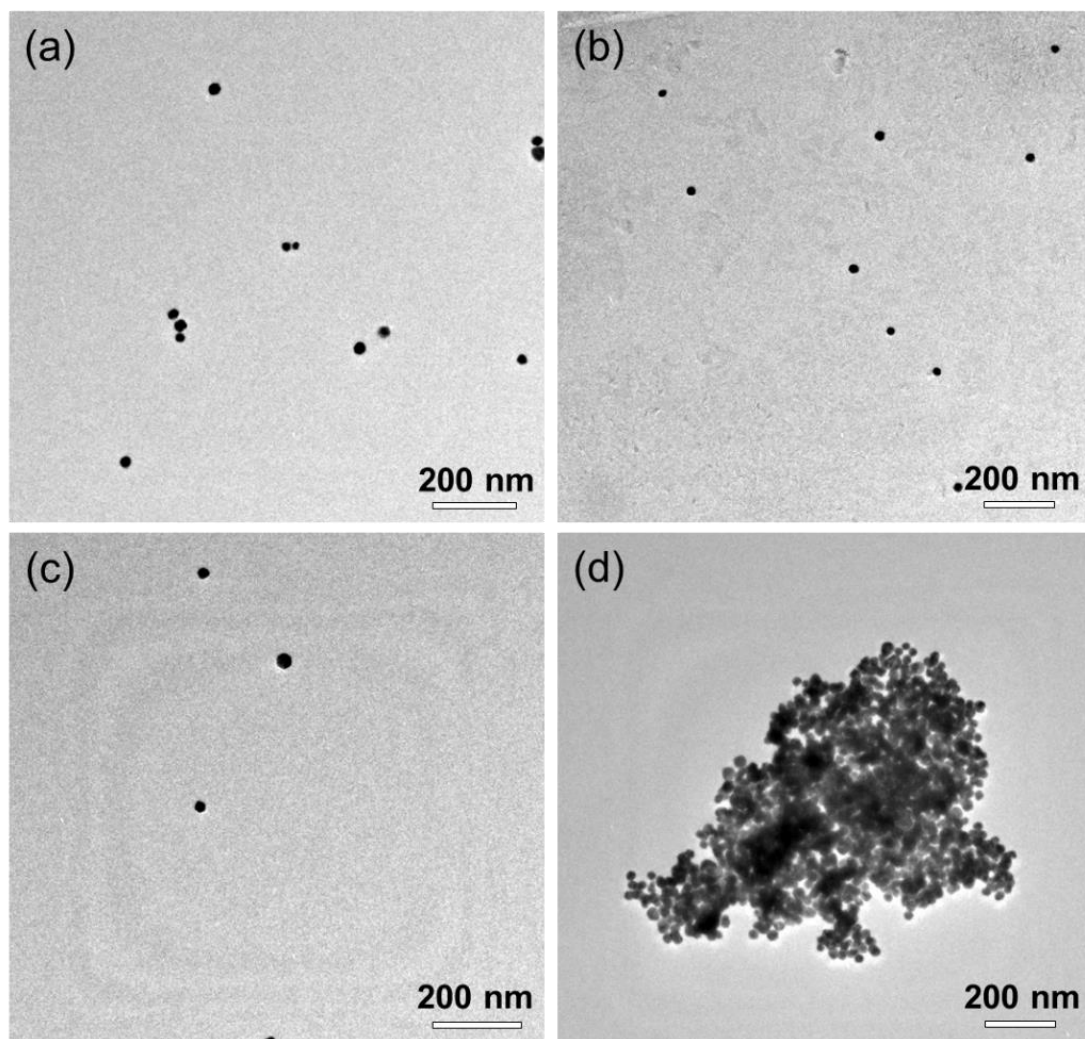


Figure 4.3. TEM images of AuNP solutions. (a) Bare AuNPs, (b) in the presence of lysine, (c) in the presence of Hg^{2+} ions, and (d) in the presence of both lysine and Hg^{2+} ions. AuNPs aggregated when both lysine and Hg^{2+} were added.

4.1.2. Effect of Amino Acids on Aggregation of Hg^{2+} -Capped AuNPs

As we mentioned above, it is believed that aggregation of Hg^{2+} -capped AuNPs is due to their strong interaction with two amino residues of lysine molecules. To verify this hypothesis, we tested several amino acids with the assay. First, we added Hg^{2+} (final Hg^{2+} concentration in the assay is $10\ \mu\text{M}$) to AuNP solutions, and then amino acid solutions were added to these solutions to give a final amino acid concentration of $0.4\ \text{mM}$. As shown in Figure 4.4a, among the tested 14 amino acids only lysine and arginine produced a colorimetric response by aggregating the AuNPs. Note that both amino acids have more than one amino group; lysine contains two primary amino groups, and arginine contains two primary and two

secondary amino groups. Therefore, aggregation of Hg^{2+} -capped AuNPs can be promoted by more than one amino group-containing molecule, which can interact with more than one AuNP and provide bridge formation between particles, resulting in aggregation. We also studied the effect of the amino acids on the colloidal stability of the citrate-capped AuNPs in the absence of Hg^{2+} ions (Figure 4.4b). It was observed that except for arginine, none of the amino acids significantly affected the extinction spectrum of AuNPs. On the other hand, addition of arginine resulted in a neck formation in the extinction spectrum of the AuNP solution, indicating the AuNP aggregation. Nevertheless, in the absence of Hg^{2+} the aggregation was much lower compared to that of the Hg^{2+} -capped particles. Figure 4.4c shows the ratio between extinction intensity of aggregated (around 725 nm) and separated particles (at 525 nm). As expected, the extinction intensity ratio ($\text{Ex}_{725}/\text{Ex}_{525}$) of lysine and arginine was significantly higher than that of control (i.e., bare AuNP solution) and as well as other amino acids in the presence of 10 μM Hg^{2+} . In the absence of Hg^{2+} , all amino acids had $\text{Ex}_{725}/\text{Ex}_{525}$ values similar to that of control except for arginine, which gave a ratio slightly higher than that of the other amino acids and control. These results indicate that both lysine and arginine can be used to promote aggregation of AuNPs in the presence of Hg^{2+} . However, arginine also gave a slight response in the absence of Hg^{2+} ions, which can interact with the assay especially at low Hg^{2+} concentrations. Also, the ratios between the responses, in the presence and absence of Hg^{2+} ions, of lysine and arginine are 9.89 and 7.91, respectively. Obviously, higher selectivity between these two conditions is desired for sensitive colorimetric sensors. Therefore, we used lysine as an aggregation promoter in the remainder of the study.

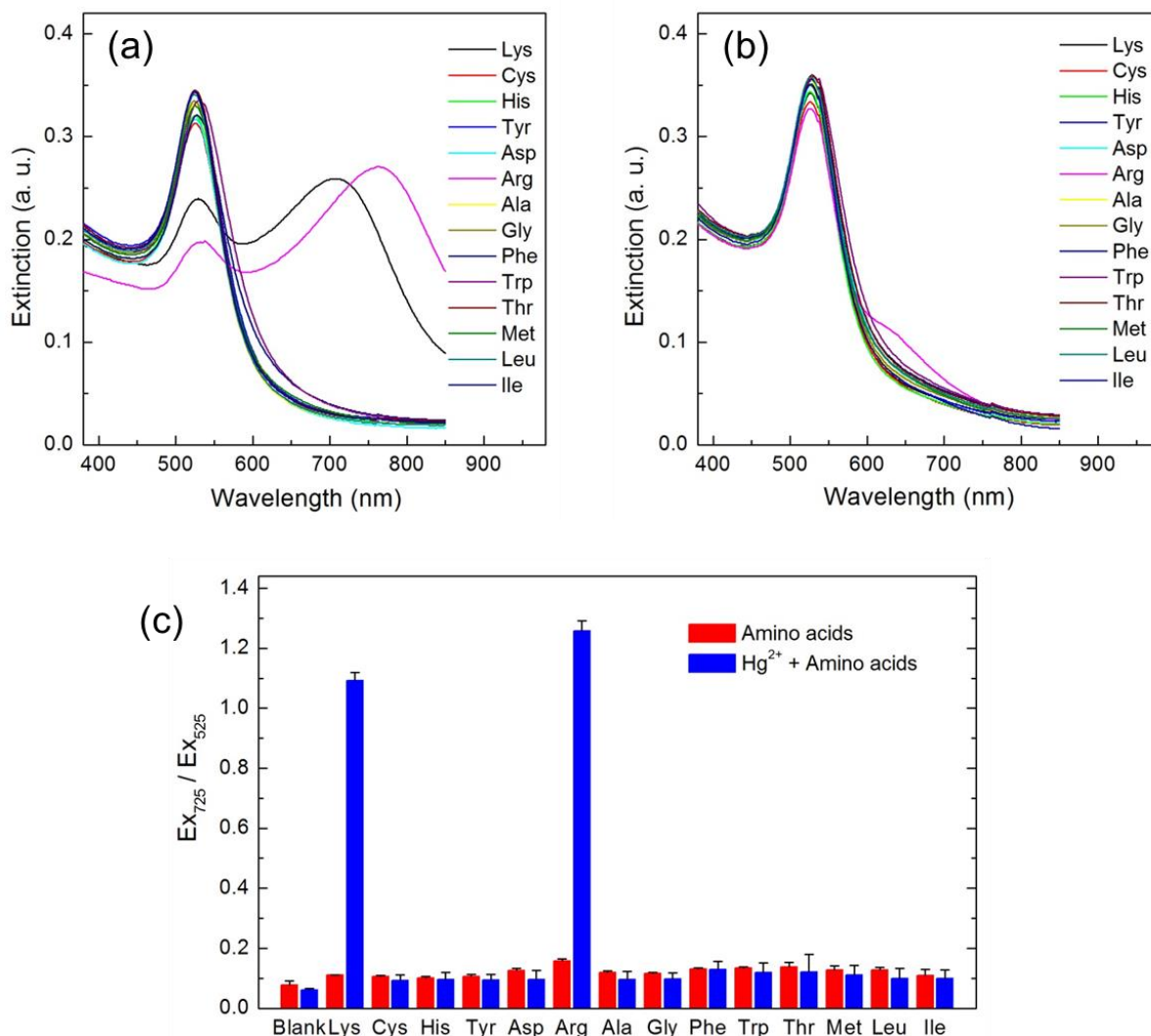


Figure 4.4. Effect of amino acids on colorimetric response of the assay. Extinction spectra of the colorimetric assay tested with 14 different amino acids: (a) in the presence and (b) in the absence of $10 \mu\text{M Hg}^{2+}$. (c) Extinction intensity ratios (EX_{725}/EX_{525}) of the colorimetric assay for 14 different amino acids in the presence or absence of $10 \mu\text{M Hg}^{2+}$ ions. (Lys: lysine, Cys: cysteine, His: histidine, Tyr: tyrosine, Asp: aspartic acid, Arg: arginine, Ala: alanine, Gly: glycine, Phe: phenylalanine, Trp: tryptophan, Met: methionine, Leu: leucine, Ile: isoleucine).

4.1.3. Colorimetric Detection of Hg^{2+}

To obtain higher aggregation and accordingly better colorimetric response through Hg^{2+} ions, first we optimized the lysine concentration in the assay. Figure 4.5 shows the effect of lysine concentration on the EX_{725}/EX_{525} value of the assay in the presence of $10 \mu\text{M Hg}^{2+}$. The EX_{725}/EX_{525} value increased sharply between the lysine concentrations of 0.05 mM and 0.1 mM and reached a maximum value of 1.35. Further increasing the lysine concentration up to 1 mM did not significantly affect the EX_{725}/EX_{525} ratio. Therefore, we used a lysine concentration of 0.4 mM in

the assay, which ensures the strong aggregation of AuNPs in the presence of Hg^{2+} . We also investigated the change in $\text{EX}_{725}/\text{EX}_{525}$ ratio with time (Figure 4.6). After addition of lysine, the $\text{EX}_{725}/\text{EX}_{525}$ ratio rapidly increased to 0.9 within 1 min and reached a plateau around 1.3 after 5 min, indicating the rapid response of the assay.

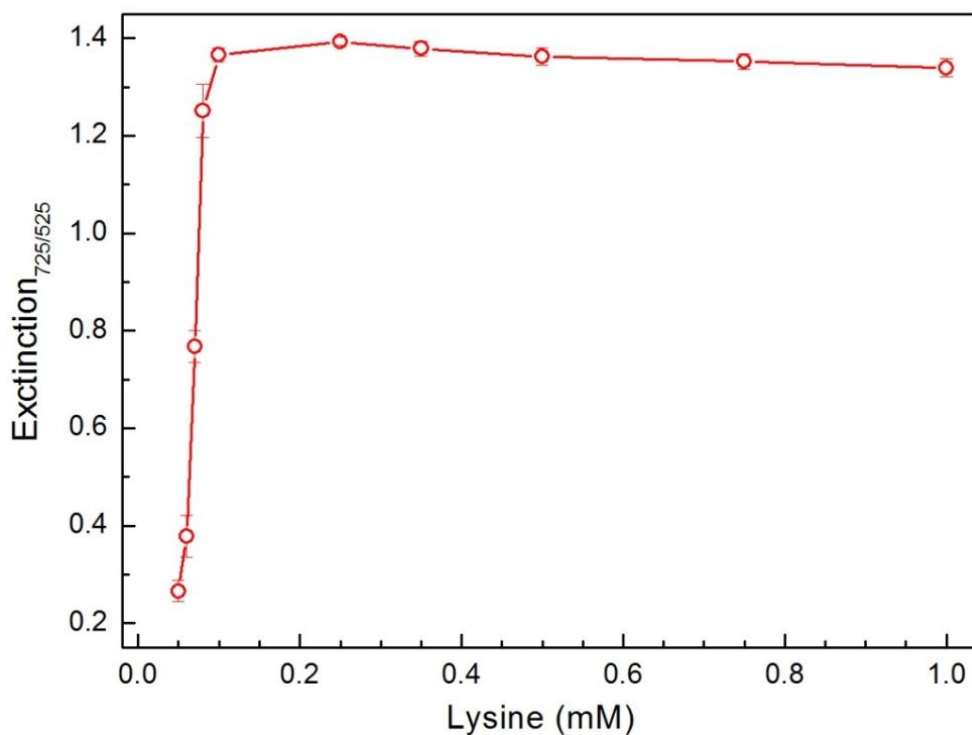


Figure 4.5. Effect of lysine concentration on the response ($\text{EX}_{725}/\text{EX}_{525}$) of the colorimetric assay (Hg^{2+} concentration is $10 \mu\text{M}$ in all measurements).

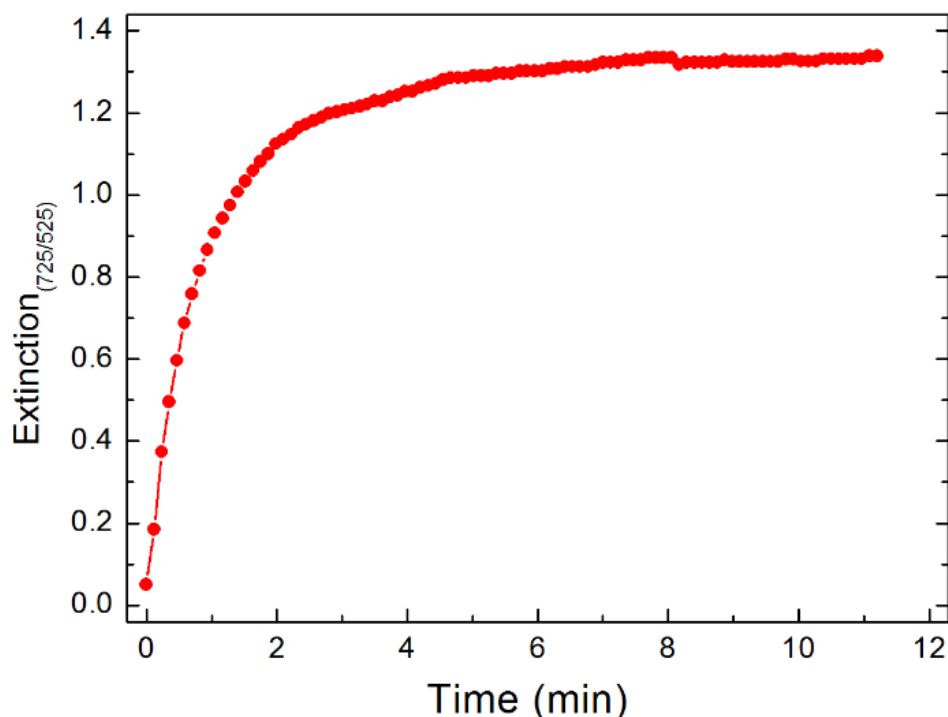


Figure 4.6. Change of the colorimetric array response with time.

To determine the sensitivity of the colorimetric assay, we tested several Hg^{2+} solutions, which had concentrations between 1 nM and 20 μM . As the concentration of the Hg^{2+} increases, the color of the AuNPs gradually changes from red to purple and finally to gray (Figure 4.7a), suggesting the Hg^{2+} concentration-dependent aggregation of AuNPs. The extinction spectra of solutions (Figure 4.7b) reveal that with increasing Hg^{2+} concentration, extinction at 525 nm decreased and extinction at 725 nm increased, which also indicates gradually increasing aggregation of the particles. Figure 4.7c shows the concentration-dependent colorimetric response ($\text{Ex}_{725}/\text{Ex}_{525}$ values) of the assay. In the Hg^{2+} concentration range of 1 nM to 1 μM , $\text{Ex}_{725}/\text{Ex}_{525}$ values regularly increase. Further increasing the Hg^{2+} concentration up to 20 μM only slightly increased the colorimetric response. The response of the assay is highly linear, with a linear regression correlation coefficient of 0.996 at the Hg^{2+} concentration range of 1 nM to 1 μM (Figure 4.8).

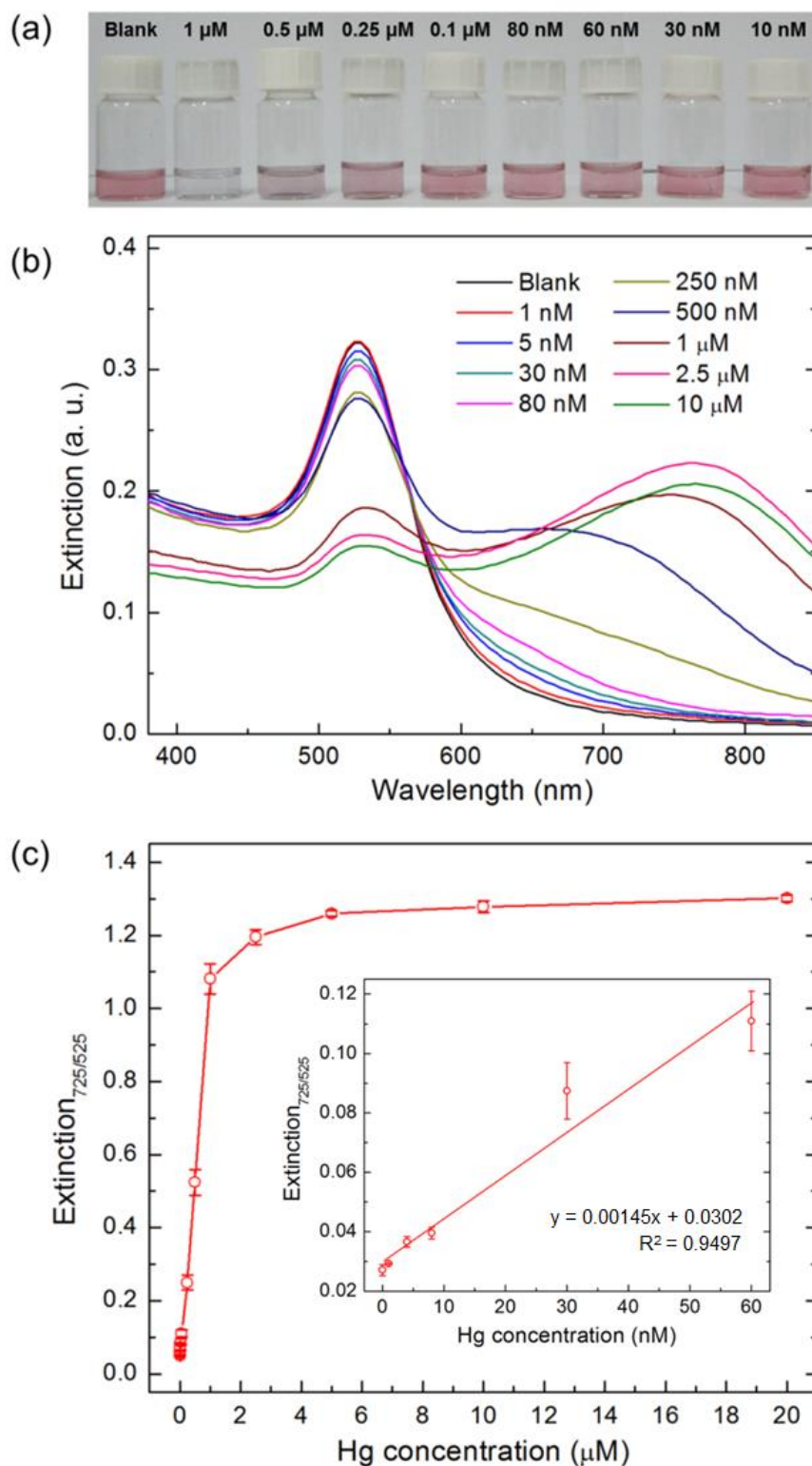


Figure 4.7. Colorimetric sensing of Hg^{2+} . (a) Photographs of AuNP solutions with different Hg^{2+} concentrations. (b) Extinction spectra of the solutions. (c) Response ($\text{Ex}_{725}/\text{Ex}_{525}$) of the colorimetric assay against increasing Hg^{2+} concentrations. Inset shows the response linearity of the assay at low Hg^{2+} concentrations (Lysine concentration is 0.4 mM in all measurements).

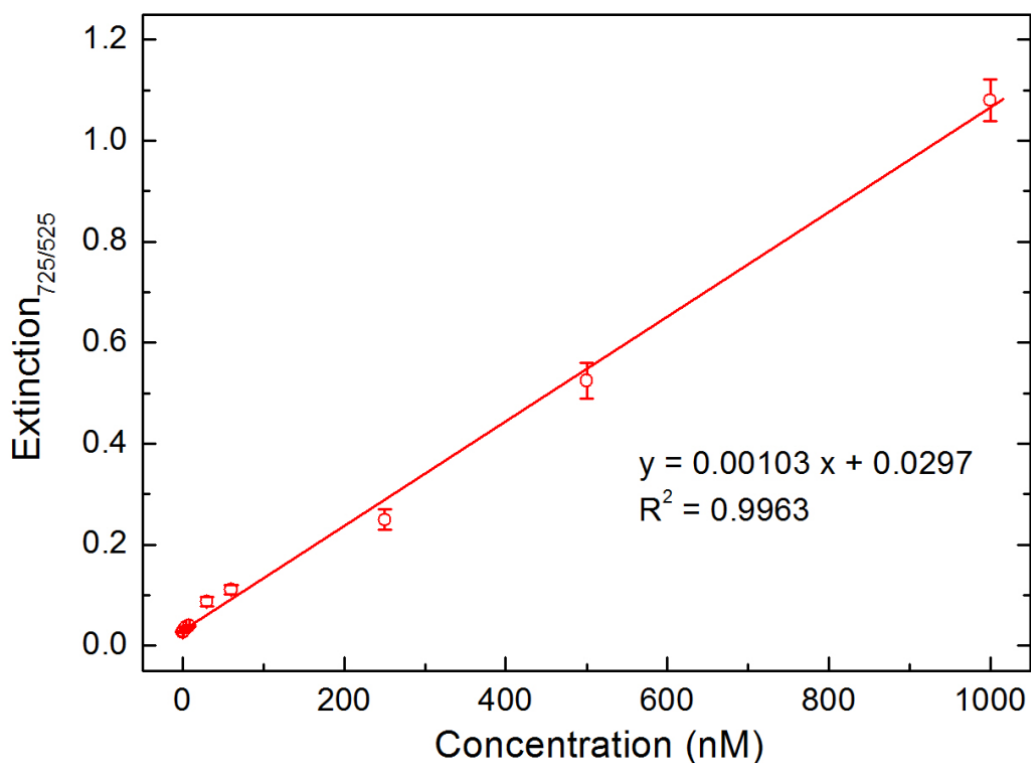


Figure 4.8. Linearity of the array response against Hg^{2+} in distilled water.

The lowest detectable Hg^{2+} concentration using this assay was calculated to be 2.9 nM, which is significantly below the allowed Hg^{2+} concentration limit (10 nM) defined by EPA. Figure 4.7c inset shows the response of the assay at the low Hg^{2+} concentration range (1 to 60 nM). The assay also demonstrated good separation and linear response at Hg^{2+} concentrations of around 10 nM. Our simple assay is one of the most sensitive and rapid colorimetric Hg^{2+} sensors compared with many metal nanoparticle-based methods (Table 4.1).

Table 4.1. Comparison of our assay with other colorimetric approaches.

Probe	Read out	Surface modification	LOD (nM)	Selectivity	Time (min)	Ref
DNA-AuNPs	Absorption	Yes	100	Hg ²⁺	10	[18]
DNA-AuNPs	Fluorescence	Yes	1	Hg ²⁺	10	[21]
DNA-AuNPs	Absorption	Yes	10	Hg ²⁺	30	[22]
DNA-AuNPs	Absorption	Yes	10	Hg ^{2+ a}	20	[23]
DNA-AuNPs	Fluorescence	Yes	40	Hg ²⁺	30	[133]
Dye-DNA-AuNPs	Fluorescence	Yes	25	Hg ²⁺	1	[27]
Citrate-AgNPs-DNA	Absorption	No	17	Hg ²⁺	5	[24]
Citrate-AuNPs-Aptamer	Absorption	No	0.6	Hg ²⁺	10	[134]
Peptide-AuNPs	Absorption	Yes	26	Multiple ions	1	[25]
BSA-AuNCs	Fluorescence	No	0.5	Hg ²⁺	<1	[26]
Dye-PEG-AuNPs	Fluorescence	Yes	2.3	Hg ²⁺	1	[28]
QA-AuNPs	Absorption	Yes	30	Hg ²⁺	<1	[29]
MPA-AuNPs	Fluorescence	Yes	5	Hg ^{2+ a}	10	[30]
MPA-AuNPs	Absorption	Yes	100	Hg ^{2+ a}	60	[31]
MPA-homocysteine-AuNPs	Absorption	Yes	10	Hg ^{2+ a}	30	[32]
Alkanethiol-AgNPRs	Absorption	Yes	3.3	Hg ²⁺	15	[6]
NTA-AuNPs-Tris	Absorption	Yes	7	Hg ²⁺	60	[135]
Tween20-AuNPs	Absorption	Yes	5	Hg ^{2+ a} , Ag ^{+ a}	30	[15]
Tween20-AuNPs	Absorption	Yes	100	Hg ^{2+ a} , Ag ^{+ a}	5	[124]
Citrate-AuNPS-Urine	Absorption	Yes	50	Hg ²⁺	30	[125]
Citrate-AuNPs-Lysine	Absorption	No	2.9	Hg ²⁺	5	This work

^a Masking agents were added to eliminate interfering metal ions

4.1.4. Selectivity of the Colorimetric Assay

To determine the selectivity of the colorimetric assay against Hg^{2+} , 13 other metal ions (Cu^{2+} , Ni^{2+} , Pb^{2+} , Co^{2+} , Zn^{2+} , Ca^{2+} , Al^{3+} , K^+ , Fe^{3+} , Cd^{2+} , Ag^+ , Na^+ , Au^{3+}) were tested in the assay. Figure 4.9 shows the response of the colorimetric assay against competing metal ions (50 μM) and Hg^{2+} (1 μM) in the presence or absence of lysine. In the absence of lysine none of the metal ions significantly changed the $\text{EX}_{725}/\text{EX}_{525}$ value of the AuNP solutions. On the other hand, after lysine addition, Hg^{2+} led to a large increase in the $\text{EX}_{725}/\text{EX}_{525}$ value of the assay, as expected. Except for Ag^+ , none of the metal ions interacted with the colorimetric assay. However, Ag^+ ions resulted in a slight increase in the colorimetric assay response. Yet the response was considerably lower than the response of the assay against Hg^{2+} ions although the concentration of Ag^+ ions was 50 fold higher than the concentration of Hg^{2+} ions. The reason for the slight colorimetric response of Ag^+ ions may be because of their spontaneous reduction tendency on the surface of citrate-capped AuNPs as for the Hg^{2+} ions [124]. However, interaction between the amino functionalities of lysine and soft Ag^+ ions can be expected to be much weaker than the interaction between lysine and hard Hg^{2+} ions. Therefore, the colorimetric assay gave only a slight response against Ag^+ ions even at a very high ion concentration, and it shows a high selectivity for the Hg^{2+} ions. To further demonstrate the selectivity of the colorimetric assay, we measured its response against 1 μM of Hg^{2+} in the presence of a mixture of the other 13 metal ions (each metal ion concentration was 10 μM) (Figure 4.9). The response of the assay was only slightly reduced in this complex environment, indicating the excellent selectivity of the colorimetric assay for Hg^{2+} ions.

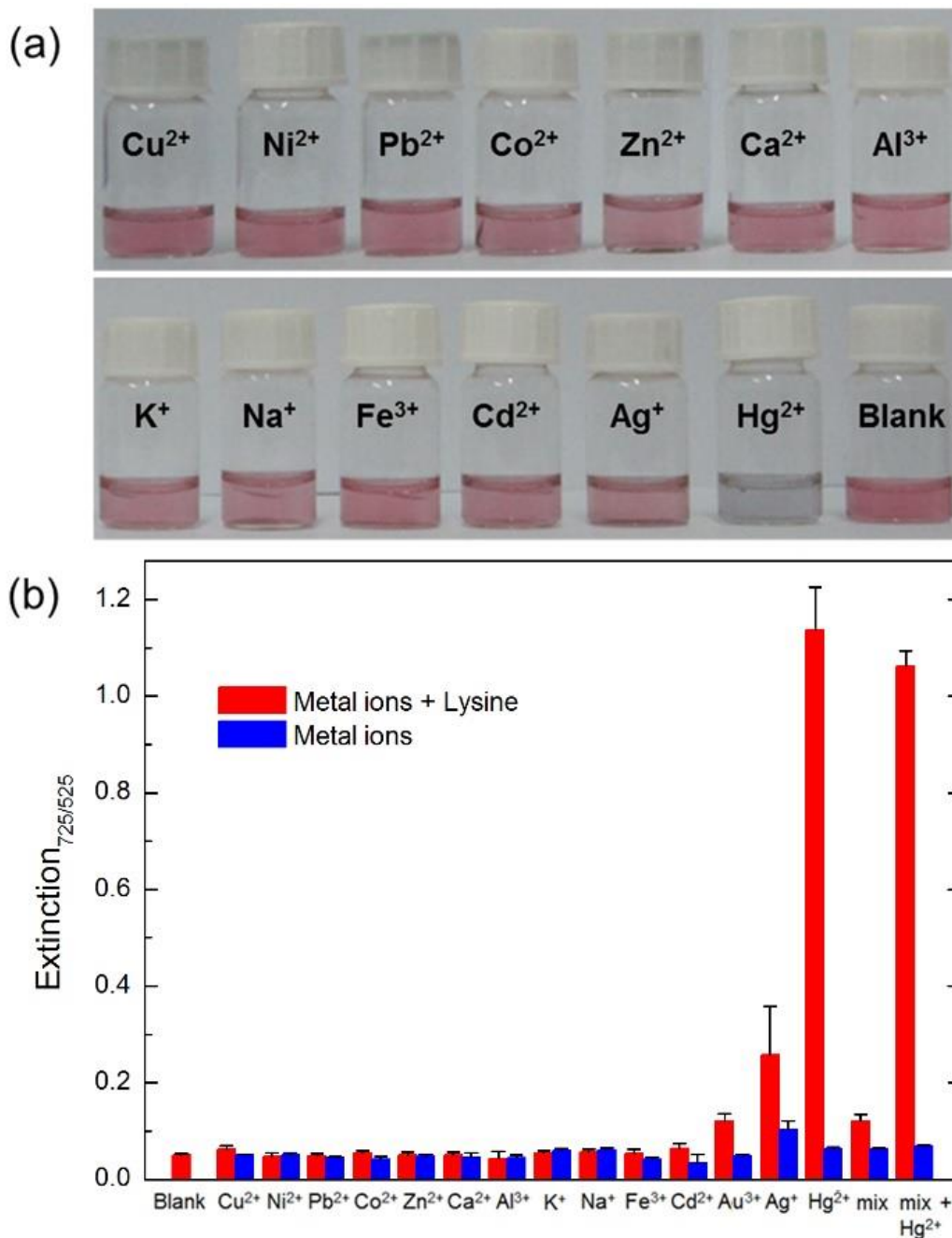


Figure 4.9. Selectivity of the sensor. (a) Photographs showing the AuNP solutions in the presence of lysine (0.4 mM) and several competing metal ions (50 μ M) or Hg^{2+} (1 μ M). (b) Response ($\text{EX}_{725}/\text{EX}_{525}$) of the colorimetric assay against several competing metal ions (50 μ M) or mixture of competing metal ions (Cu^{2+} , Ni^{2+} , Pb^{2+} , Co^{2+} , Zn^{2+} , Ca^{2+} , Al^{3+} , K^{+} , Na^{+} , Fe^{3+} , Cd^{2+} , Au^{3+} , Ag^{+}) (10 μ M) and Hg^{2+} (1 μ M) in the presence (0.4 mM) or absence of lysine.

4.1.5. Practical Application

To evaluate the applicability of the colorimetric assay to real samples, tap water (sampled from Beytepe, Ankara; see Table 4.2 for ion composition of the tap water) was spiked with Hg^{2+} and tested in the assay.

Table 4.2. Ion concentrations of tap water of Ankara^a.

Ion	Content (mg/L)
Ammonia	0.50
Nitrite	0.5
Nitrate	50
Sodium	200
Chloride	250
Sulphide	250
Floride	1.5

^aData was obtained in June 2013 (see ref. [136]).

Figure 4.10 shows the response of the colorimetric assay to tap water samples with Hg^{2+} concentrations of 1 nM to 1 μM . The sensor response linearly increased with increasing Hg^{2+} concentration in this concentration range (Figure 4.11). Sensor responses in distilled water and tap water are very similar, suggesting that the colorimetric assay can detect Hg^{2+} without being affected by the interfering tap water environment (other metal ions and organic contaminants). Accordingly, we calculated a limit of detection value (3.9 nM) for Hg^{2+} in tap water experiments similar to that in the experiments performed in distilled water. Figure 4.10b shows the response of the assay at low Hg^{2+} concentration range (2 to 100 nM). Even at low Hg^{2+} concentrations, the assay response demonstrated a high linearity ($R^2 = 0.99$). To further demonstrate the applicability of our assay in practical applications, we performed recovery experiments using spiked tap water samples with 5 nM of Hg^{2+} (Table 4.3). We observed an average recovery value of 97%, indicating that the colorimetric assay can be used for the detection of Hg^{2+} in real samples even at concentrations below the allowed Hg^{2+} concentration (10 nM) defined by the EPA. High recovery percentages even at very low Hg^{2+}

concentration and low standard deviation in the experiments indicate the high accuracy of our colorimetric assay.

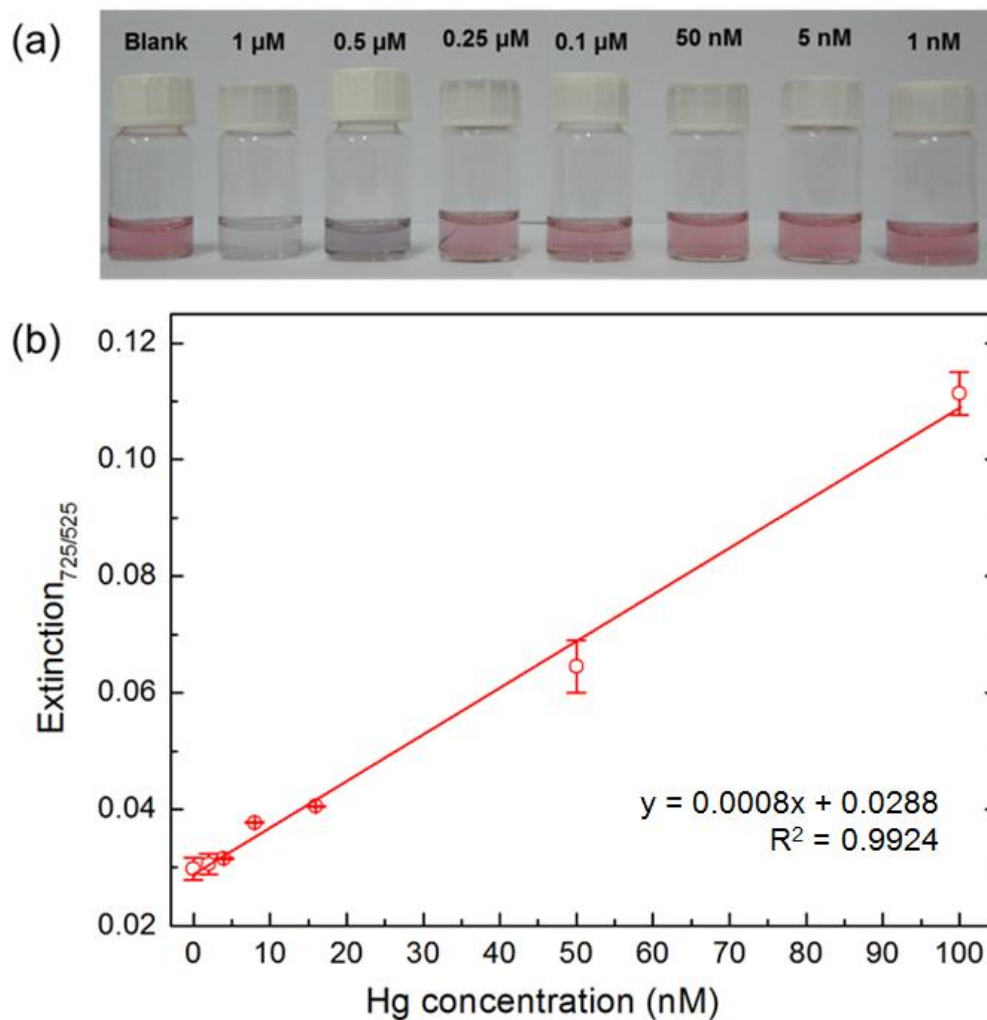


Figure 4.10. Colorimetric sensing of Hg^{2+} in tap water. (a) Photographs of AuNP solutions in tap water with different Hg^{2+} concentrations. (b) Colorimetric response of the assay against Hg^{2+} containing tap water samples at different concentrations (Lysine concentration is 0.4 mM in all measurements).

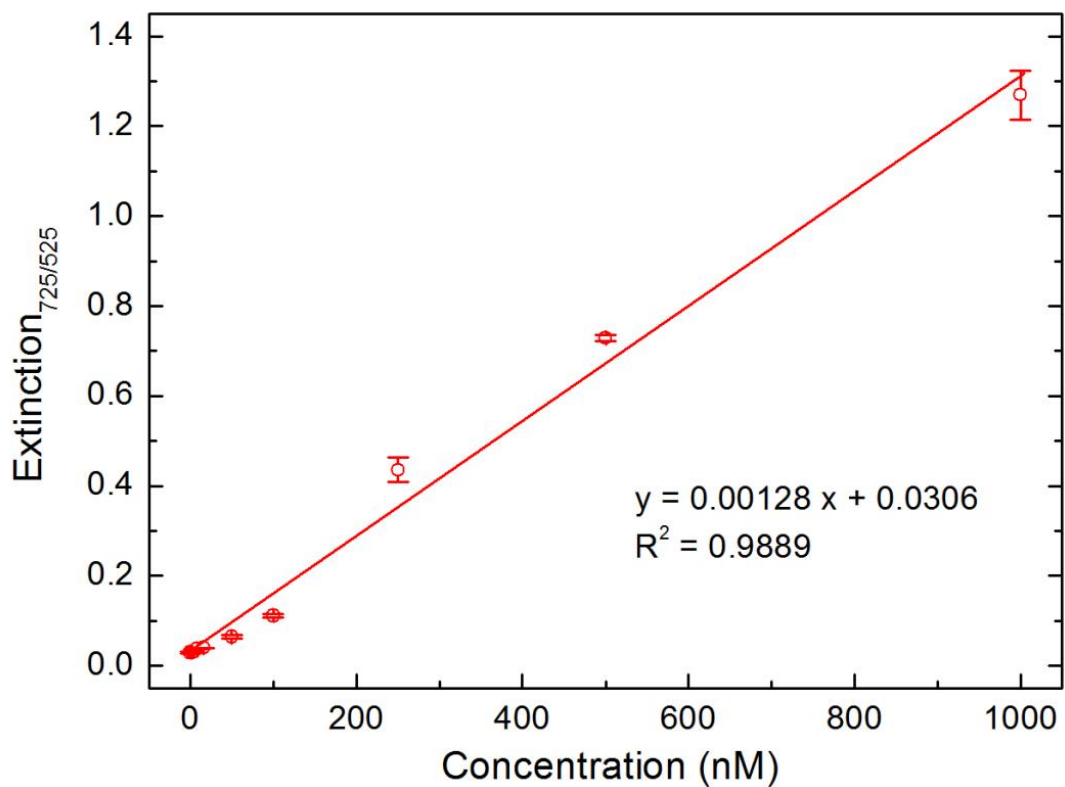


Figure 4.11. Linearity of the assay response against Hg^{2+} in tap water.

Table 4.3. Results of the recovery experiments performed in tap water samples.

Added (nM)	Found (nM)	Recovery (%)
5	4.72	94.5
5	4.99	99.8

4.2. Development of a Colorimetric Sensor Array for Detection of Multiple Metal Ions based on AuNPs and Amino Acids

Although many successful colorimetric probes have been reported for detection of single specific metal ions; colorimetric sensor arrays that are capable of detection of multiple metal ions are very rare [7,25,137]. One example of such colorimetric assays is reported by Kim et al. [7], which uses simple MUA-capped AuNPs for simultaneous detection of Hg^{2+} , Pb^{2+} , Cd^{2+} ions through ion-templated chelation process between these divalent metal ions and carboxyl groups of MUA molecules. However, the assay lacks of selectivity between the metal ions. Same problem is applicable for the other multiple metal ion colorimetric assays.

In this thesis, we describe a colorimetric sensor array that is capable of discrimination of seven metal ions (Hg^{2+} , Cd^{2+} , Fe^{3+} , Pb^{2+} , Al^{3+} , Cu^{2+} , and Cr^{3+}) simultaneously with excellent selectivity. The colorimetric assay is based on metal ion induced aggregation of MUA-capped AuNPs in the presence of different amino acids (lysine, cysteine, histidine, tyrosine, and arginine). Amino acids were used because they can bind AuNPs through their amino groups and also can form complexes with metal ions through their carboxyl and amino groups [7,17,138,139]. In addition, their side chains may also contain functional groups that have affinity to both AuNPs and metal ions; for example mercapto group of cysteine or second amino group of lysine. Accordingly, use of amino acids provides the selectivity by interacting AuNPs and metal ions with many different pathways. Each of the amino acids and MUA-capped AuNPs forms a distinct sensor element of the colorimetric array. We observed that presence of amino acids could either enhance or diminish the metal induced aggregation. Aggregation of AuNPs changes the color of nanoparticle solution from red to purple or blue [13]. Therefore, by analyzing the combinatorial colorimetric response (e.g., using hierarchical cluster analysis or simply by naked eye) of the each sensor element, it is possible to discriminate all of the seven metal ions tested in this study.

4.2.1. Amino Acid Binding onto the MUA-capped AuNP Surface

The binding ability of amino acids onto the surface of MUA-capped AuNPs was investigated using Raman spectroscopy and zeta potential measurements. In order to obtain the Raman spectra, we incubated the AuNPs with amino acids for approximately 15 min and washed the AuNPs several times in order to remove the unbound amino acids. Then, we dried the solutions onto the glass substrates and collected Raman spectra of AuNPs. The Raman peaks corresponding to the organic groups [140] (e.g., $-\text{CH}_2-$ and $-\text{COOH}$) increased significantly after interacting the AuNPs with amino acids (Figure 4.12) indicating the amino acid binding to the AuNP surface.

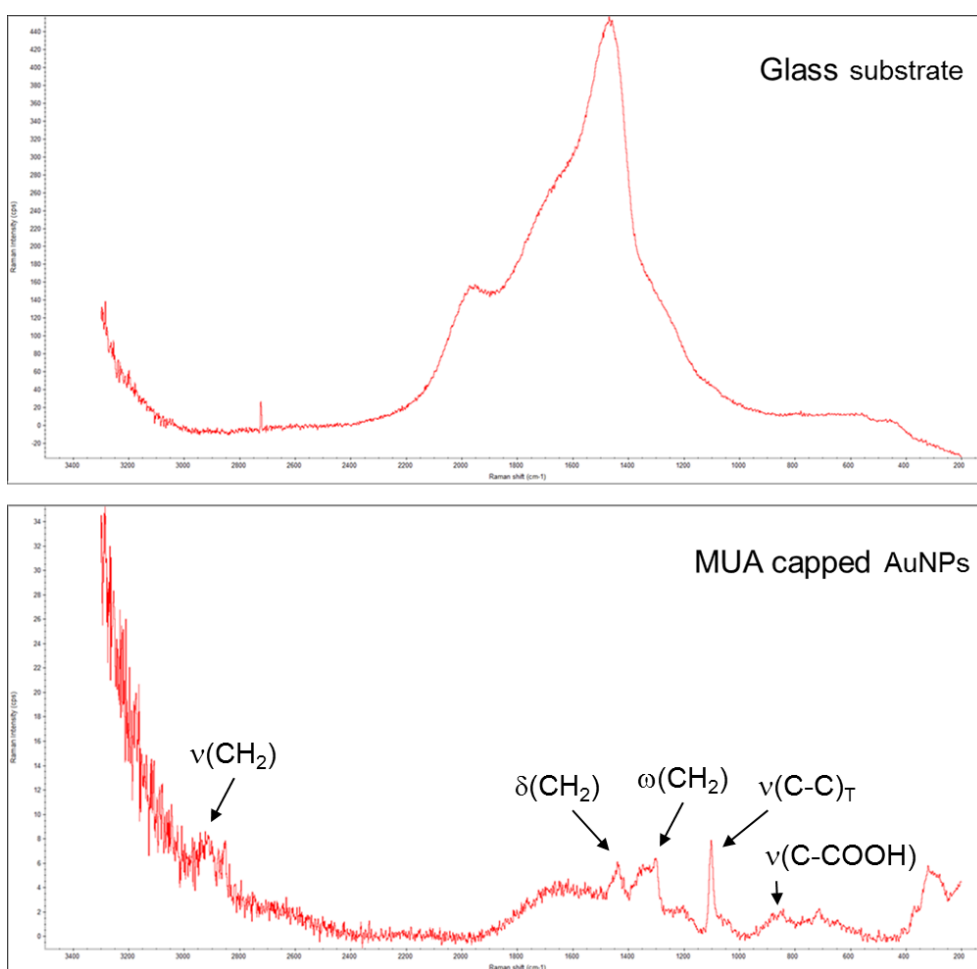


Figure 4.12. Raman Spectra of glass substrate and MUA capped AuNPs and amino acid treated AuNPs which were dried on glass substrates.

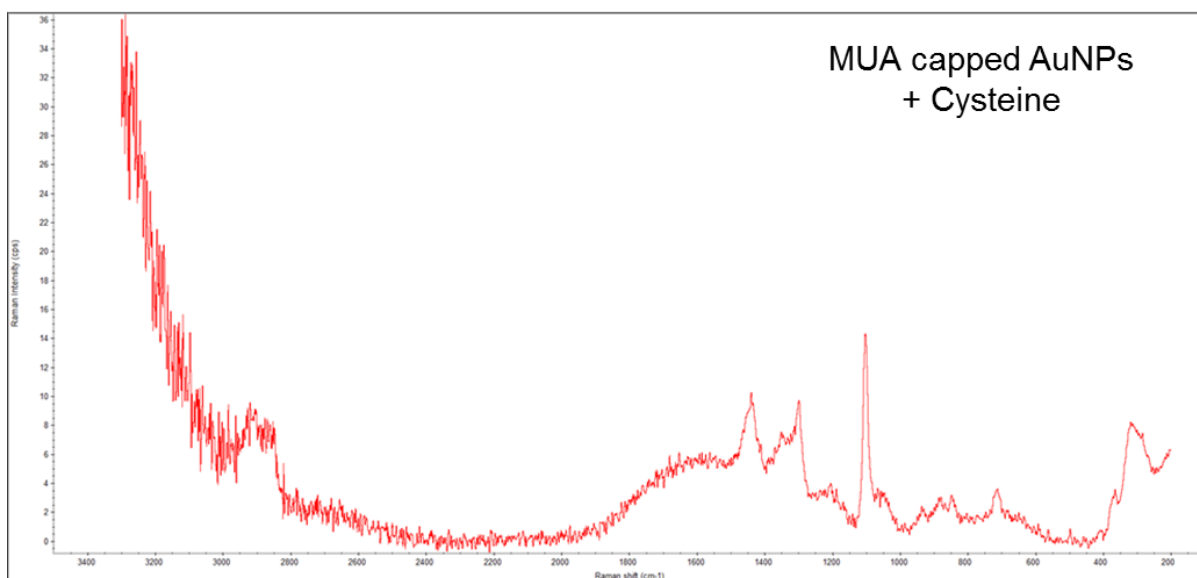
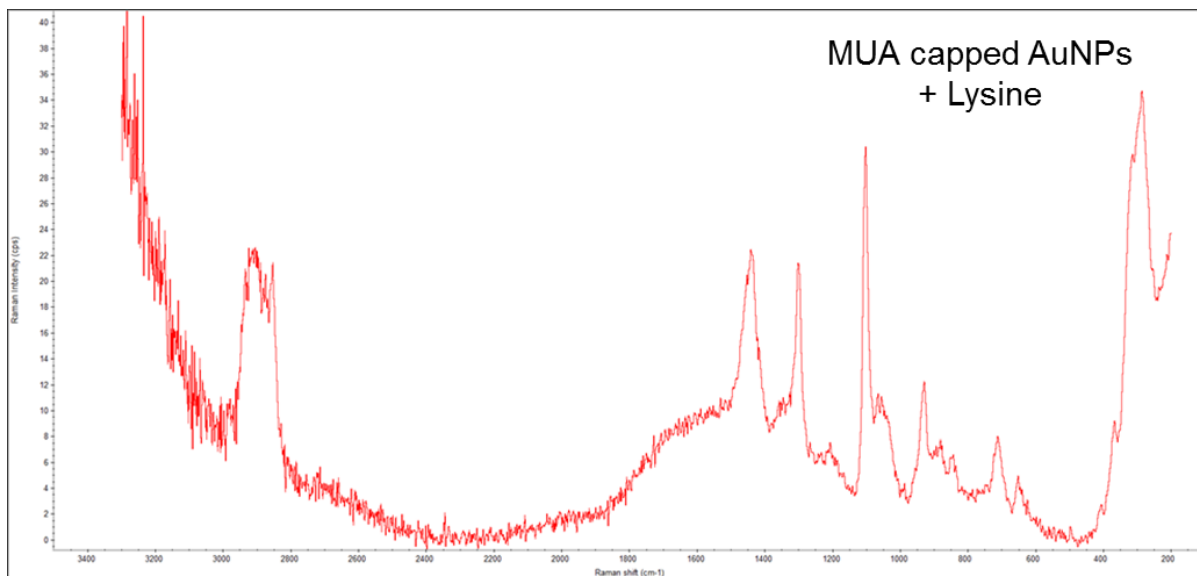


Figure 4.12. Cont'd.

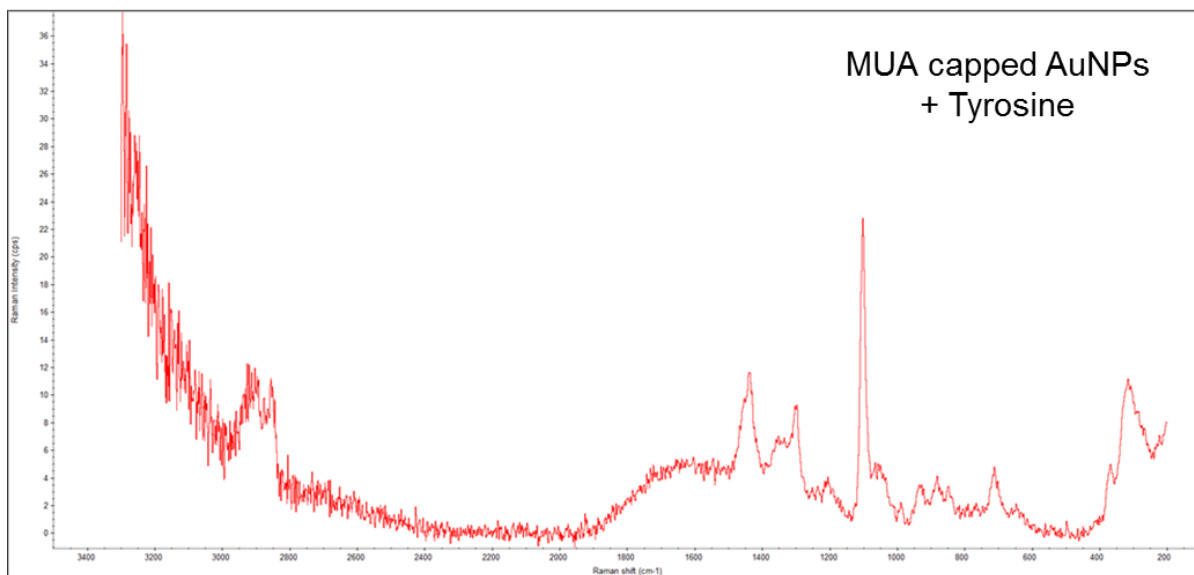
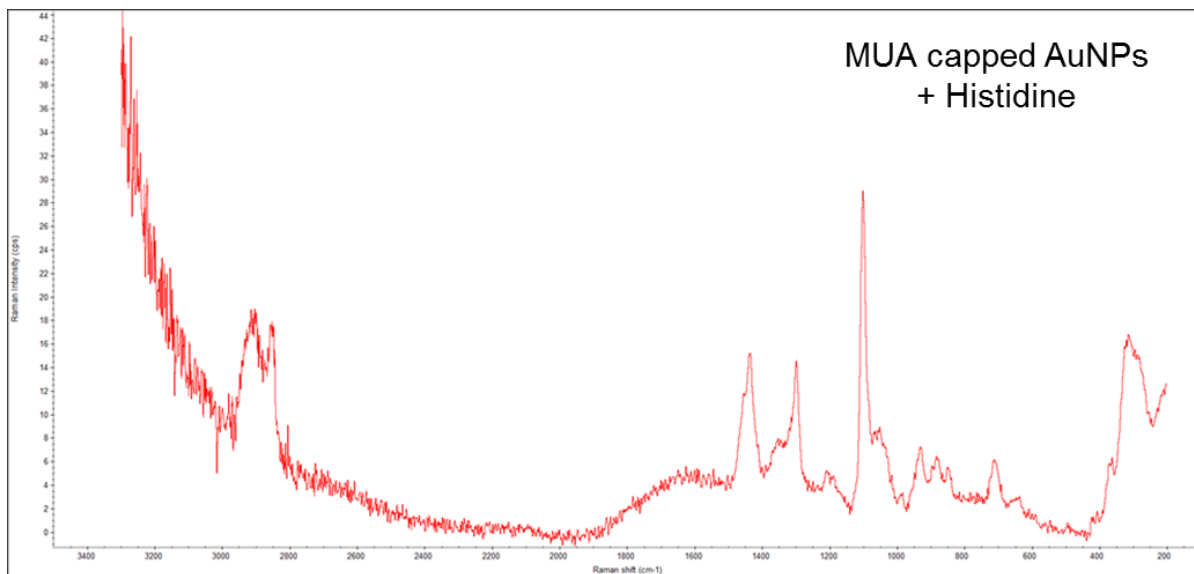


Figure 4.12. Cont'd.

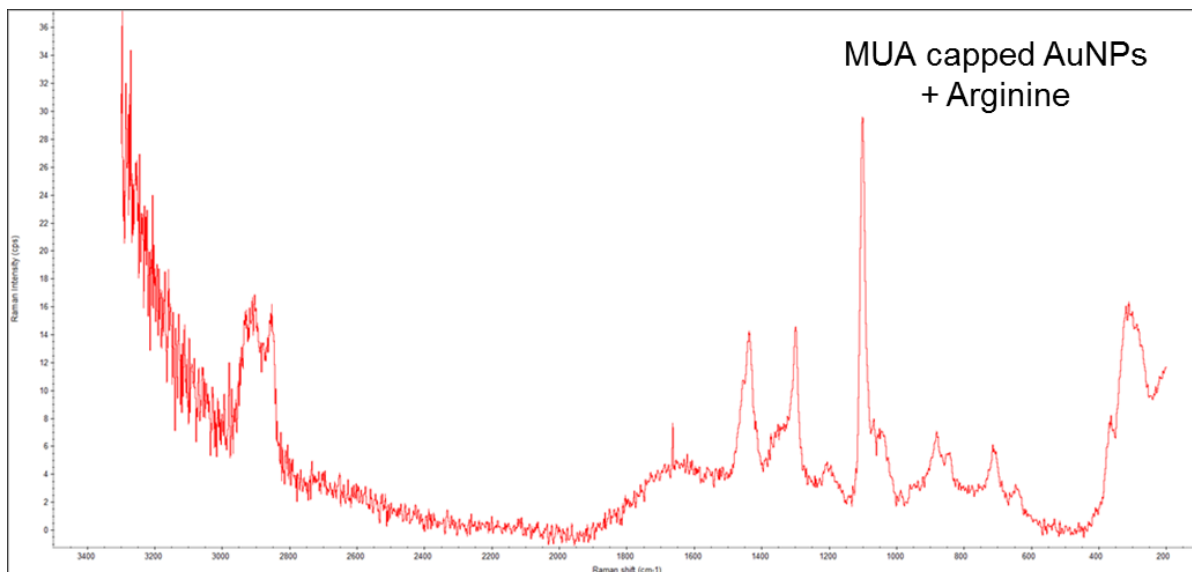


Figure 4.12. Cont'd.

In addition, zeta potential measurements showed that after amino acid treatment zeta potential of the AuNPs become more negative which also points out the amino acid binding to the surface (Table 4.4). Amino acids can easily bind onto the AuNP surfaces through their amino groups [141].

Table 4.4. Zeta potentials of MUA capped AuNPs before and after interacting with different amino acids.

Sample	Zeta potential (mV)
MUA capped AuNPs	-12.3 ± 2.0
Lysine + MUA capped AuNPs	-14.1 ± 2.2
Cysteine + MUA capped AuNPs	-14.2 ± 0.9
Histidine + MUA capped AuNPs	-13.7 ± 0.6
Tyrosine + MUA capped AuNPs	-16.2 ± 1.2
Arginine + MUA capped AuNPs	-16.0 ± 1.4

4.2.2. Sensing Mechanism

In the colorimetric assay, many different interactions between AuNPs, amino acids, and metal ions are possible (Figure 4.13). The results of Raman spectroscopy and Zeta potential measurements indicated that amino acids can bind to the MUA-capped AuNP surfaces and form mixed ligand surfaces. Accordingly, we considered that some of the amino acids attached to the surface of AuNPs and some are free in the solution and we proposed the following mechanisms.

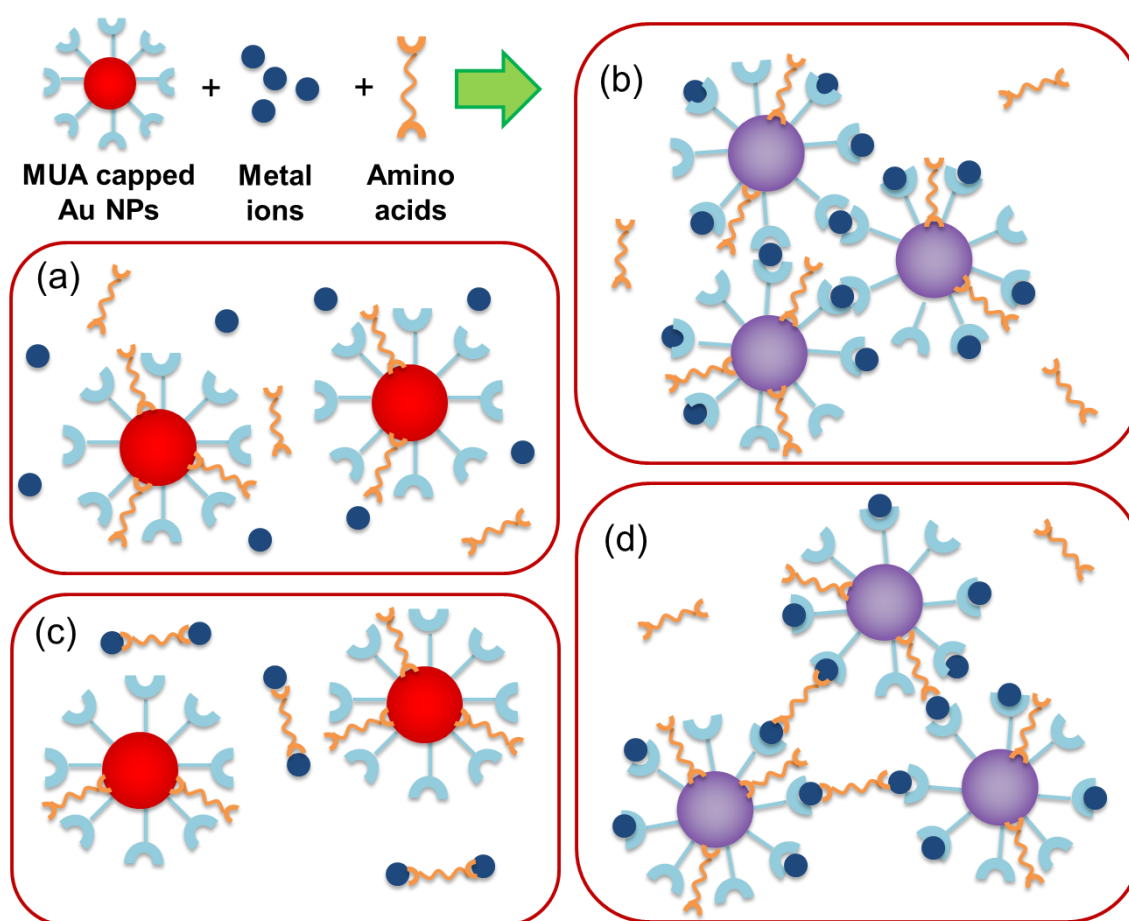


Figure 4.13. Schematic Representation of Proposed Metal Ions, Amino Acids, and AuNP Interactions: (a) No interaction, (b) Metal Ions Induce the Aggregation of AuNPs, (c) Amino Acids Interact with Metal Ions and Prevent Aggregation of AuNPs; and (d) Metal Ions and Amino Acids Co-Contribute the Aggregation of AuNPs

First of all, there may be no interaction with AuNPs and they are not aggregated (Figure 4.13a). Note that in this scenario, there may be interaction between amino acids and metal ions but in the both cases AuNPs well-dispersed in the solution. In the second mechanism, metal ions can induce the aggregation of AuNPs (Figure 4.13b) and result in a color change. Here, presence of amino acids has no effect on the colorimetric response. In the third scenario, amino acids can interact with metal ions that normally aggregate AuNPs and prevent the aggregation (Figure 4.13c). Lastly, metal ions and amino acids can co-contribute the aggregation of AuNPs (Figure 4.13d). Also, mechanisms related with amino acid induced aggregation of AuNPs can be proposed. However, in our experimental conditions, amino acids did not cause any aggregation of AuNPs in the absence of metal ions; therefore mechanisms related with amino acid induced aggregation are not applicable for our colorimetric array. In addition, structure of MUA-capped AuNPs and some possible interactions between functional groups and metal ions were demonstrated in Figure 4.14.

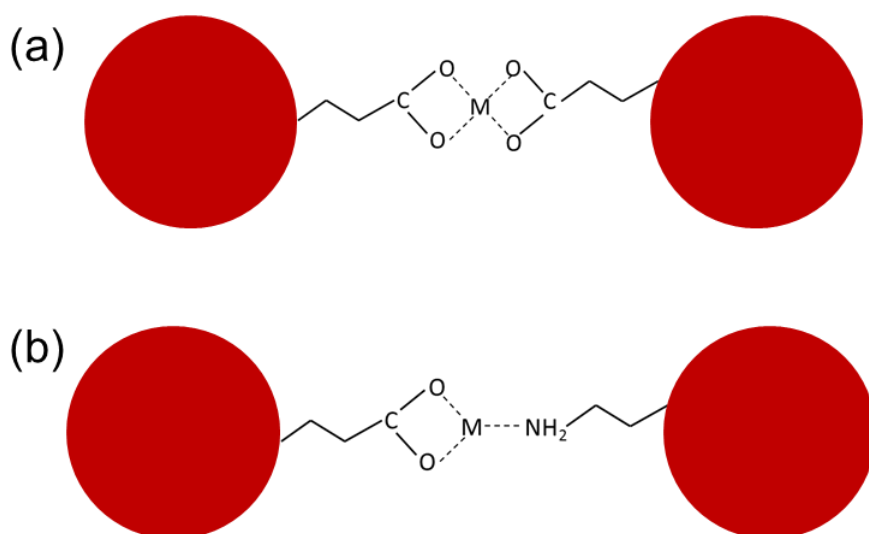


Figure 4.14. Structure of MUA capped AuNPs and some possible interaction between metal ions and amino acid or MUA molecules.

4.2.3. Colorimetric Sensing of Metal Ions Using the Colorimetric Array

Figure 4.15 shows the response (i.e., extinction at 625 nm/525 nm; Ex_{625}/Ex_{525}) of the colorimetric assay against seven metal ions (Hg^{2+} , Cd^{2+} , Fe^{3+} , Pb^{2+} , Al^{3+} , Cu^{2+} , and Cr^{3+}) at different concentrations between 2 and 50 μM . The representative UV-Vis spectra of AuNPs in the presence of Cd^{2+} (20 μM) and lysine are given in Figure 4.16. There was only a slight change in the UV-Vis spectra of AuNPs in the presence only Cd^{2+} and Ex_{625}/Ex_{525} value is almost same with the blank control. In the presence of both lysine and Cd^{2+} , on the other hand, absorption at around 625 nm increased, which indicates the aggregation of AuNPs [14] and accordingly colorimetric response is increased significantly which can be also observed from Figure 15. The aggregation of AuNPs was also investigated using TEM (Figure 4.17). In the absence of lysine and Cd^{2+} AuNPs were well separated and dispersed onto the TEM grid (Figure 4.17a); however in the presence of lysine and Cd^{2+} AuNPs aggregated and formed large clusters (Figure 4.17b). The average particles size of AuNPs was calculated to be 29.8 ± 5.3 nm from TEM images (Figure 4.17a).

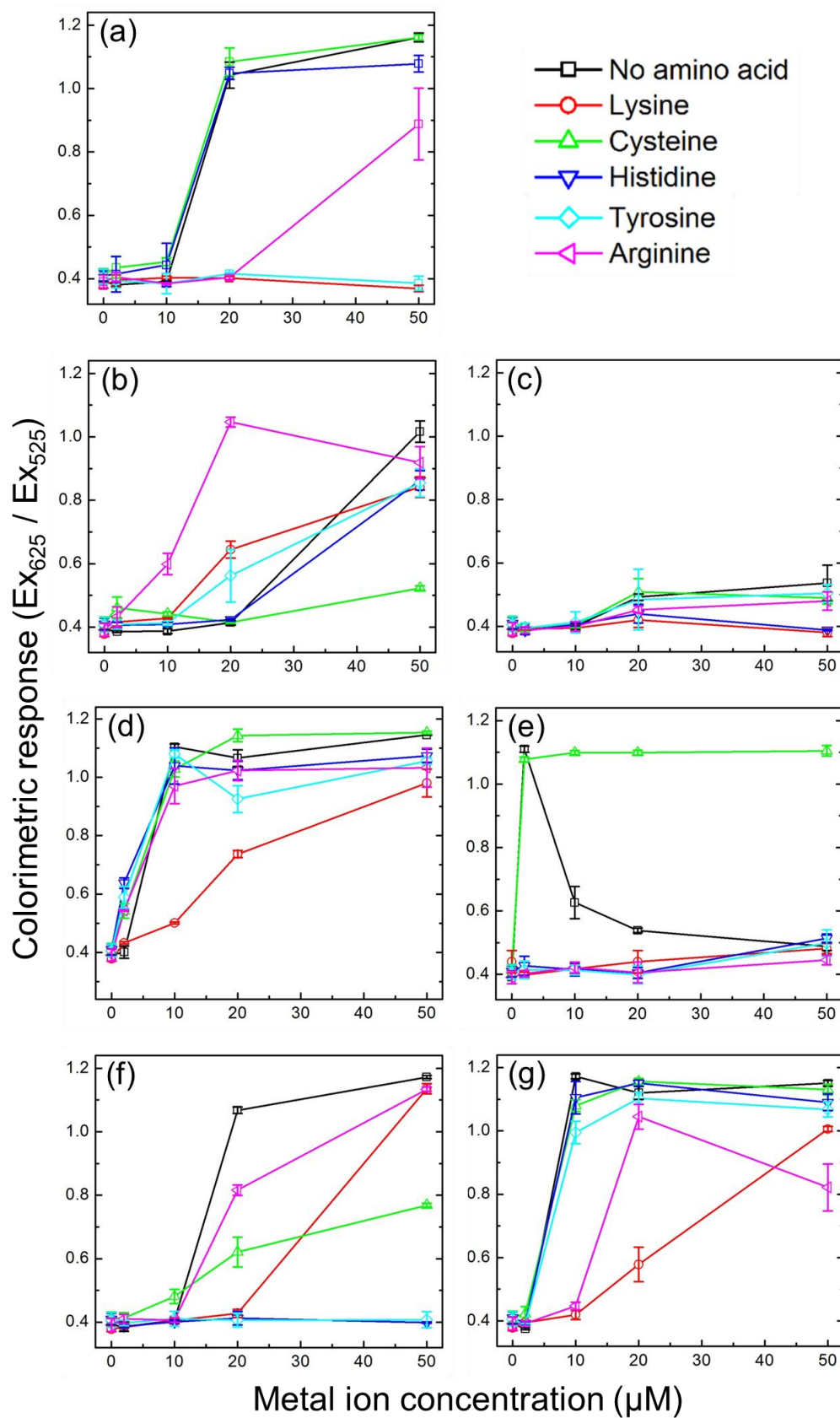


Figure 4.15. Effect of metal ion concentration (0-50 μM) on the response (EX_{625}/EX_{525}) of the colorimetric sensor array. (a) Hg^{2+} , (b) Cd^{2+} , (c) Fe^{3+} , (d) Pb^{2+} , (e) Al^{3+} , (f) Cu^{2+} , and (g) Cr^{3+} .

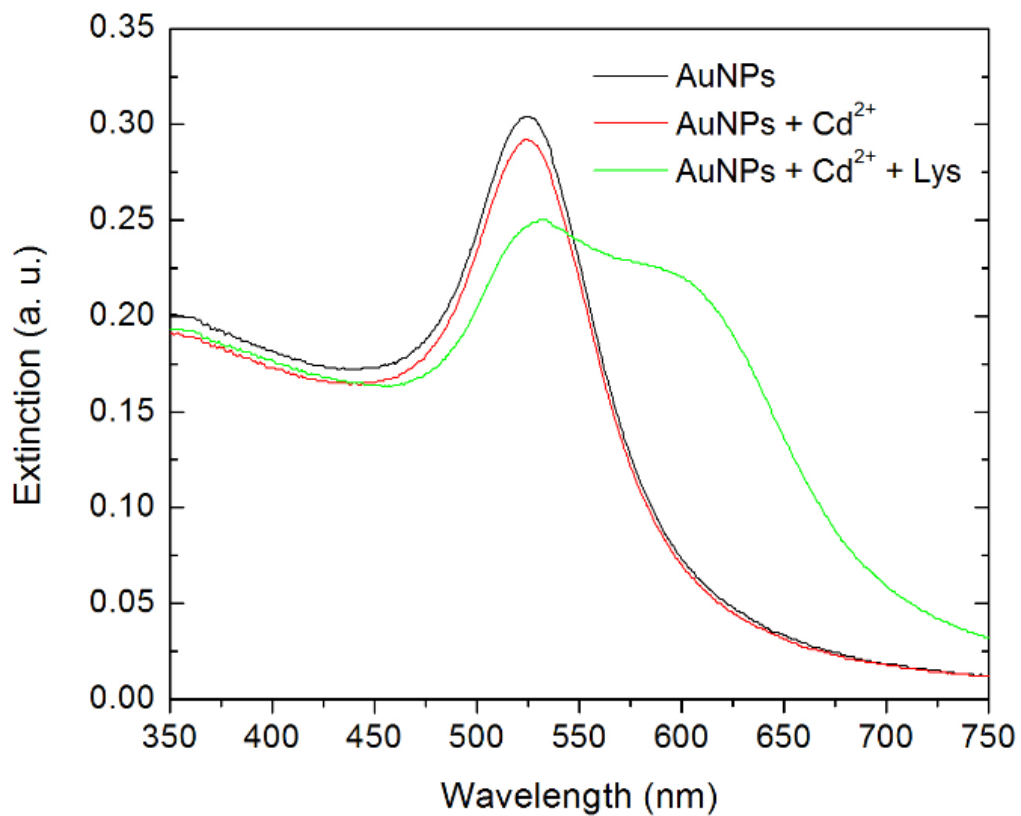


Figure 4.16. Representative UV-Vis spectra for AuNPs in the presence or absence of metal ions and amino acids.

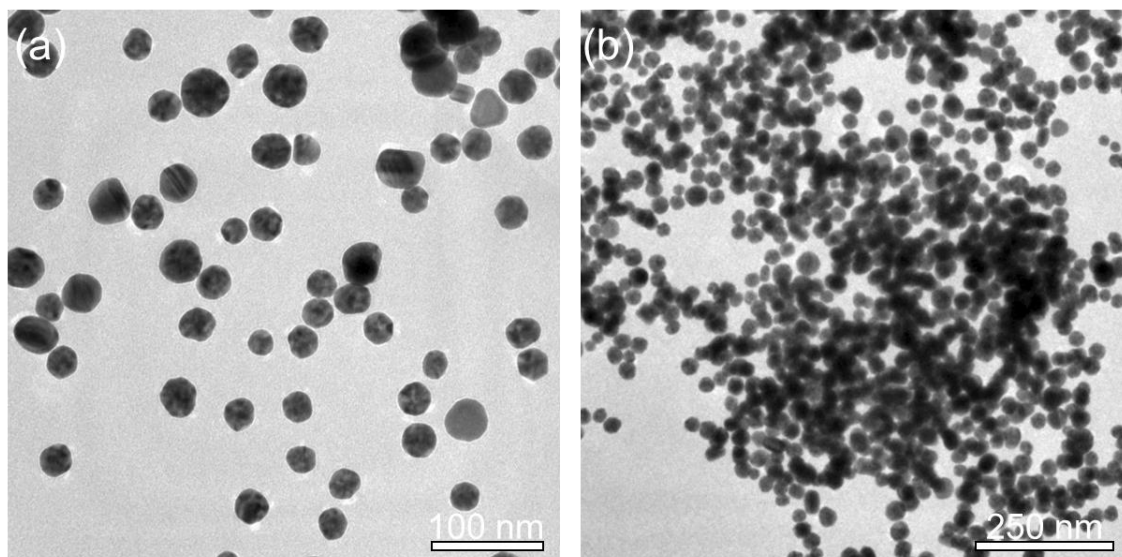


Figure 4.17. TEM images of well-dispersed as prepared MUA capped AuNPs (a) and aggregated AuNPs in the presence of 20 μM of Cd^{2+} and 200 μM of lysine.

AuNP concentration in the assay is 0.1 nM (which was calculated according to a previous report using the TEM size of particles [123]) and amino acid concentration is 50 μM for cysteine and 200 μM for other amino acids. Amino acid concentrations were selected to ensure no aggregation of AuNPs in the absence of metal ions (Figures 4.18 and 4.19). We studied the effect of amino acid concentration on the aggregation of AuNPs in the concentration range of 0 to 500 μM . It was observed that except cysteine none of the amino acids cause significant aggregation of AuNPs; $\text{Ex}_{625}/\text{Ex}_{525}$ values remained almost unaffected. For cysteine, on the other hand, a concentration-dependent aggregation and increase in $\text{Ex}_{625}/\text{Ex}_{525}$ value was observed. Nevertheless, up to a concentration of 100 μM cysteine did not cause significant aggregation. Accordingly, we selected the amino acid concentrations as 50 μM for cysteine and 200 μM for other amino acids (Figure 4.18). In addition, we studied the stability of the amino acid (above selected amino acid concentrations were used) added AuNP solutions for 1 h. No aggregation was observed even after 1 h (Figure 4.19).

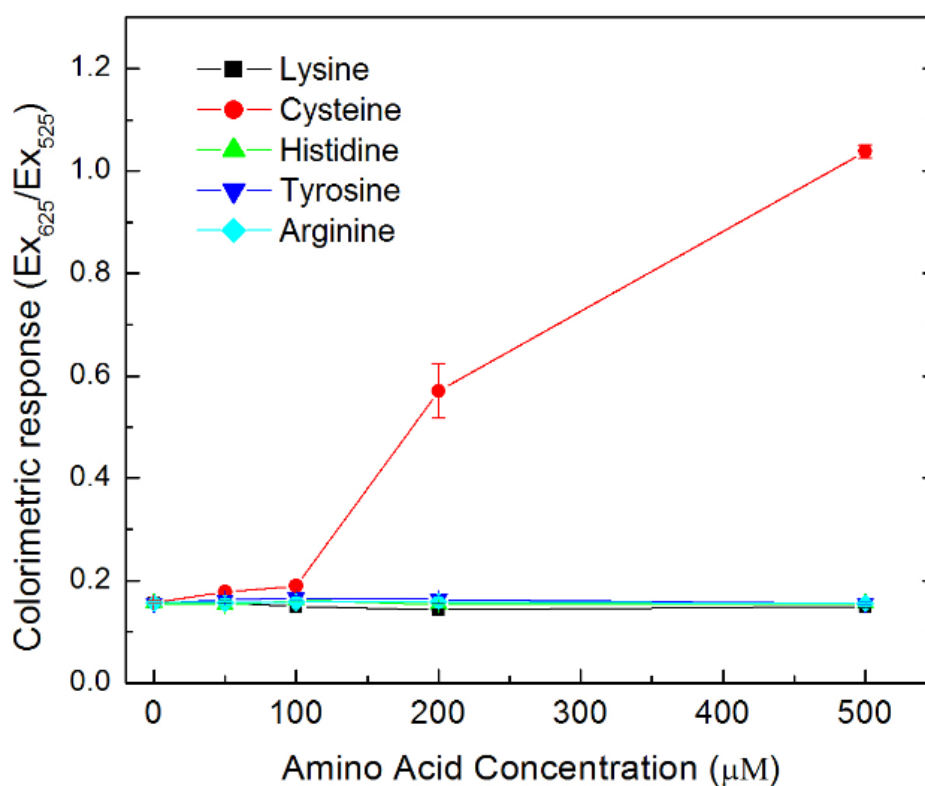


Figure 4.18. Colorimetric response ($\text{Ex}_{625}/\text{Ex}_{525}$) of AuNPs depending on amino acid concentrations in the absence of metal ions.

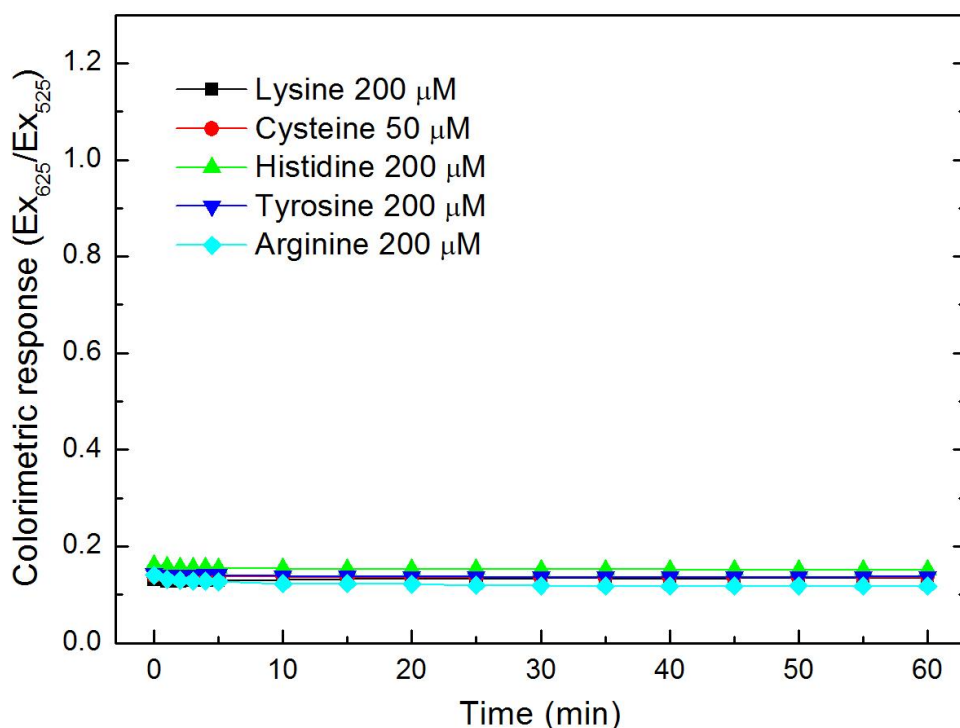


Figure 4.19. Time dependent colorimetric response (Ex_{625}/Ex_{525}) of AuNPs in the presence of amino acids at their concentrations used in the assay.

In addition, to investigate effect of salinity on the response of AuNPs, we added different amounts of phosphate buffered saline (PBS) (pH 7.4, 10 mM) on to the MUA-capped AuNPs. It was observed that above the final PBS concentration of 2 mM AuNPs aggregated and Ex_{625}/Ex_{525} values gradually increases with the increasing PBS solution (Figure 4.20). Nevertheless, the assay can be used in mild salinity conditions. Also, it is important to note that MUA-capped AuNPs were stable at least for two months at 4 °C.

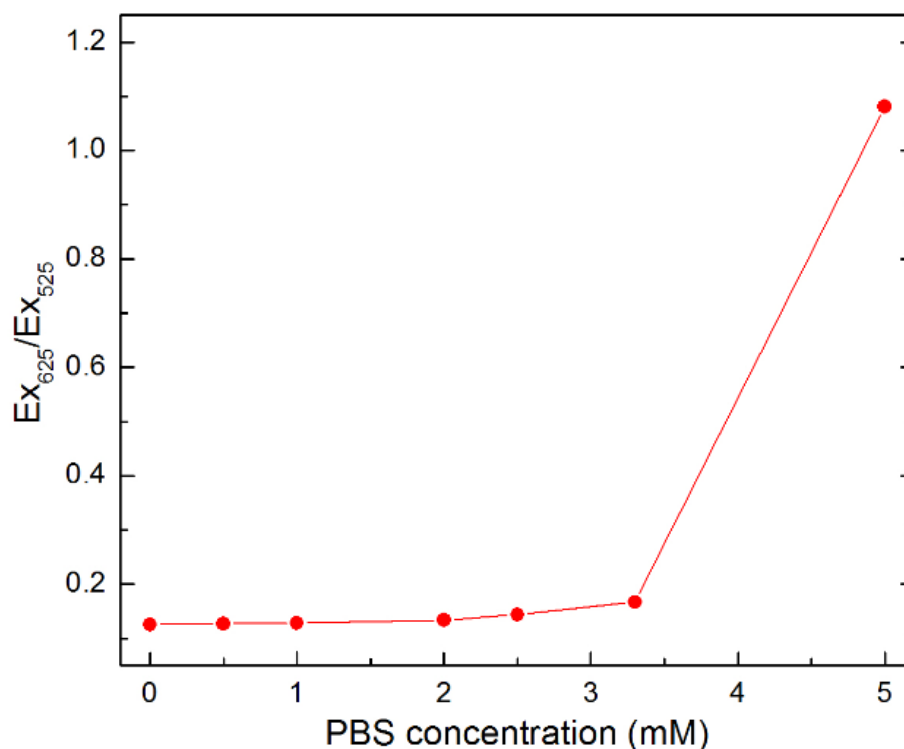


Figure 4.20. Effect of salinity on the stability of MUA capped AuNPs.

All proposed mechanisms of AuNP aggregation can be observed from Figure 4.15. For example, in the presence of lysine and 10 μM of Hg^{2+} , the response of the assay is similar to the blank (i.e., only AuNPs), which indicates that MUA-capped AuNPs are not aggregated (proposed mechanism a). In the presence of 20 μM of Cr^{3+} , AuNPs aggregate independent from the presence of cysteine, which can be given as an example of mechanism b. In the presence of 20 μM Cu^{2+} , AuNPs aggregate; however, when tyrosine is in the solution, no aggregation is observed and the response of the assay remains unchanged (proposed mechanism c). Lastly, in the absence of arginine 10 μM Cd^{2+} does not interact with MUA-capped AuNPs, whereas the aggregation is observed if arginine was added (proposed mechanism d).

The colorimetric sensor array enables naked eye discrimination of the seven metal ions. For instance, Figure 4.21 shows a representative photograph of the colorimetric array response against 20 μM of metal ions. As it can be clearly seen from the photograph each of the metal ions produce different color pattern. We observed that some metal ions produce more colorimetric response (i.e., changing

the original red color of AuNPs in more channels) than others. For example, Pb^{2+} and Cr^{3+} promoted aggregation at five of the six channels; on the other hand addition of Al^{3+} produced slight color change at only one of the channels. In addition, we tested nine more metal ions (Ag^+ , Ca^{2+} , Zn^{2+} , Co^{2+} , Ni^{2+} , Sr^{2+} , K^+ , Na^+ , and Fe^{2+}) and their mixtures with the assay. We observed that none of these metal ions produce significant color change (i.e., response) in any channel (Figure 4.22). It is important to note that, the response of the assay against the same metal ion with different valence numbers is different. For example, for ferric ions; Fe^{3+} produced colorimetric response in three channels of the assay (Figure 4.21), whereas, ferrous ions, Fe^{2+} did not produce any response (Figure 4.22). This result indicate that the colorimetric assay can be also used for discriminate the metal ions with different valence numbers.

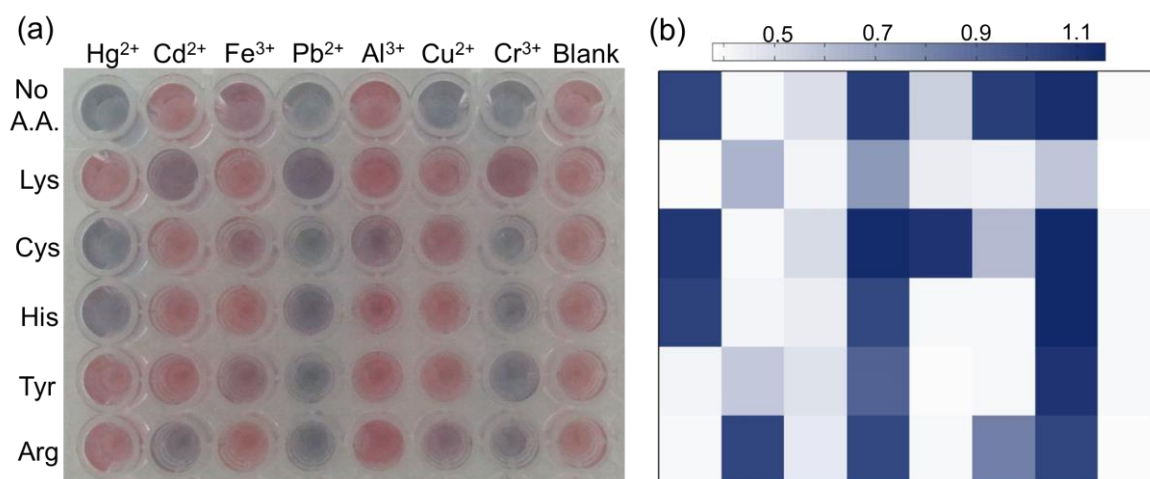


Figure 4.21. (a) Representative photograph of the colorimetric sensor array response against 20 μM of metal ions. (b) Blue-scale representation of the colorimetric sensor array response. White corresponds to no aggregation and blue corresponds to aggregation of AuNPs.

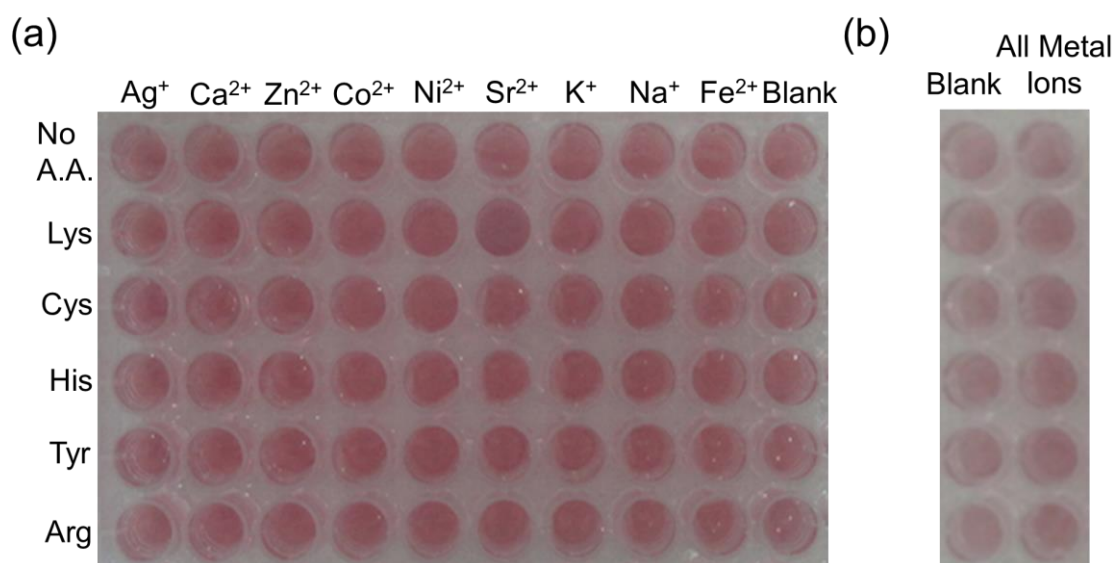


Figure 4.22. Representative photograph of the colorimetric sensor array response against (a) 20 μM of 9 nonresponsive metal ions with the assay (b) mixture of all metal ions.

The different affinity of the metal ions with the colorimetric sensor array can be explained with the difference in chelate formation capability of metal ions with carboxyl groups of MUA molecules and functional groups (amino, carboxyl, thiol etc.) of amino acids [142]. The colorimetric response of the array against metal ions in Figure 4.21a can be also expressed as color mapping using simple software for clearer representation. Figure 4.21b shows blue-scale color map of averaged response from three separate measurements of the array against 20 μM of each metal ion. The color map demonstrates the excellent discrimination among all tested metal ions.

To demonstrate reproducibility of the colorimetric sensor array response, a HCA was performed using the Euclidean algorithm [143,144]. Figure 4.23 shows the results of HCA analysis of the array response against metal ions at different concentrations for three separate experiments. The dendrogram demonstrates that at high metal ion concentrations (20 and 50 μM) all of the metal ions can be successfully identified without a mistake for all of the three separate experiments indicating the good reproducibility of the colorimetric sensor array. At low concentrations (2 and 10 μM), on the other hand, response of some metal ions interfere with each other; at 2 μM , only 2 of 7 metal ions, and at 10 μM , 4 of 7 metal ions can be identified.

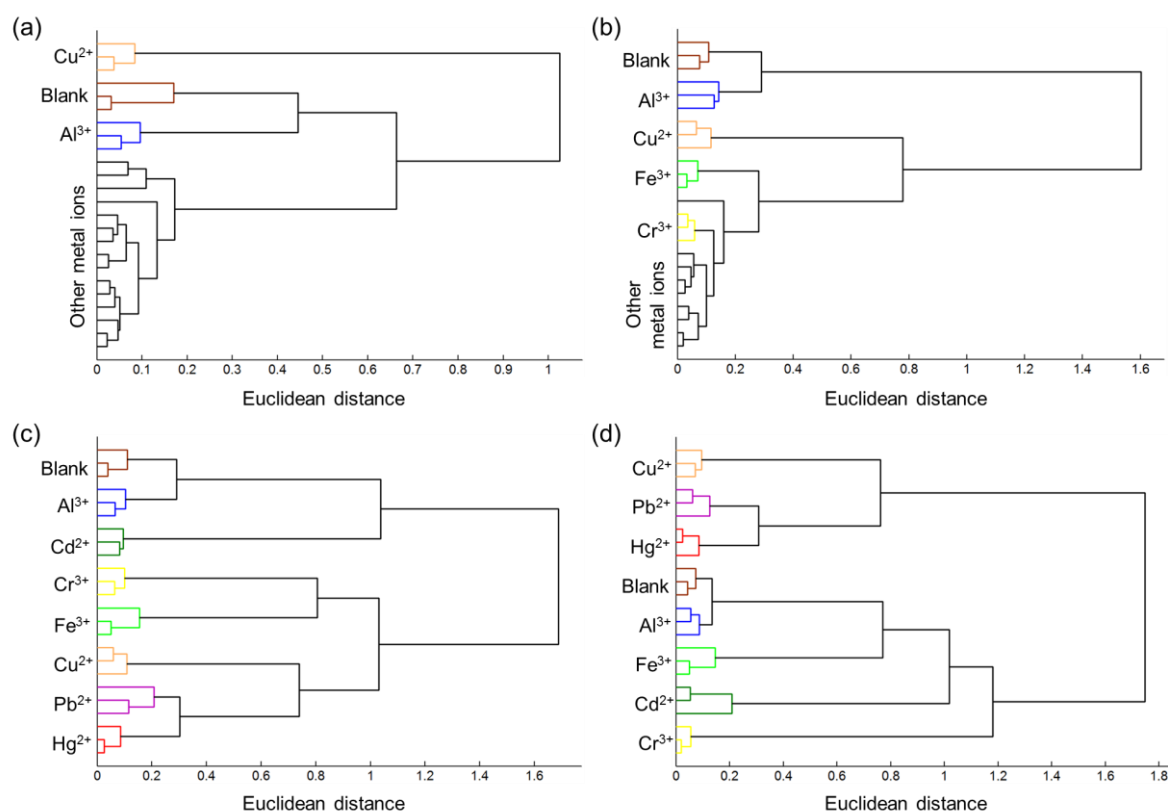
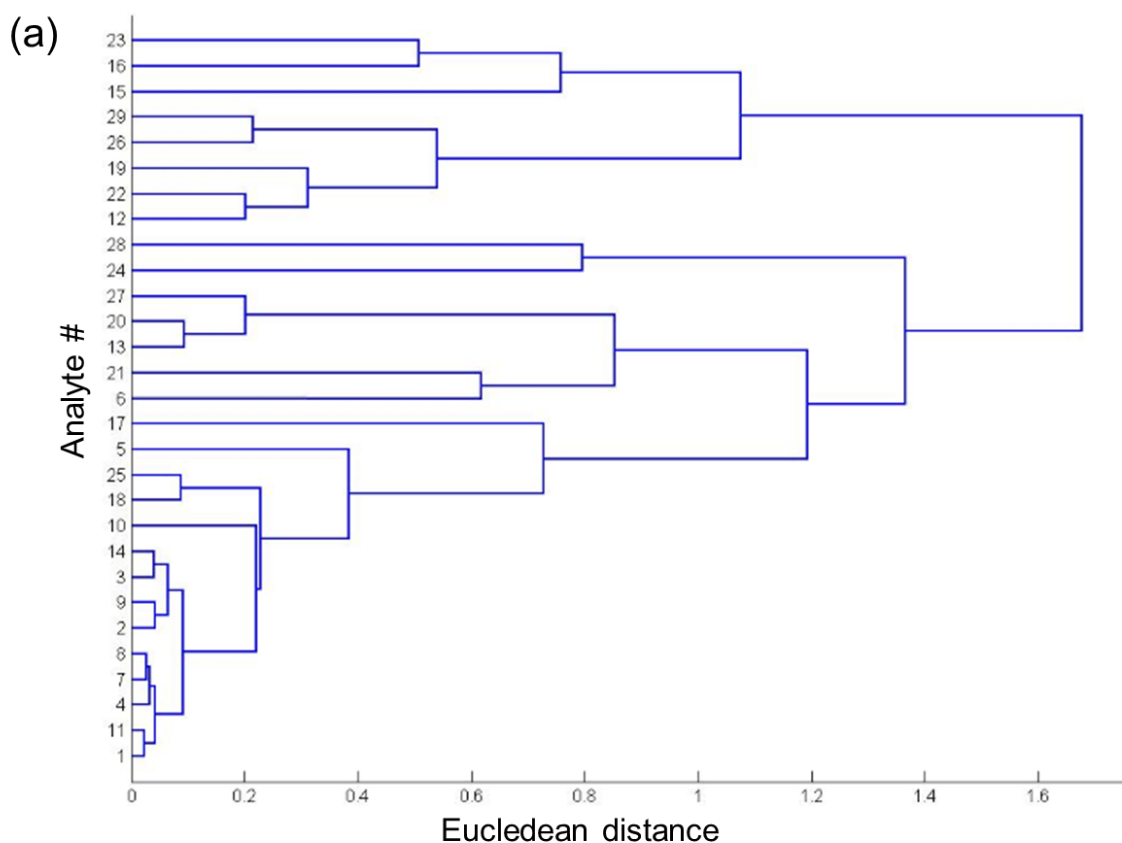


Figure 4.23. Hierarchical cluster analysis of colorimetric sensor array of seven different metal ions at different metal ion concentrations: (a) at 2 μM , (b) at 10 μM , (c) at 20 μM , and (d) at 50 μM .

In addition, we performed HCA analysis for the averaged response of all concentrations between 2 μM and 50 μM (using the data represented in Figure 4.15). There is good discrimination between most of the tested solutions especially at high metal ion concentrations (Figure 4.24). At low concentrations (2 and 10 μM) of weakly responsive metal ions (e.g., Hg^{2+} , Fe^{2+} and Cu^{2+}), discrimination (e.g., difference from the response of blank) is not very clear. Nevertheless, the colorimetric sensor array can identify most of the cases depending on the metal ion concentration and responsivity.



(b)

Analyte#	Metal ion	Analyte#	Metal ion	Analyte#	Metal ion
1	Blank	11	Cd ²⁺ (10 μM)	21	Cu ²⁺ (20 μM)
2	Hg ²⁺ (2 μM)	12	Fe ³⁺ (10 μM)	22	Cr ³⁺ (20 μM)
3	Cd ²⁺ (2 μM)	13	Pb ²⁺ (10 μM)	23	Hg ²⁺ (50 μM)
4	Fe ³⁺ (2 μM)	14	Al ³⁺ (10 μM)	24	Cd ²⁺ (50 μM)
5	Pb ²⁺ (2 μM)	15	Cu ²⁺ (10 μM)	25	Fe ³⁺ (50 μM)
6	Al ³⁺ (2 μM)	16	Cr ³⁺ (10 μM)	26	Pb ²⁺ (50 μM)
7	Cu ²⁺ (2 μM)	17	Hg ²⁺ (20 μM)	27	Al ³⁺ (50 μM)
8	Cr ³⁺ (2 μM)	18	Cd ²⁺ (20 μM)	28	Cu ²⁺ (50 μM)
9	Hg ²⁺ (10 μM)	19	Fe ³⁺ (20 μM)	29	Cr ³⁺ (50 μM)
10	Cd ²⁺ (10 μM)	20	Pb ²⁺ (20 μM)		

Figure 4.24. (a) Dendrogram showing the discrimination between all the tested metal ions at different concentrations. (b) Table listing the names and concentrations of analytes in (a).

4.2.4. Simultaneous Sensing of Multiple Metal Ions

Lastly, we tested binary and ternary mixtures of three metal ions (Hg²⁺, Cd²⁺, Fe³⁺) with the colorimetric assay. The assay successfully discriminates all combinations (Figure 4.25). One can expect that in the presence of two metal ions the response of the colorimetric assay should be the addition of their responses with the assay. Although this is true for most of the cases, we observed that for

some cases it is more complicated (Figure 4.25a). For example, when there was only Cd^{2+} present in the assay, color change in the lysine channel was observed. Interestingly, presence of Hg^{2+} prevents the colorimetric response of Cd^{2+} in this channel. Whereas, presence of Fe^{3+} has no effect on the colorimetric response of Cd^{2+} in the lysine channel.

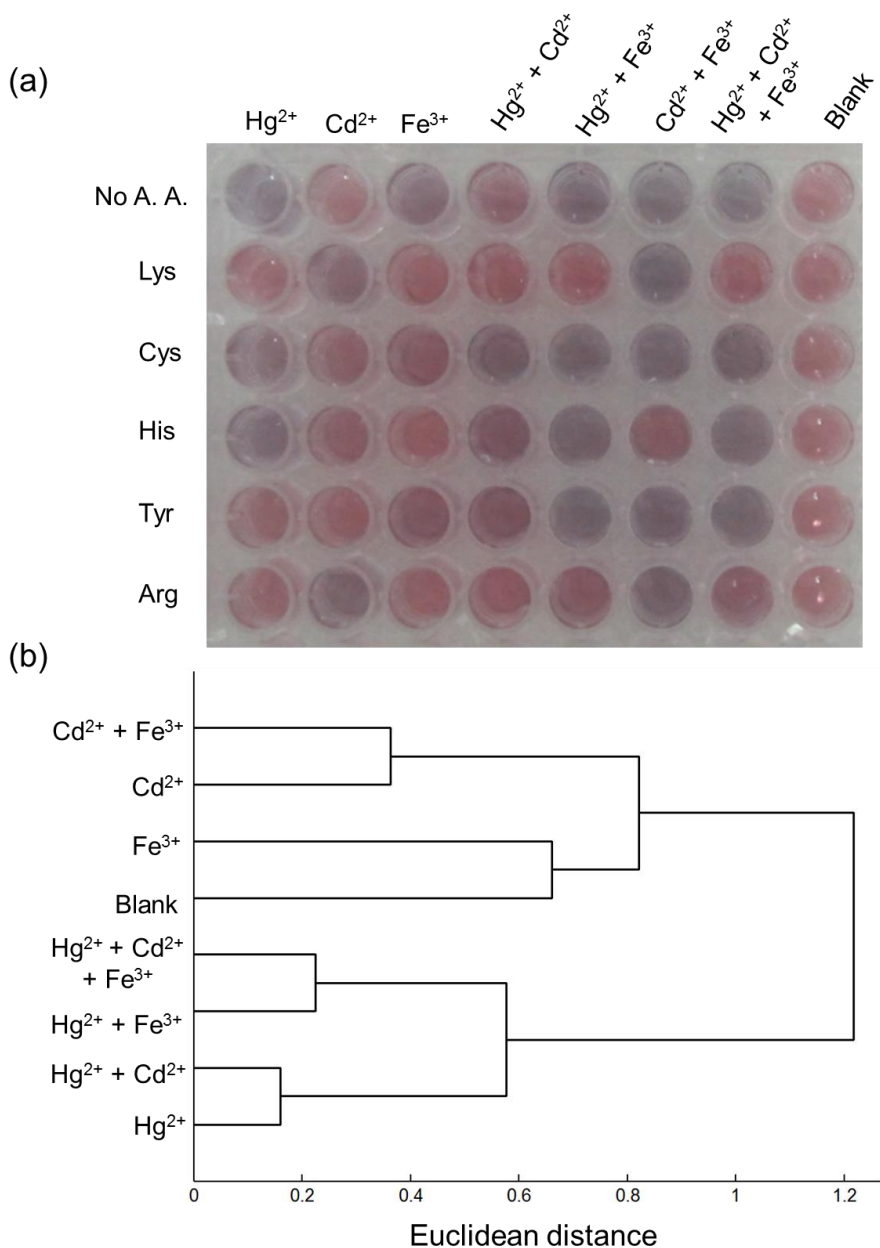


Figure 4.25. Colorimetric response of the colorimetric array against Hg^{2+} , Cd^{2+} and Fe^{3+} ions (20 M) and their binary and ternary mixtures. (a) Representative photograph and (b) Hierarchical cluster analysis.

5. CONCLUSIONS

In conclusion, we demonstrated two different AuNP-based colorimetric sensors for detection of toxic heavy metal ion contaminated water. First, we prepared and characterized the AuNPs. Then, if needed, we modified their surfaces with proper ligands and designed the sensors. Finally, we investigated the performance of sensors in terms of sensitivity, selectivity, reliability and repeatability and we applied them to real-samples.

In the first project, we have developed a simple, rapid, and very sensitive colorimetric assay for Hg^{2+} ion detection in drinking water, which utilizes lysine as an aggregation promoter of AuNPs. The assay uses common citrate-capped AuNPs without the need for tedious surface modification steps (e.g., DNA oligomers and peptides), which makes the sensor practical and cost-effective. The detection limit of the colorimetric assay is around 2.9 nM, which is below the limit (10 nM) defined by the EPA in drinkable water. The assay response is highly linear in a wide concentration range (1 nM to 1000 nM) for experiments performed using either tap or distilled water. Also, selectivity of the sensor was demonstrated in the presence of several other heavy metal ions at high concentrations (50 μM). In addition, the response of the colorimetric assay is very fast, and all analyses can be completed within a few minutes. Furthermore, the cost of one test performed using our colorimetric assay is very low (around 0.5 cent), which is calculated based on reagent prices. Because of its simplicity, excellent sensitivity, and selectivity, our colorimetric assay is advantageous over several metal nanoparticle-based methods (Table 4.1) and feasible for practical applications.

In the second project, we have demonstrated a colorimetric sensor array that can simultaneously detect and identify several heavy metal ions (Hg^{2+} , Cd^{2+} , Fe^{3+} , Pb^{2+} , Al^{3+} , Cu^{2+} , and Cr^{3+}) in aqueous media, to our knowledge for the first time. The colorimetric sensor array utilizes MUA-capped AuNPs and amino acids. In the absence of amino acids MUA-capped AuNPs are aggregated by most of the studied metal ions. The presence of amino acids (lysine, cysteine, histidine, tyrosine, and arginine) either enhances or prevents the aggregation of the MUA-capped AuNPs. The possible mechanisms of aggregation/colloidal stability were discussed. By analyzing the combinatorial response of the array components (i.e., each AuNP and amino acid couple), all of the tested metal ions can be

discriminated in a broad concentration range. This concentration range is highly dependent to the responsivity (i.e., ability to induce aggregation of AuNPs) of the metal ions. For example, highly responsive Pb^{2+} ions can be identified between 2 and 50 μM ; on the other hand, weakly responsive Fe^{3+} ions can be identified at the concentrations above 10 μM . In addition, the response of the colorimetric sensor array is highly reproducible; it discriminated all tested metal ions for three separate experiments without a mistake at the metal ion concentration of 20 μM . Although the reached sensitivity (low μM level) using MUA-capped AuNPs does not satisfy the needed detection limit (around low nM level) for real-world applications, it is possible to design colorimetric arrays for metal ion detection from real samples using simply metal nanoparticles that are capped with different ligands (peptides, aptamers, citrate, etc.) according to the general method described in this study. In addition, we believe that the introduced straightforward colorimetric detection method can be easily adopted to other metal ions and as well as other chemical sensing platforms including proteins, peptides sugars, and organic contaminants.

REFERENCES

- [1] Clarkson, T.W., Magos, L., Myers, G.J., The toxicology of mercury - Current exposures and clinical manifestations, *New England Journal of Medicine*, 349, 1731-1737, **2003**.
- [2] Uzun, L., Kara, A., Osman, B., Yilmaz, E., Besirli, N., Denizli, A., Removal of Heavy-Metal Ions by Magnetic Beads Containing Triazole Chelating Groups, *Journal of Applied Polymer Science*, 114, 2246-2253, **2009**.
- [3] Kim, Y.R., Mahajan, R.K., Kim, J.S., Kim, H., Highly Sensitive Gold Nanoparticle-Based Colorimetric Sensing of Mercury(II) through Simple Ligand Exchange Reaction in Aqueous Media, *ACS Applied Materials & Interfaces*, 2, 292-295, **2010**.
- [4] Du, J., Liu, M., Lou, X., Zhao, T., Wang, Z., Xue, Y., Zhao, J., Xu, Y., Highly Sensitive and Selective Chip-Based Fluorescent Sensor for Mercuric Ion: Development and Comparison of Turn-On and Turn-Off Systems, *Analytical Chemistry*, 84, 8060-8066, **2012**.
- [5] Kim, H.N., Ren, W.X., Kim, J.S., Yoon, J., Fluorescent and colorimetric sensors for detection of lead, cadmium, and mercury ions, *Chemical Society Reviews*, 41, 3210-3244, **2012**.
- [6] Chen, L., Fu, X.L., Lu, W.H., Chen, L.X., Highly Sensitive and Selective Colorimetric Sensing of Hg²⁺ Based on the Morphology Transition of Silver Nanoprisms, *ACS Applied Materials & Interfaces*, 5, 284-290, **2013**.
- [7] Kim, Y.J., Johnson, R.C., Hupp, J.T., Gold nanoparticle-based sensing of "spectroscopically silent" heavy metal ions, *Nano Letters*, 1, 165-167, **2001**.
- [8] Udhayakumari, D., Suganya, S., Velmathi, S., MubarakAli, D., Naked eye sensing of toxic metal ions in aqueous medium using thiophene-based ligands and its application in living cells, *Journal of Molecular Recognition*, 27, 151-159, **2014**.
- [9] Bontidean, I., Berggren, C., Johansson, G., Csöregi, E., Mattiasson, B., Lyoyd, J.R., Jakeman, K., Brown, N.L., Detection of heavy metal ions at femtomolar levels using protein-based biosensors, *Analytical Chemistry*, 70, 4162-4169, **1998**.
- [10] Du, J., Jiang, L., Shao, Q., Liu, X., Marks, R.S., Ma, J., Chen, X., Colorimetric Detection of Mercury Ions Based on Plasmonic Nanoparticles, *Small*, 9, 1467-1481, **2013**.
- [11] Lin, Y.W., Huang, C.C., Chang, H.T., Gold nanoparticle probes for the detection of mercury, lead and copper ions, *Analyst*, 136, 863-871, **2011**.
- [12] Sepulveda, B., Angelome, P.C., Lechuga, L.M., Liz-Marzan, L.M., LSPR-based nanobiosensors, *Nano Today*, 4, 244-251, **2009**.
- [13] Saha, K., Agasti, S.S., Kim, C., Li, X.N., Rotello, V.M., Gold Nanoparticles in Chemical and Biological Sensing, *Chemical Reviews*, 112, 2739-2779, **2012**.
- [14] Sener, G., Uzun, L., Denizli, A., Lysine-Promoted Colorimetric Response of Gold Nanoparticles: A Simple Assay for Ultrasensitive Mercury(II) Detection, *Analytical Chemistry*, 86, 514-520, **2014**.

- [15] Lou, T.T., Chen, Z.P., Wang, Y.Q., Chen, L.X., Blue-to-Red Colorimetric Sensing Strategy for Hg²⁺ and Ag⁺ via Redox-Regulated Surface Chemistry of Gold Nanoparticles, *ACS Applied Materials & Interfaces*, 3, 1568-1573, **2011**.
- [16] Zheng, Q.L., Han, C.P., Li, H.B., Selective and efficient magnetic separation of Pb²⁺ via gold nanoparticle-based visual binding enrichment, *Chemical Communications*, 46, 7337-7339, **2010**.
- [17] Chai, F., Wang, C.A., Wang, T.T., Li, L., Su, Z.M., Colorimetric Detection of Pb²⁺ Using Glutathione Functionalized Gold Nanoparticles, *ACS Applied Materials & Interfaces*, 2, 1466-1470, **2010**.
- [18] Lee, J.S., Han, M.S., Mirkin, C.A., Colorimetric detection of mercuric ion (Hg²⁺) in aqueous media using DNA-functionalized gold nanoparticles, *Angewandte Chemie-International Edition*, 46, 4093-4096, **2007**.
- [19] Wu, Y.G., Zhan, S.S., Wang, F.Z., He, L., Zhi, W., Zhou, P., Cationic polymers and aptamers mediated aggregation of gold nanoparticles for the colorimetric detection of arsenic(III) in aqueous solution, *Chemical Communications*, 48, 4459-4461, **2012**.
- [20] Dang, Y.Q., Li, H.W., Wang, B., Li, L., Wu, Y.Q., Selective Detection of Trace Cr³⁺ in Aqueous Solution by Using 5,5'-Dithiobis (2-Nitrobenzoic acid)-Modified Gold Nanoparticles, *ACS Applied Materials & Interfaces*, 1, 1533-1538, **2009**.
- [21] Ye, B.C., Yin, B.C., Highly Sensitive Detection of Mercury(II) Ions by Fluorescence Polarization Enhanced by Gold Nanoparticles, *Angewandte Chemie-International Edition*, 47, 8386-8389, **2008**.
- [22] Lee, J.S., Mirkin, C.A., Chip-based scanometric detection of mercuric ion using DNA-functionalized gold nanoparticles, *Analytical Chemistry*, 80, 6805-6808, **2008**.
- [23] Li, D., Wieckowska, A., Willner, I., Optical analysis of Hg(2+) ions by oligonucleotide-gold-nanoparticle hybrids and DNA-based machines, *Angewandte Chemie-International Edition*, 47, 3927-3931, **2008**.
- [24] Wang, Y., Yang, F., Yang, X.R., Colorimetric Detection of Mercury(II) Ion Using Unmodified Silver Nanoparticles and Mercury-Specific Oligonucleotides, *ACS Applied Materials & Interfaces*, 2, 339-342, **2010**.
- [25] Slocik, J.M., Zabinski, J.S., Phillips, D.M., Naik, R.R., Colorimetric response of peptide-functionalized gold nanoparticles to metal ions, *Small*, 4, 548-551, **2008**.
- [26] Xie, J.P., Zheng, Y.G., Ying, J.Y., Highly selective and ultrasensitive detection of Hg²⁺ based on fluorescence quenching of Au nanoclusters by Hg²⁺-Au⁺ interactions, *Chemical Communications*, 46, 961-963, **2010**.
- [27] Liu, C.W., Huang, C.C., Chang, H.T., Control over surface DNA density on gold nanoparticles allows selective and sensitive detection of mercury(II), *Langmuir*, 24, 8346-8350, **2008**.
- [28] Liu, D.B., Wang, S.J., Swierczewska, M., Huang, X., Bhirde, A.A., Sun, J., Wang, Z., Yang, M., Jiang, X., Chen, X., Highly Robust, Recyclable

- Displacement Assay for Mercuric Ions in Aqueous Solutions and Living Cells, *ACS Nano*, 6, 10999-11008, **2012**.
- [29] Liu, D.B., Qu, W.S., Chen, W.W., Zhang, W., Wang, Z., Jiang, X., Highly Sensitive, Colorimetric Detection of Mercury(II) in Aqueous Media by Quaternary Ammonium Group-Capped Gold Nanoparticles at Room Temperature, *Analytical Chemistry*, 82,9606-9610, **2010**.
- [30] Huang, C.C., Yang, Z., Lee, K.H., Chang, H.T., Synthesis of highly fluorescent gold nanoparticles for sensing Mercury(II), *Angewandte Chemie-International Edition*, 46, 6824-6828, **2007**.
- [31] Huang, C.C., Chang, H.T., Parameters for selective colorimetric sensing of mercury(II) in aqueous solutions using mercaptopropionic acid-modified gold nanoparticles, *Chemical Communications*, 1215-1217, **2007**.
- [32] Tan, Z.Q., Liu, J.F., Liu, R., Yin, Y.G., Jiang, G.B., Visual and colorimetric detection of Hg²⁺ by cloud point extraction with functionalized gold nanoparticles as a probe, *Chemical Communications*, 7030-7032, **2009**.
- [33] World Health Organization, *Guidelines for Drinking-Water Quality*, 4th ed., WHO Press, Geneva, **2011**.
- [34] Carvalho, C.M.L., Chew, E.H., Hashemy, S.I., Lu, J., Holmgren, A., Inhibition of the human thioredoxin system-A molecular mechanism of mercury toxicity, *Journal of Biological Chemistry*, 283, 11913-11923, **2008**.
- [35] Fen, Y.W., Yunus, W.M.M., Surface plasmon resonance spectroscopy as an alternative for sensing heavy metal ions: a review, *Sensor Review*, 33, 305-314, **2013**.
- [36] Zatta, P., Drago, D., Bolognin, S., Sensi, S.L., Alzheimer's disease, metal ions and metal homeostatic therapy, *Trends in Pharmacological Sciences*, 30, 346-355, **2009**.
- [37] Uversky, V.N., Li, J., Fink, A.L., Metal-triggered structural transformations, aggregation, and fibrillation of human alpha-synuclein-A possible molecular link between Parkinson's disease and heavy metal exposure, *Journal of Biological Chemistry*, 276, 44284-44296, **2001**.
- [38] Fong, B.M.W., Siu, T.S., Lee, J.S.K., Tam, S., Determination of mercury in whole blood and urine by inductively coupled plasma mass spectrometry, *Journal of Analytical Toxicology*, 31, 281-287, **2007**.
- [39] Maciel, C.J.D., Miranda, G.M., de Oliveira, D.P., de Siqueira, M.E.P.B., Silveira, J.N., Leite, E.M.A., da Silva, J.B.B., Determination of cadmium in human urine by electrothermal atomic absorption spectrometry, *Analytica Chimica Acta*, 491, 231-237, **2003**.
- [40] Pesavento, M., Alberti, G., Biesuz, R., Analytical methods for determination of free metal ion concentration, labile species fraction and metal complexation capacity of environmental waters: A review, *Analytica Chimica Acta*, 631, 129-141, **2009**.
- [41] Van Leeuwen, H.P., Town, R.M., Buffle, J., Cleven, R.F.M.J., Davison, W., Puy, J., Van Riemsdijk, W.H., Sigg, L., Dynamic speciation analysis and bioavailability of metals in aquatic systems, *Environmental Science & Technology*, 39, 8545-8556, **2005**.

- [42] Fraday, M., The Bakerian Lecture: Experimental Relations of Gold (and Other Metals) to Light, *Philosophical Transactions of the Royal Society of London*, 147, 145-185, **1857**.
- [43] Turkevich, J., Stevenson, P.C., Hillier, J., A study of the nucleation and growth processes in the synthesis of colloidal gold, *Discussions of the Faraday Society*, 11, 55-75, **1951**.
- [44] Frens, G., Controlled nucleation for regulation of particle-size in monodisperse gold suspensions, *Nature-Physical Science*, 241, 20-22, **1973**.
- [45] Brust, M., Walker, M., Bethell, D., Schiffrin, D.J., Whyman, R., Synthesis of thiol-derivatized gold nanoparticles in a 2-phase liquid-liquid system, *Journal of the Chemical Society-Chemical Communications*, 801-802, **1994**.
- [46] Yee, C.K., Jordan, R., Ulman, A., White, H., King, A., Rafailovich, M., Sokolov, J., Novel one-phase synthesis of thiol-functionalized gold, palladium, and iridium nanoparticles using superhydride, *Langmuir*, 15, 3486-3491, **1999**.
- [47] Negishi, Y., Takasugi, Y., Sato, S., Yao, H., Kimura, K., Tsukuda, T., Magic-numbered Au-n clusters protected by glutathione monolayers (n=18, 21, 25, 28, 32, 39): Isolation and spectroscopic characterization, *Journal of the American Chemical Society*, 126, 6518-6519, **2004**.
- [48] Li, N., Zhao, P.X., Astruc, D., Anisotropic Gold Nanoparticles: Synthesis, Properties, Applications, and Toxicity, *Angewandte Chemie-International Edition*, 53, 1756-1789, **2014**.
- [49] Jana, N.R., Gearheart, L., Murphy, C.J., Seed-mediated growth approach for shape-controlled synthesis of spheroidal and rod-like gold nanoparticles using a surfactant template, *Advanced Materials*, 13, 1389-1393, **2001**.
- [50] Jana, N.R., Gearheart, L., Murphy, C.J., Wet chemical synthesis of high aspect ratio cylindrical gold nanorods, *Journal of Physical Chemistry B*, 105, 4065-4067, **2001**.
- [51] Sharma, V., Park, K., Srinivasarao, M., Colloidal dispersion of gold nanorods: Historical background, optical properties, seed-mediated synthesis, shape separation and self-assembly, *Materials Science & Engineering R-Reports*, 65, 1-38, **2009**.
- [52] Busbee, B.D., Obare, S.O., Murphy, C.J., An improved synthesis of high-aspect-ratio gold nanorods, *Advanced Materials*, 15, 414-416, **2003**.
- [53] Gole A, Murphy CJ. Seed-mediated synthesis of gold nanorods: Role of the size and nature of the seed, *Chemistry of Materials*, 16, 3633-3640, **2004**.
- [54] Wu, H.Y., Chu, H.C., Kuo, T.J., Kuo, C.L., Huang, M.H., Seed-mediated synthesis of high aspect ratio gold nanorods with nitric acid, *Chemistry of Materials*, 17, 6447-6451, **2005**.
- [55] Nikoobakht, B., El-Sayed, M.A., Preparation and growth mechanism of gold nanorods (NRs) using seed-mediated growth method, *Chemistry of Materials*, 15, 1957-1962, **2003**.

- [56] Esumi, K., Matsuhisa, K., Torigoe, K., Preparation of rodlike gold particles by uv irradiation using cationic micelles as a template, *Langmuir*, 11, 3285-3287, **1995**.
- [57] Leontidis, E., Kleitou, K., Kyprianidou-Leodidou, T., Bekiari, V., Lianos, P., Gold colloids from cationic surfactant solutions 1. Mechanisms that control particle morphology, *Langmuir*, 18, 3659-3668, **2002**.
- [58] Miranda, O.R., Ahmadi, T.S., Effects of intensity and energy of CWUV light on the growth of gold nanorods, *Journal of Physical Chemistry B*, 109, 15724-15734, **2005**.
- [59] Eustis, S., Hsu, H.Y., El-Sayed, M.A., Gold nanoparticle formation from photochemical reduction of Au³⁺ by continuous excitation in colloidal solutions. A proposed molecular mechanism, *Journal of Physical Chemistry B*, 109, 4811-4815, **2005**.
- [60] Wang, C.Y., Liu, C.P., Chen, J., Shen, T., The surface chemistry of hybrid nanometer-sized particles 2. Characterization and microstructure of Au clusters supported on TiO₂, *Journal of Colloid and Interface Science*, 191, 464-470, **1997**.
- [61] Wang, C.Y., Liu, C.Y., Zheng, X., Chen, J., Shen, T., The surface chemistry of hybrid nanometer-sized particles I. Photochemical deposition of gold on ultrafine TiO₂ particles, *Colloids and Surfaces a-Physicochemical and Engineering Aspects*, 131, 271-280, **1998**.
- [62] Huang, X., Qi, X., Huang, Y., Li, S., Xue, C., Gan, C.L., Boey, F., Zhang, H., Photochemically Controlled Synthesis of Anisotropic Au Nanostructures: Platelet-like Au Nanorods and Six-Star Au Nanoparticles, *ACS Nano*, 4, 6196-6202, **2010**.
- [63] Huang, X., Zhou, X., Wu, S., Wei, Y., Qi, X., Zhang, J., Boey, F., Zhang, H., Reduced Graphene Oxide-Templated Photochemical Synthesis and in situ Assembly of Au Nanodots to Orderly Patterned Au Nanodot Chains, *Small*, 6, 513-516, **2010**.
- [64] Kim, F., Song, J.H., Yang, P.D., Photochemical synthesis of gold nanorods, *Journal of the American Chemical Society*, 124, 14316-14317, **2002**.
- [65] Nishioka, K., Niidome, Y., Yamada, S., Photochemical reactions of ketones to synthesize gold nanorods, *Langmuir*, 23, 10353-10356, **2007**.
- [66] Niidome, Y., Nishioka, K., Kawasaki, H., Yamada, S., Rapid synthesis of gold nanorods by the combination of chemical reduction and photoirradiation processes; morphological changes depending on the growing processes, *Chemical Communications*, 2376-2377, **2003**.
- [67] Miranda, O.R., Dollahon, N.R., Ahmadi, T.S., Critical concentrations and role of ascorbic acid (vitamin C) in the crystallization of gold nanorods within hexadecyltrimethyl ammonium bromide (CTAB)/tetraoctyl ammonium bromide (TOAB) micelles, *Crystal Growth & Design*, 6, 2747-2753, **2006**.
- [68] Yu, Y.Y., Chang, S.S., Lee, C.L., Wang, C.R.C., Gold nanorods: Electrochemical synthesis and optical properties, *Journal of Physical Chemistry B*, 101, 6661-6664, **1997**.

- [69] Chang, S.S., Shih, C.W., Chen, C.D., Lai, W.C., Wang, C.R.C., The shape transition of gold nanorod, *Langmuir*, 15, 701-709, **1999**.
- [70] Barbour, K., Ashokkumar, M., Caruso, R.A., Grieser, F., Sonochemistry and sonoluminescence in aqueous AuCl₄⁻ solutions in the presence of surface-active solutes, *Journal of Physical Chemistry B*, 103, 9231-9236, **1999**.
- [71] Qiu, X.F., Zhu, J.J., Chen, H.Y., Controllable synthesis of nanocrystalline gold assembled whiskery structures via sonochemical route, *Journal of Crystal Growth*, 257, 378-383, **2003**.
- [72] Zhang, J., Du, J., Han, B., Liu, Z., Jiang, T., Zhang, Z., Sonochemical formation of single-crystalline gold nanobelts, *Angewandte Chemie-International Edition*, 45, 1116-1119, **2006**.
- [73] Burda, C., Chen, X.B., Narayanan, R., El-Sayed, M.A., Chemistry and properties of nanocrystals of different shapes, *Chemical Reviews*, 105, 1025-1102, **2005**.
- [74] Lu, G., Zhao, R., Qian, G., Qi, Y., Wang, X., Suo, J., A highly efficient catalyst Au/MCM-41 for selective oxidation cyclohexane using oxygen, *Catalysis Letters*, 97, 115-118, **2004**.
- [75] Henzie, J., Kwak, E.S., Odom, T.W., Mesoscale metallic pyramids with nanoscale tips, *Nano Letters*, 5, 1199-1202, **2005**.
- [76] Antonietti, M., Thunemann, A., Wenz, E., Synthesis and characterization of non spherical gold colloids in block-copolymer micelles, *Colloid and Polymer Science*, 274, 795-800, **1996**.
- [77] Skrabalak, S.E., Chen, J., Au, L., Lu, X., Li, X., Xia, Y., Gold nanocages for biomedical applications, *Advanced Materials*, 19, 3177-3184, **2007**.
- [78] Zhang, Y., Dai, H.J., Formation of metal nanowires on suspended single-walled carbon nanotubes, *Applied Physics Letters*, 77, 3015-3017, **2000**.
- [79] El-Sayed, M.A., Some interesting properties of metals confined in time and nanometer space of different shapes, *Accounts of Chemical Research*, 34, 257-264, **2001**.
- [80] Dujardin, E., Peet, C., Stubbs, G., Culver, J.N., Mann, S., Organization of metallic nanoparticles using tobacco mosaic virus templates, *Nano Letters*, 3, 413-417, **2003**.
- [81] Brown, S., Sarikaya, M., Johnson, E., A genetic analysis of crystal growth, *Journal of Molecular Biology*, 299, 725-735, **2000**.
- [82] Lee, W., Scholz, R., Niesch, K., Gosele, U., A template-based electrochemical method for the synthesis of multisegmented metallic nanotubes, *Angewandte Chemie-International Edition*, 44, 6050-6054, **2005**.
- [83] Pham, T., Jackson, J.B., Halas, N.J., Lee, T.R., Preparation and characterization of gold nanoshells coated with self-assembled monolayers, *Langmuir*, 18, 4915-4920, **2002**.
- [84] Wang, H., Brandl, D.W., Le, F., Nordlander, P., Halas, N.J., Nanorice: A hybrid plasmonic nanostructure, *Nano Letters*, 6, 827-832, **2006**.

- [85] Sun, Y.G., Xia, Y.N., Mechanistic study on the replacement reaction between silver nanostructures and chloroauric acid in aqueous medium, *Journal of the American Chemical Society*, 126, 3892-3901, **2004**.
- [86] Sun, Y.G., Mayers, B.T., Xia, Y.N., Template-engaged replacement reaction: A one-step approach to the large-scale synthesis of metal nanostructures with hollow interiors, *Nano Letters*, 2:481-485, **2002**.
- [87] Chen, J., Wiley, B., McLellan, J., Xiong, Y., Li, Z.Y., Xia, Y., Optical properties of Pd-Ag and Pt-Ag nanoboxes synthesized via galvanic replacement reactions, *Nano Letters*, 5, 2058-2062, **2005**.
- [88] Au, L., Lu, X.M., Xia, Y.N., A comparative study of galvanic replacement reactions involving Ag nanocubes and AuCl_2^- or AuCl_4^- , *Advanced Materials*, 20, 2517-2522, **2008**.
- [89] Booth, J.M., Bhargava, S.K., Bond, A.M., O'Mullane, A.P., Voltammetric monitoring of gold nanoparticle formation facilitated by glycyl-L-tyrosine: Relation to electronic spectra and transmission electron microscopy images, *Journal of Physical Chemistry B*, 110, 12419-12426, **2006**.
- [90] Bhargava, S.K., Booth, J.M., Agrawal, S., Coloe, P., Kar, G., Gold nanoparticle formation during bromoaurate reduction by amino acids, *Langmuir*, 21, 5949-5956, **2005**.
- [91] Harnish, B., Robinson, J.T., Pei, Z.C., Ramstrom, O., Yan, M.D., UV-cross-linked poly(vinylpyridine) thin films as reversibly responsive surfaces, *Chemistry of Materials*, 17, 4092-4096, **2005**.
- [92] Pucci, A., Bernabo, M., Elvati, P., Meza, L.I., Galembeck, F., Leite, C.A.P., Tirelli, N., Ruggeri, G., Photoinduced formation of gold nanoparticles into vinyl alcohol based polymers, *Journal of Materials Chemistry*, 16, 1058-1066, **2006**.
- [93] Huang, H.Z., Yang, X.R., Synthesis of chitosan-stabilized gold nanoparticles in the absence/presence of tripolyphosphate, *Biomacromolecules*, 5, 2340-2346, **2004**.
- [94] Mandal, T.K., Fleming, M.S., Walt, D.R., Preparation of polymer coated gold nanoparticles by surface-confined living radical polymerization at ambient temperature, *Nano Letters*, 2, 3-7, **2002**.
- [95] Choi, J., Yang, J., Park, J., Kim, E., Suh, J.-S., Huh, Y.-M., Haam, S., Specific Near-IR Absorption Imaging of Glioblastomas Using Integrin-Targeting Gold Nanorods, *Advanced Functional Materials*, 21, 1082-1088, **2011**.
- [96] Zeng, S.W., Yong, K.T., Roy, I., Din, X.-Q., Yu, X., Luan, F., A Review on Functionalized Gold Nanoparticles for Biosensing Applications, *Plasmonics*, 6, 491-506, **2011**.
- [97] Chanana, M., Liz-Marzan, L.M., Coating matters: the influence of coating materials on the optical properties of gold nanoparticles, *Nanophotonics*, 1, 199-220, **2012**.
- [98] Njoki, P.N., Lim, I.I.S., Mott, D., Park, H.-Y., Khan, B., Mishra, S., Sujakumar, R., Luo, J., Zhong, C.-J., Size correlation of optical and

- spectroscopic properties for gold nanoparticles, *Journal of Physical Chemistry C*, 111, 14664-14669, **2007**.
- [99] Taladriz-Blanco, P., Buurma, N.J., Rodriguez-Lorenzo, L., Perez-Juste, J., Liz-Marzan, L.M., Hervas, P., Reversible assembly of metal nanoparticles induced by penicillamine. Dynamic formation of SERS hot spots, *Journal of Materials Chemistry*, 21, 16880-16887, **2011**.
- [100] Link, S., El-Sayed, M.A., Size and temperature dependence of the plasmon absorption of colloidal gold nanoparticles, *Journal of Physical Chemistry B*, 103, 4212-4217, **1999**.
- [101] Lin, S.Y., Wu, S.H., Chen, C.H., A simple strategy for prompt visual sensing by gold nanoparticles: General applications of interparticle hydrogen bonds, *Angewandte Chemie-International Edition*, 45, 4948-4951, **2006**.
- [102] Lee, I.L., Sung, Y.M., Wu, S.P., Triazole-acetate functionalized gold nanoparticles for colorimetric Pb(II) sensing, *RSC Advances*, 4, 25251-25256, **2014**.
- [103] Yu, C.J., Tseng, W.L., Colorimetric Detection of Mercury(II) in a High-Salinity Solution Using Gold Nanoparticles Capped with 3-Mercaptopropionate Acid and Adenosine Monophosphate, *Langmuir*, 24, 12717-12722, **2008**.
- [104] Su, D.Y., Yang, X., Xia Q.D., Wang, C., Qu, F., Colorimetric detection of Hg²⁺ using thioctic acid functionalized gold nanoparticles, *RSC Advances*, 3, 24618-24624, **2013**.
- [105] Placido, T., Aragay, G., Pons, J., Comparelli, R., Curri, M., L., Merkoci, A., Ion-Directed Assembly of Gold Nanorods: A Strategy for Mercury Detection, *ACS Applied Materials & Interfaces*, 5, 1084-1092, **2013**.
- [106] Yao, Y., Tian, D.M., Li, H.B., Cooperative Binding of Bifunctionalized and Click-Synthesized Silver Nanoparticles for Colorimetric Co²⁺ Sensing, *ACS Applied Materials & Interfaces*, 2, 684-690, **2010**.
- [107] Krpetic, Z., Guerrini, L., Larmour, I.A., Reglinski, J., Faulds, K., Graham, D., Importance of Nanoparticle Size in Colorimetric and SERS-Based Multimodal Trace Detection of Ni(II) Ions with Functional Gold Nanoparticles, *Small*, 8, 707-714, **2012**.
- [108] Chen, Z.P., Liu, R.L., Wang, S.S., Qu, C., Chen, L., Wang, Z., Colorimetric sensing of copper(II) based on catalytic etching of gold nanorods. *RSC Advances*, 3, 13318-13323, **2013**.
- [109] Lin, S.Y., Liu, S.W., Lin, C.M., Chen, C.H., Recognition of potassium ion in water by 15-crown-5 functionalized gold nanoparticles, *Analytical Chemistry*, 74, 330-335, **2002**.
- [110] Lin, S.Y., Chen, C.H., Lin, M.C., Hsu, H.F., A cooperative effect of bifunctionalized nanoparticles on recognition: Sensing alkali ions by crown and carboxylate moieties in aqueous media, *Analytical Chemistry*, 77, 4821-4828, **2005**.
- [111] Obare, S.O., Hollowell, R.E., Murphy, C.J., Sensing strategy for lithium ion based on gold nanoparticles, *Langmuir*, 18, 10407-10410, **2002**.

- [112] Reynolds, A.J., Haines, A.H., Russell, D.A., Gold glyconanoparticles for mimics and measurement of metal ion-mediated carbohydrate-carbohydrate interactions, *Langmuir*, 22, 1156-1163, **2006**.
- [113] Lisowski, C.E., Hutchison, J.E., Malonamide-Functionalized Gold Nanoparticles for Selective, Colorimetric Sensing of Trivalent Lanthanide Ions, *Analytical Chemistry*, 81, 10246-10253, **2009**.
- [114] Li, X.K., Wang, J.N., Sun, L.L., Wang, Z.X., Gold nanoparticle-based colorimetric assay for selective detection of aluminium cation on living cellular surfaces, *Chemical Communications*, 46, 988-990, **2010**.
- [115] Lee, J.H., Wang, Z.D., Liu, J.W., Lu, Y., Highly Sensitive and Selective Colorimetric Sensors for Uranyl (UO_2^{2+}): Development and Comparison of Labeled and Label-Free DNAzyme-Gold Nanoparticle Systems, *Journal of the American Chemical Society*, 130, 14217-14226, **2008**.
- [116] Modi, R.P., Mehta, V.N., Kailasa, S.K., Bifunctionalization of silver nanoparticles with 6-mercaptopurinic acid and melamine for simultaneous colorimetric sensing of Cr^{3+} and Ba^{2+} ions, *Sensors and Actuators B-Chemical*, 195, 562-571, **2014**.
- [117] Alizadeh, A., Khodaei, M.M., Hamidi, Z., Bin, Shamsuddin, M., Naked-eye colorimetric detection of Cu^{2+} and Ag^+ ions based on close-packed aggregation of pyridines-functionalized gold nanoparticles, *Sensors and Actuators B-Chemical*, 190, 782-791, **2014**.
- [118] Karthiga, D., Anthony, S.P., Selective colorimetric sensing of toxic metal cations by green synthesized silver nanoparticles over a wide pH range, *RSC Advances*, 3, 16765-16774, **2013**.
- [119] Kumar, V.V., Anthony, S.P., Silver nanoparticles based selective colorimetric sensor for Cd^{2+} , Hg^{2+} and Pb^{2+} ions: Tuning sensitivity and selectivity using co-stabilizing agents, *Sensors and Actuators B-Chemical*, 191, 31-36, **2014**.
- [120] Wei, Q.S., Nagi, R., Sadeghi, K., Feng, S., Yan, E., Ki, S.J., Caire, R., Tseng, D., Ozcan, A., Detection and Spatial Mapping of Mercury Contamination in Water Samples Using a Smart-Phone, *ACS Nano*, 8, 1121-1129, **2014**.
- [121] Chen, G.H., Chen, W.Y., Yen, Y.C., Wang, C.W., Chang, H.T., Chen, C.F., Detection of Mercury(II) Ions Using Colorimetric Gold Nanoparticles on Paper-Based Analytical Devices, *Analytical Chemistry*, 86, 6843-6849, **2014**.
- [122] Enustun, B.V., Turkevich, J., Coagulation of colloidal gold, *Journal of the American Chemical Society*, 85, 3317, **1963**.
- [123] Haiss, W., Thanh, N.T.K., Aveyard, J., Fernig, D.G., Determination of size and concentration of gold nanoparticles from UV-Vis spectra, *Analytical Chemistry*, 79, 4215-4221, **2007**.
- [124] Lin, C.Y., Yu, C.J., Lin, Y.H., Tseng, W.L., Colorimetric Sensing of Silver(I) and Mercury(II) Ions Based on an Assembly of Tween 20-Stabilized Gold Nanoparticles, *Analytical Chemistry*, 82, 6830-6837, **2010**.

- [125] Du, J.J., Zhu, B.W., Chen, X.D., Urine for Plasmonic Nanoparticle-Based Colorimetric Detection of Mercury Ion, *Small*, 9, 4104-4111, **2013**.
- [126] Chai, F., Wang, C.G., Wang, T.T., Ma, Z.F., Su, Z.M., L-cysteine functionalized gold nanoparticles for the colorimetric detection of Hg²⁺ induced by ultraviolet light, *Nanotechnology*, 21, 6, **2010**.
- [127] Lee, J.S., Ulmann, P.A., Han, M.S., Mirkin, C.A., A DNA-gold nanoparticle-based colorimetric competition assay for the detection of cysteine, *Nano Letters*, 8, 529-533, **2008**.
- [128] Xu, H., Hepel, M., "Molecular Beacon"-Based Fluorescent Assay for Selective Detection of Glutathione and Cysteine, *Analytical Chemistry* 83, 813-819, **2011**.
- [129] You, J., Hu, H., Zhou, J., Zhang, L., Kondo, T., Novel Cellulose Polyampholyte-Gold Nanoparticle-Based Colorimetric Competition Assay for the Detection of Cysteine and Mercury(II), *Langmuir*, 29, 5085-5092, **2013**.
- [130] Hamaguchi, K., Kawasaki, H., Arakawa, R., Photochemical synthesis of glycine-stabilized gold nanoparticles and its heavy-metal-induced aggregation behavior, *Colloids and Surfaces a-Physicochemical and Engineering Aspects*, 367, 167-173, **2010**.
- [131] Zhu, J.Z., Yang, J., Deng, B.L., Enhanced mercury ion adsorption by amine-modified activated carbon, *Journal of Hazardous Materials*, 166, 866-872, **2009**.
- [132] Radhakumary, C., Sreenivasan, K., Gold nanoparticles generated through "green route" bind Hg²⁺ with a concomitant blue shift in plasmon absorption peak, *Analyst*, 136, 2959-2962, **2011**.
- [133] Wang, H., Wang, Y.X., Jin, J.Y., Yang, R.H., Gold Nanoparticle-Based Colorimetric and "Turn-On" Fluorescent Probe for Mercury(II) Ions in Aqueous Solution, *Analytical Chemistry*, 80, 9021-9028, **2008**.
- [134] Li, L., Li, B.X., Qi, Y.Y., Jin, Y., Label-free aptamer-based colorimetric detection of mercury ions in aqueous media using unmodified gold nanoparticles as colorimetric probe, *Analytical and Bioanalytical Chemistry*, 393, 2051-2057, **2009**.
- [135] Chen, X.J., Zu, Y.B., Xie, H., Kemas, A.M., Gao, Z.Q., Coordination of mercury(II) to gold nanoparticle associated nitrotriazole towards sensitive colorimetric detection of mercuric ion with a tunable dynamic range, *Analyst*, 136, 1690-1696, **2011**.
- [136] <http://www.ankara.bel.tr/haberler/ankaranin-icme-suyu-tertemizpirilpiril/#.UmanZvIshIE> (accessed October 22, 2013).
- [137] Zhang, G., Lin, W., Yang, W., Lin, Z., Guo, L., Qiu, B., Chen, G., Logic gates for multiplexed analysis of Hg²⁺ and Ag⁺, *Analyst*, 137, 2687-2691, **2012**.
- [138] Cush, R., Cronin, J.M., Stewart, W.J., Maule, C.H., Molloy, J., Goard, N.J., The resonant mirror: a novel optical biosensor for direct sensing of biomolecular interactions Part I: principle of operation and associated instrumentation, *Biosensors and Bioelectronics*, 8, 347-353, **1993**.

- [139] Promnimit, S., Bera, T., Baruah, S., Dutta, J., Chitosan Capped Colloidal Gold Nanoparticles for Sensing Zinc Ions in Water, *Journal of Nano Research*, 16, 55-61, **2011**.
- [140] Ma, C.X., Harris, J.M., Surface-Enhanced Raman Scattering Study of the Kinetics of Self-Assembly of Carboxylate-Terminated n-Alkanethiols on Silver, *Langmuir*, 28, 2628-2636, **2012**.
- [141] Zakaria, H.M., Shah, A., Konieczny, M., Hoffmann, J.A., Nijdam, A.J., Reeves, M.E., Small Molecule- and Amino Acid-Induced Aggregation of Gold Nanoparticles, *Langmuir*, 29, 7661-7673, **2013**.
- [142] Rulisek, L., Havlas, Z., Theoretical studies of metal ion selectivity. 1. DFT calculations of interaction energies of amino acid side chains with selected transition metal ions (Co^{2+} , Ni^{2+} , Cu^{2+} , Zn^{2+} , Cd^{2+} , and Hg^{2+}), *Journal of the American Chemical Society*, 122, 10428-10439, **2000**.
- [143] Musto, C.J., Lim, S.H., Suslick, K.S., Colorimetric Detection and Identification of Natural and Artificial Sweeteners, *Analytical Chemistry*, 81, 6526-6533, **2009**.
- [144] Yildirim, A., Ozturk, F.E., Bayindir, M., Smelling in Chemically Complex Environments: An Optofluidic Bragg Fiber Array for Differentiation of Methanol Adulterated Beverages, *Analytical Chemistry*, 85, 6384-6391, **2013**.

CURRICULUM VITAE

Credentials

Name, Surname : Gülsu Şener Yildirim
Place of Birth : Ankara
Marital Status : Married
E-mail : gulsu@hacettepe.edu.tr
Address : Hacettepe University, Department of Chemistry, Beytepe,
Ankara

Education

High School : Hacı Ömer Tarman Anadolu Lisesi, Ankara
BSc. : Hacettepe University
MSc. : Hacettepe University
PhD. : Hacettepe University

Foreign Languages

English (fluent), German (Sprachdiplom)

Work Experience

Hacettepe University 2007 – present
Department of Chemistry and
Nanotechnology and Nanomedicine Division,

Areas of Experiences

Nanoparticle synthesis, molecular imprinted polymers, biosensors, colorimetric sensors.

Projects and Budgets

Principal Investigator

- Ağır Metal Tayini İçin Yüzey Plazmon Rezonans Temelli Nanosensörlerin Tasarımı ve Seçici, Duyarlı ve Eş Zamanlı Gümüş İyonu Tayininde Kullanımının İncelenmesi
The Scientific and Technological Research Council of Turkey, Project number: 113 Z 442, 2013-2014.
Budget: 29.500 TL

Publications

1. G. Sener, L. Uzun and A. Denizli “A Colorimetric Sensor Array based on Gold Nanoparticles and Amino Acids for Identification of Toxic Metal Ions in Water” *ACS Applied Materials and Interfaces*, 2014, 6, 18395.
2. G. Sener, L. Uzun and A. Denizli “Lysine Promoted Colorimetric Response of Gold Nanoparticles: A Simple Assay for Ultra-Sensitive Mercury(II) Detection” *Analytical Chemistry*, 2014, 86, 514.
3. G. Sener, E. Ozgur, A. Y. Rad, L. Uzun, R. Say and A. Denizli “Rapid Real-time Detection of Procalcitonin using a Microcontact Imprinted Surface Plasmon Resonance Biosensor” *Analyst*, 2013, 138, 6422.
4. E. Ozgur, E. Yilmaz, G. Sener, L. Uzun, R. Say and A. Denizli “A New Molecular Imprinting-Based Mass-Sensitive Sensor for Real-Time Detection of 17 beta-Estradiol from Aqueous Solution” *Environmental Progress & Sustainable Energy*, 2013, 32, 1164.
5. G. Sener, L. Uzun, R. Say and A. Denizli “Use of Molecular Imprinted Nanoparticles as Biorecognition Element on Surface Plasmon Resonance Sensor” *Sensors and Actuators B: Chemical*, 2011, 160, 791.
6. N. Bereli, G. Sener, H. Yavuz and A. Denizli “Oriented Immobilized anti-LDL Antibody Carrying Poly(hydroxyethyl methacrylate) Cryogel for Cholesterol Removal from Human Plasma” *Materials Science and Engineering: C*, 2011, 31, 1078.
7. G. Sener, E. Ozgur, E. Yilmaz, L. Uzun, R. Say and A. Denizli “Quartz Crystal Microbalance Based Nanosensor for Lysozyme Detection with Lysozyme Imprinted Nanoparticles” *Biosensors and Bioelectronics*, 2010, 26, 815.

8. N. Bereli, G. Sener, E. B. Altintas, H. Yavuz and A. Denizli "Poly(glycidyl methacrylate) Beads Embedded Cryogels for Pseudo-specific Affinity Depletion of Albumin and Immunoglobulin G" *Materials Science and Engineering: C*, 2010, 30, 323.

Oral and Poster Presentations

1. G. Sener, L. Uzun, A. Denizli, Lysine Promoted Formation of Hg/Au Nanoparticle Aggregates for Simple and Ultra-Sensitive Mercury (II) Detection. MRS Spring Meeting & Exhibit, San Francisco, USA, April 21-25, 2014. (Poster presentation)
2. G. Sener, E. Ozgur, A. Y. Rad, L. Uzun, R. Say, A. Denizli, Microcontact Imprinted Surface Plasmon Resonance Biosensor for Rapid Procalcitonin Detection. ACS Fall Meeting, Indianapolis, USA, September 8-12, 2013. (Poster presentation)
3. G. Sener, E. Ozgur, E. Yilmaz, L. Uzun, R. Say, A. Denizli, Preparation of Ion Imprinted SPR Sensor for Real-Time Detection of Silver(I) Ion from Aqueous Solution. 2nd International Conference Nanomaterials: Applications and Properties, Ukraine, September 17-22, 2012. (Poster presentation)
4. G. Sener, E. Yilmaz, S. Ozkara, L. Uzun, R. Say, A. Denizli, Imprinting Based SPR Ion Sensor for Real-time Monitoring of Cu(II) Ions from Aqueous Solutions. 2nd International Conference on Bio Sensing Technology 2011, Amsterdam, Holland October 10-12, 2011. (Poster presentation)
5. G. Sener, E. Ozgur, E. Yilmaz, L. Uzun, R. Say, A. Denizli, Quartz Crystal Microbalance Based Nanosensor for Lysozyme Detection with Lysozyme Imprinted Nanoparticles. Biosensors 2010, 20th Anniversary World Congress on Biosensors, Glasgow, Great Britain, May 26-28, 2010. (Poster presentation)